Impulsive Noise Suppression in Modern Communication Systems

by

Jia Jia

M. Phil., University of Bradford, Bradford, England, 2009

B. Sc., University of Electronic Science and Technology of China, Chengdu, China, 2005

A Dissertation Submitted in Partial Fulfillment of the Requirements for the Degree of

Doctor of Philosophy

in the Graduate Academic Unit of Electrical and Computer Engineering

Supervisor:	Julian Meng, Ph. D., Electrical and Computer Engineering
Examining Board:	Richard Tervo, Ph. D., Electrical and Computer Engineering
	Brent Petersen, Ph. D., Electrical and Computer Engineering
	Wei Song, Ph. D., Computer Science
External Examiner:	Weimin Huang, Ph. D., Electrical and Computer Engineering, Memorial University of Newfoundland, St. John's, Canada

This dissertation is accepted by the
Dean of Graduate Studies

THE UNIVERSITY OF NEW BRUNSWICK

September, 2015

ABSTRACT

Compared to additive white Gaussian noise (AWGN), impulsive noise has unique characteristics which include random occurrence, short time duration, wide band spectrum, and high-energy content. Due to these distinctive features, impulsive noise with significant power can degrade the transmission quality of various communication systems.

In this research, the impact of impulsive noise on Orthogonal Frequency-Division Multiplexing (OFDM)-based communication systems and ZigBee wireless sensor networks (WSNs) based on direct sequence spread spectrum (DSSS) modulation are addressed. For the purpose of improving system performance, several impulsive noise suppression approaches are proposed for both of the two communication systems mentioned above. First, this research proposes a novel time domain filtering approach for both OFDM and DSSS modulation with the aid of Reed-Solomon (RS) coding and noise estimation to mitigate the influence of impulsive noise on the transmitted signal. This filter utilizes a composite comparison value (CCV) algorithm to improve the accuracy of impulsive noise detection. Performance comparisons with previously proposed filtering and coding methods demonstrate the effectiveness of the CCV filter. In the second case, we describe a new Error-Balanced Wavelet (EB-Wavelet) filtering process for the impulsive noise suppression in ZigBee-based WSNs utilizing DSSS modulation. Theoretical analysis shows that the bit error rate (BER) of ZigBee systems is related to the received noise power and any filter generated distortion. The EB-Wavelet filter employs a multiresolution analysis and weighting matrix for bandwidth management to

limit the presence of impulsive noise power while balancing the overall filter distortion. Computer simulations are performed to compare the performance of the proposed EB-Wavelet approach with conventional finite impulse response filters. Results show that the EB-Wavelet filter can further improve the BER performance of ZigBee systems in the presence of significant impulsive noise while maintaining a low complexity of ZigBee receiver design.

Additionally, in this dissertation, the impulsive noise performances of 915 MHz and 2.4 GHz band ZigBee communication systems are compared. A novel impulsive noise model based on the statistical characteristics of the impulsive noise measured in electricity substations is proposed and utilized for the comparison procedure. Both theoretical and simulation results show the advantage of deploying the 2.4 GHz band ZigBee in impulsive noise environments in order to enhance transmission quality. However, it may be possible to deploy the 915 MHz band ZigBee for partial discharge fault monitoring in related environments.

DEDICATION

This dissertation is dedicated to my parents, for their heartfelt support and unconditional love.

This work is also dedicated to my grandparents who are in my memory forever.

ACKNOWLEDGEMENTS

I would like to express my special appreciation and thanks to my supervisor Dr. Julian Meng, for his invaluable guidance, constant encouragement, and financial support in my PhD research program. I gained valuable knowledge and research experience from him during the past years. My academic goals could never be accomplished without his careful supervision. Also, I wish to extend my appreciation to Drs. Saleh Saleh and Eduardo Guerra for their selfless help and support during my PhD studies.

I would like to express my gratitude to the examining committee for taking the time to review this dissertation and provide valuable suggestions. I also wish to thank Ms. Shelley Cormier, Ms. Denise Burke, and Ms. Karen Annett for their sincere assistance in my PhD program.

I am very grateful to the Natural Science and Engineering Research Council of Canada (NSERC) and the University of New Brunswick (UNB) for the financial support which made this research work possible.

Last but not least, I am thankful to all the researchers in the Sustainable Power Research Group UNB for their memorable friendship and help.

Table of Contents

List of Tables

List of Figures

List of Abbreviations

4G	the fourth generation
16-QAM	16-ary quadrature amplitude modulation
ADCI	adjacent channel interference
ADSL	Asymmetric Digital Subscriber Line
ALCI	alternate channel interference
AM	amplitude modulation
APL	application layer
ASK	amplitude shift keying
AWGN	additive white Gaussian noise
BER	bit error rate
BM	Berlekamp-Massey
BPF	bandpass filter
CCV	composite comparison value
CCV-OFDM	OFDM with the composite comparison value filter
CCV-ZigBee	ZigBee with the composite comparison value filter
CDF	cumulative distribution function
CP	cyclic prefix
DAB	Digital Audio Broadcasting
DFT	discrete Fourier transform
DSP	digital signal processing
DSSS	direct sequence spread spectrum

DWT	discrete wavelet transform
EB-Wavelet	Error-Balanced Wavelet
FDM	Frequency-Division Multiplexing
FFT	Fast Fourier transform
FIR	finite impulse response
HBH	high band quasi-transverse electromagnetic horn antenna
HDTV	High-Definition Television
ICI	inter-channel interference
IDFT	inverse discrete Fourier transform
IFFT	inverse Fast Fourier transform
ISI	inter-symbol interference
ITU	International Telecommunication Union
LBH	low band quasi-transverse electromagnetic horn antenna
LPF	lowpass filter
LTE-Advanced	Long Term Evolution advanced
MAC	media access layer
MRA	multiresolution analysis
MSE	mean squared error
NRZ	nonreturn-to-zero
NWK	network layer
O-QPSK	offset-quadrature phase-shift keying
OFDM	Orthogonal Frequency-Division Multiplexing
P/S	parallel-to-serial

PBC	passband clipping
PD	partial discharge
PDF	probability distribution density
PE	probability of error
PER	packet error rate
PHY	physical layer
PN	pseudorandom noise
PSD	power spectral density
PSSS	parallel sequence spread spectrum
RF	radio frequency
RS-OFDM	Reed-Solomon coded Orthogonal Frequency-Division Multiplexing
RS-ZigBee	Reed-Solomon coded ZigBee
RS	Reed-Solomon
RSCCV-OFDM	Reed-Solomon coded Orthogonal Frequency-Division Multiplexing with the composite comparison value filter
RSCCV-ZigBee	Reed-Solomon coded ZigBee with the composite comparison value filter
S/P	serial-to-parallel
SAR	signal-to-additive white Gaussian noise ratio
SER	symbol error rate
SNR	signal-to-noise ratio
VBF	variance-based filter

VBF-OFDM	OFDM with the variance-based filter
VLSI	very-large-scale integrated circuit
WLAN	Wireless Local Area Network
WSN	wireless sensor network

Chapter 1 Introduction

1.1 Background

The concept of Orthogonal Frequency-Division Multiplexing (OFDM) was first proposed in the 1960s [1]. In the 1970s, a multi-carrier modulation process utilizing the discrete Fourier transform (DFT) was developed by Weinstein which made the practical implementation of OFDM possible [2]. Later in the 1980s, Cimini systemically analyzed the existing challenges and possible solutions for applying the OFDM technique in mobile communications [3]. From then on, the OFDM technology was developed quickly with the driving force from the continuously growing mobile communications market. Nowadays, OFDM has been widely used in various modern communication systems such as Asymmetric Digital Subscriber Line (ADSL), Digital Audio Broadcasting (DAB), High-Definition Television (HDTV), and Wireless Local Area Network (WLAN) [4, 5]. In 2011, the Long Term Evolution Advanced (LTE-Advanced) was standardized as a candidate for the fourth generation (4G) mobile communication network where the OFDM was adopted as the uplink/downlink modulation of the Physical (PHY) Layer [6].

The advantages of OFDM which are of interest can be summarized as follows:

1. With the serial-to-parallel conversion (S/P) on the high speed data stream, the duration of OFDM symbols is therefore extended. When the number of OFDM sub-carriers is fairly large, this duration extension can be significant resulting in an almost flat-fading channel response compared to a wideband single tone modulation. Furthermore, with the aid of added cyclic prefix (CP), OFDM has a good robustness to the inter-symbol interference (ISI) caused by the multipath propagations [7].

2. The sub-carriers of OFDM are orthogonal to each other which creates the possibility of spectrum overlapping among adjacent sub-channels. This characteristic improves the spectral efficiency without introducing extra inter-channel interference (ICI) when compared to conventional Frequency-Division Multiplexing (FDM) systems [8].

3. With the development of digital signal processing (DSP) and very-large-scale integrated circuit (VLSI), the practical implementation of OFDM can be expediently achieved using the Fast Fourier transform (FFT) and inverse Fast Fourier transform (IFFT) DSP technologies. This development reduces the implementation complexity of OFDM-based systems.

In contrast to the OFDM which is usually utilized for long distance communication transmissions, the ZigBee technology is implemented for short range wireless sensor networks (WSNs) due to its unique advantages. Established in 2001, the ZigBee Alliance devoted itself to providing a flexible, low power consumption, and low cost WSN platform. The ratified ZigBee protocol is a set of wireless communication solutions which includes the industrial specifications for the PHY layer (which includes DSSS modulation), the media access layer (MAC), the network layer (NWK), the application layer (APL), etc. [9]. The PHY and MAC layers were defined by the IEEE 802.15.4 standard and utilized by the ZigBee Alliance as the kernel of its communication infrastructure. Due to its low power consumption characteristic, the ZigBee standard is limited to up to 250 kb/s data rate and a short point-to-point transmission distance indicating a local area deployment. However, with a hybrid network topology, wide area network coverage can be achieved to improve the practicability of deployment [10]. ZigBee is attracting more attention from both science and industry fields as it is

considered to be a good candidate for low data rate wireless transmission applications in various environments such as home security and automation, medical data collecting, industrial control and monitoring, and smart grid applications [10-15]. Using the DSSS coding for the PHY layer, ZigBee has a fairly good external white noise resistance benefiting from the spectrum despreading ability of the DSSS coding technology.

However, both OFDM and ZigBee systems are vulnerable to strong impulsive noise bursts. Unlike the additive white Gaussian noise (AWGN), impulsive noise has several unique characteristics: random occurrence, high-energy content within short time duration, and a wide band spectrum. An example of the impulsive noise based on the Bernoulli-Gaussian model is illustrated in Figure 1.1 [16]. When excessive impulsive noise is received by the OFDM receiver, its energy can spread to all OFDM sub-carriers through the DFT demodulation process which may cause degradation to the system performance. In ZigBee systems, the intense impulsive noise may also surpass the noise suppression capability of DSSS coding which results in increased level of bit error rate (BER). Therefore, we are motivated to propose various impulsive noise suppression schemes for the OFDM-based communication systems and ZigBee wireless networks.

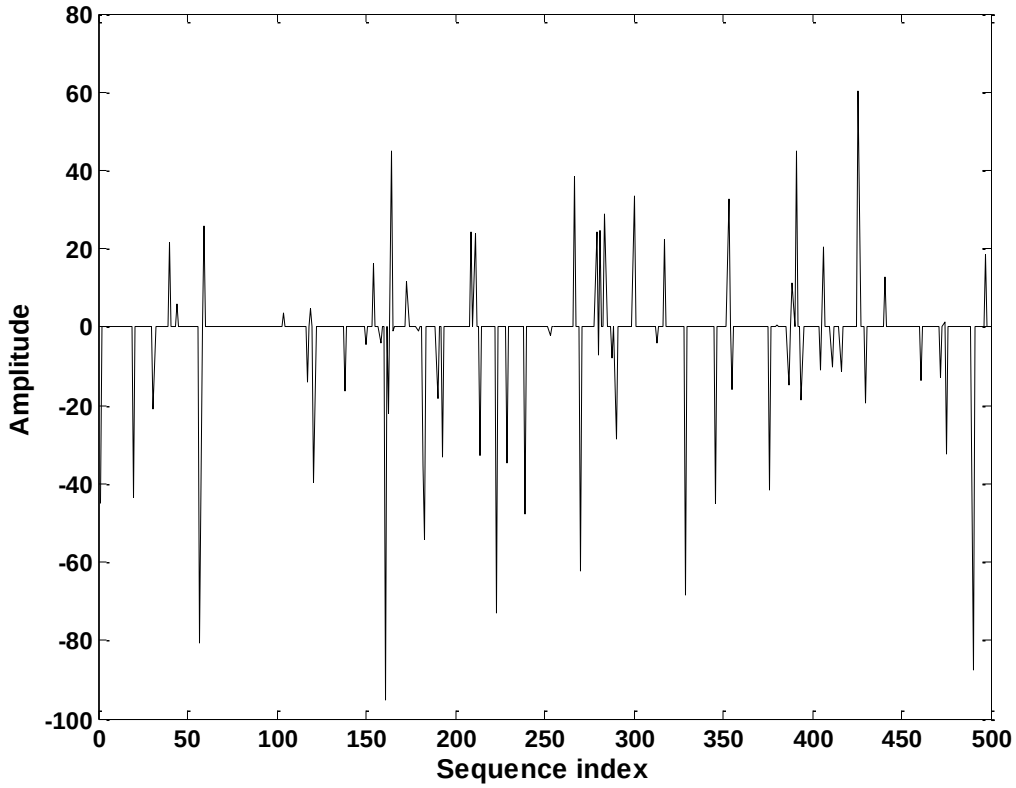

Figure 1.1 Bernoulli-Gaussian impulsive noise

1.2 Review of Impulsive Noise Suppression Methodologies

The main sources of impulsive noise can be identified as power transmission lines, transients from defective power components, vehicle ignition systems, partial discharge (PD) on deteriorated insulation, and sferic radiation from high current switching [17-20]. The amplitude of impulsive noise can be several dB over the received signal and other background noise and its frequency spectrum may reach up to 3 GHz which will overlap the operating bands of various wireless communication systems [21, 22]. As a result,

impulsive noise can significantly affect the performance of OFDM and ZigBee communication systems.

To limit the impact of impulsive noise, many approaches have been proposed and can be divided into three categories: time domain suppression, frequency domain suppression, and error-correcting code techniques.

For impulsive noise suppression in the time domain, a blanking implementation scheme was proposed for OFDM systems [23]. The sampled discrete time domain signal which is interfered by the individual impulsive noise sample is detected and discarded using the proposed adaptive threshold value. The proposed threshold is obtained by minimizing the estimated interference power after this blanking process. Another promising peak detection method based on the variance of the estimated noise was introduced to suppress impulsive noise in OFDM systems [24]. For the peak detection, a threshold value is obtained to locate the impulsive noise in the estimated noise sequence followed by a nonlinear blanking operation on the detected impulsive noise location. To mitigate the impulsive noise in DSSS-based systems, a passband clipping (PBC) approach was proposed [25]. Similar to the peak detection methods employed in OFDM systems, the PBC detects the impulsive noise using a calculated threshold and suppresses it by clipping the time domain amplitude of the detected impulsive noise. The clipping threshold is determined by the root mean squared amplitude of the received passband DSSS signal. However, for the time domain impulsive noise suppression methods, the threshold should be carefully arranged as extra symbol errors can be generated by a false detection.

The second category deals with impulsive noise in the frequency domain. The interleaving and additional orthogonal transform before the FFT demodulation were utilized to mitigate the influence of impulsive noise in OFDM systems [26]. With the aid of an additional orthogonal transform, the power of impulsive noise samples can be spread over several OFDM symbols and the symbol-to-noise ratio is therefore improved. This method can further improve system performance when compared to the interleaving approach implemented alone. In Hussien's research, a lowpass filter (LPF) was utilized at the offset-quadrature phase-shift keying (O-QPSK) demodulator to suppress the channel interference including the impulsive noise by limiting the power of interference [27]. Simulations showed that a 3rd order finite impulse response (FIR) LPF with a 1 MHz cutoff frequency obtained the best BER for ZigBee systems.

For the third category, channel coding techniques are employed to reject impulsive noise interference. The system performance can be improved by correcting errors during the decoding process. The Reed-Solomon (RS) code is a good candidate for impulsive noise cancellation due to its burst noise correcting ability. With RS codes, the transmitted bytes interfered by the impulsive noise in a codeword can be corrected irrespective of the number of bits in error [28]. Meerbergen merged the conventional RS codes with an OFDM modulator using the proposed subsampled filter bank [29]. The RS coded OFDM (RS-OFDM) performance was evaluated and results showed the impulsive noise immunity of RS-OFDM systems is further enhanced when compared to the conventional uncoded OFDM system. The International Telecommunication Union (ITU) G.9903 standard also requires the RS coding to be implemented with the OFDM modulation in order to recover lost bits which are caused by impulsive noise [30].

1.3 OFDM Modulation Systems

In this section, the basics of OFDM are introduced. The system architecture of the conventional OFDM system employed in this dissertation is illustrated in Figure 1.2.

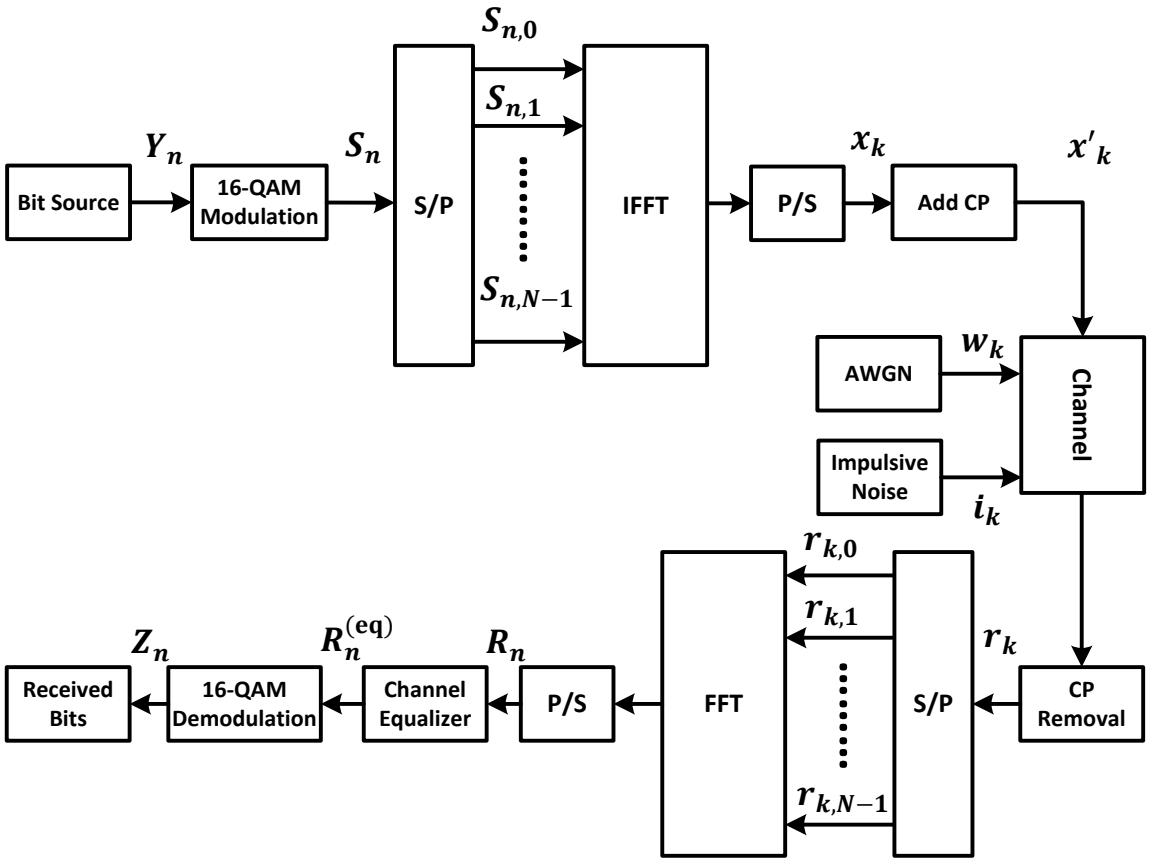

Figure 1.2 OFDM system architecture

At the OFDM transmitter, the bit sequence Y_n is first modulated by the 16-ary quadrature amplitude modulation (16-QAM) and forms the complex signal sequence S_n where $0 \leq n \leq N-1$ and N is the number of OFDM sub-carriers. The utilization of 16-QAM is to improve the system bandwidth efficiency which is explained in Appendix A.

Although a higher order QAM further improves the bandwidth efficiency, the system tolerance to noise is lowered given a higher density of QAM constellation points. With the S/P conversion, the signal to be transmitted on the ith OFDM sub-carrier is represented as $S_{n,i}$ where $0 \leq i \leq N-1$. Followed by the parallel-to-serial (P/S) conversion, the inverse discrete Fourier transform (IDFT) result is then obtained as

$$x_k = \mathrm{IDFT}(S_n) = \frac{1}{N}\sum_{n=0}^{N-1} S_n \exp\left(\mathrm{j}\frac{2\pi nk}{N}\right), 0 \leq k \leq N-1, \tag{1.1}$$

where $\mathrm{IDFT}(\cdot)$ indicates the IDFT operator. However, in a practical OFDM modulation system, the IFFT and FFT operations are employed to implement the IDFT and corresponding DFT process, respectively. (1.1) ensures the orthogonality of OFDM sub-carriers, that is

$$\frac{1}{N}\sum_{n=0}^{N-1} \exp(\mathrm{j}\frac{2\pi ni_1}{N})\exp(\mathrm{j}\frac{2\pi ni_2}{N}) = \begin{cases} 1, & i_1 = i_2 \\ 0, & i_1 \neq i_2 \end{cases}, \tag{1.2}$$

where i_1 and i_2 indicate the $i_1 th$ and $i_2 th$ sub-carrier, respectively. With the CP added into x_k, the signal to be transmitted in the channel is represented as x'_k. The insertion of CP improves multipath resistance without disturbing the orthogonality of OFDM sub-carriers.

In the transmission channel, x'_k is interfered by the impulsive noise i_k and AWGN w_k, respectively. Therefore at the receiver, the received signal processed by the CP removal is expressed as

$$r_k = x_k * h_k + i_k + w_k, \tag{1.3}$$

where $*$ denotes the linear convolution operation and h_k is the channel impulse response. After the S/P conversion, the parallel received signal streams $r_{k,i}$ are then processed by

the DFT transform. The DFT result is then P/S converted and forms the serial signal sequence R_n, that is,

$$R_n = \mathrm{DFT}(r_k) = \sum_{n=0}^{N-1} r_k \exp\left(-\mathrm{j}\frac{2\pi nk}{N}\right) = S_n H_n + I_n + W_n, 0 \le n \le N-1\ , \quad (1.4)$$

where $\mathrm{DFT}(\cdot)$ is the DFT operator, H_n is the channel frequency response, I_n and W_n are the frequency domain representation of i_k and w_k, respectively. Assuming an ideal channel equalization process is performed, the equalized signal can be expressed as

$$R_n^{(\mathrm{eq})} = R_n H_n^{-1} = S_n + I_n H_n^{-1} + W_n H_n^{-1}. \quad (1.5)$$

Finally, with the 16-QAM demodulation, we obtain the demodulated bit sequence Z_n.

As can be seen from (1.4) and (1.5), the impact of impulsive noise spreads to all OFDM sub-carriers and may cause system degradation. Obviously, an error-correcting coding process performed on the bit source sequence Y_n can mitigate the impact of impulsive noise and improve the system performance. An impulsive noise suppression in the time domain before the DFT demodulation at the receiver is another possible approach, e.g., a filtering process performed on the received noise interfered signal r_k.

1.4 ZigBee Systems

The PHY layer of ZigBee is based on the IEEE 802.15.4 standard. Three major operating bands are assigned which are the 868 MHz in Europe, 915 MHz in the USA and Australia, and 2.4 GHz worldwide. A general specification for the ZigBee PHY layer based on the 2011 version of IEEE 802.15.4 standard is given in Table 1.1, where ASK and PSSS represent amplitude-shift keying and parallel sequence spread spectrum, respectively [31]. In this dissertation, we focus on the 2.4 GHz band ZigBee since

compared to the 915 MHz band ZigBee which has the identical radio frequency (RF) and baseband coding modulation, the 2.4 GHz band ZigBee shows an improved impulsive noise resistance which is later discussed in Chapter 3.

Table 1.1 Specifications of ZigBee PHY layer

Operation band (MHz)	Frequency bandwidth (MHz)	Radio frequency modulation	Bit rate (kb/s)	Chip rate (kchip/s)	Baseband spread spectrum
868	868-868.6	ASK	250	400	PSSS
915	902-928	O-QPSK	250	1000	DSSS
2400	2400-2483.5	O-QPSK	250	2000	DSSS

The system architecture of the 2.4 GHz band ZigBee systems is illustrated in Figure 1.3. The detailed description of the ZigBee transmitter and receiver is provided in Figure 1.4 and Figure 1.5, respectively.

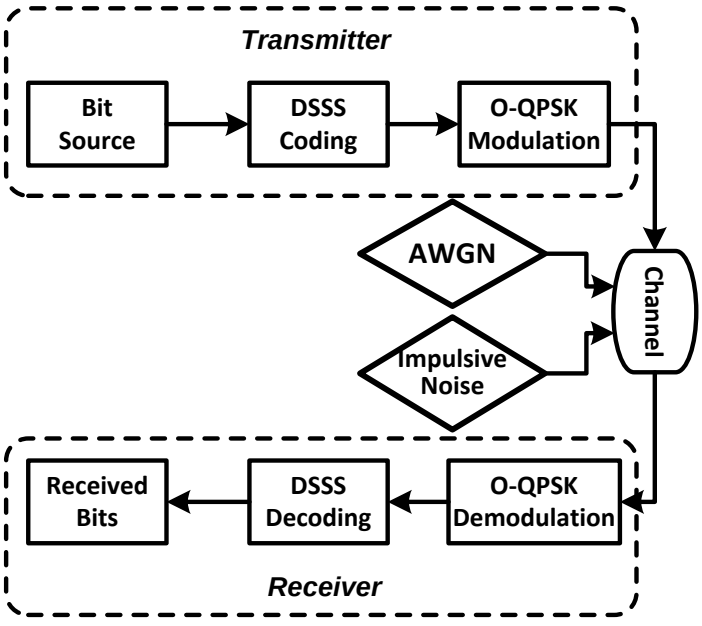

Figure 1.3 System architecture of the 2.4 GHz band ZigBee

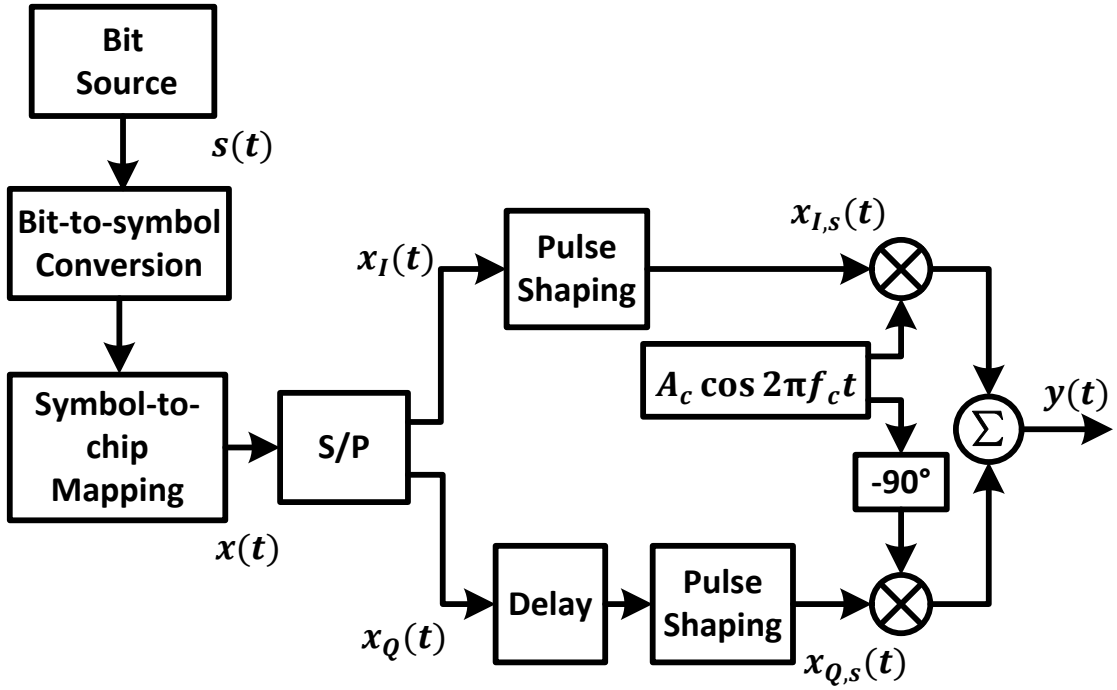

Figure 1.4 2.4 GHz band ZigBee transmitter

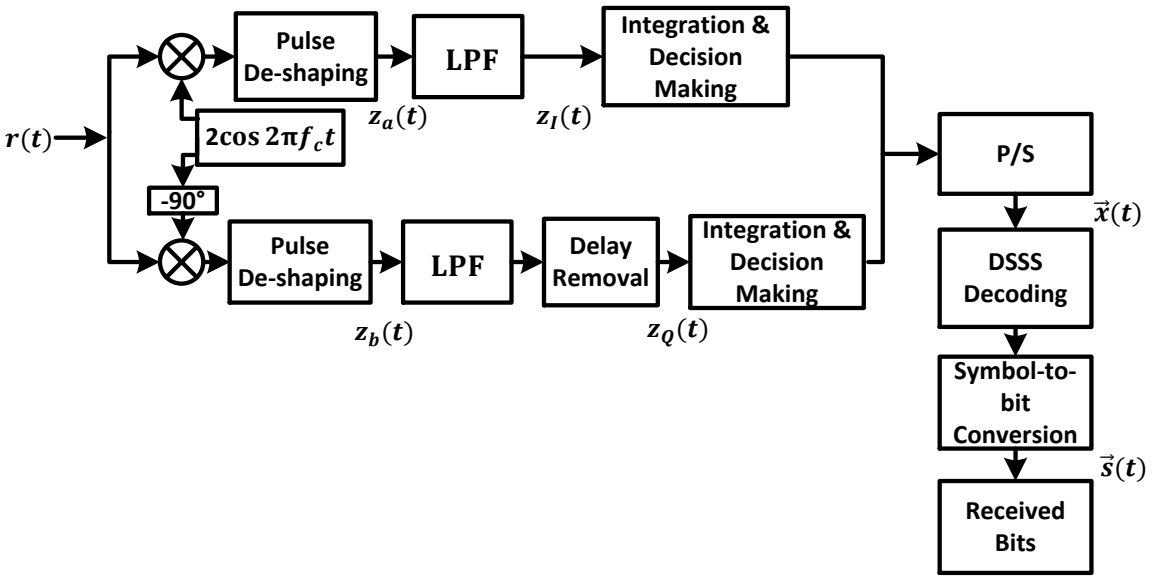

Figure 1.5 2.4 GHz band ZigBee receiver

For the 2.4 GHz band ZigBee transmitter, every 4 bits of the bit source sequence $s(t)$ which is at 250 kb/s bit rate are grouped and converted into one integer symbol. Every integer symbol is then mapped into a 32-chip pseudorandom noise (PN) sequence $x(t)$ following the symbol-to-chip mapping regulation given by IEEE 802.15.4 standard. The spectrum spreading gain is obtained by

$$\text{Gain}_{\text{ZigBee}} = 10\log_{10}\frac{32}{4} \approx 9 \text{ (dB)}. \tag{1.6}$$

The PN sequence $x(t)$ which is at 2000 kchip/s chip rate is then S/P converted and forms the two parallel data streams $x_I(t)$ and $x_Q(t)$, respectively. A pulse shaping operation is respectively performed on $x_I(t)$ and $x_Q(t)$ using the required half-sine pulse as described in IEEE 802.15.4. The pulse shaped signal $x_{I,s}(t)$ and $x_{Q,s}(t)$ are then modulated by the 2.4 GHz O-QPSK quadrature carriers for the channel transmission.

Considering the interference of impulsive noise $i(t)$ and AWGN $w(t)$ added in the channel, the received signal at the ZigBee receiver is represented by

$$r(t) = y(t) + i(t) + w(t), \tag{1.7}$$

where $y(t)$ is the originally transmitted signal. After the coherent detection and pulse de-shaping, the in-phase sub-channel signal $z_a(t)$ and quadrature sub-channel signal $z_b(t)$ are obtained. The employed LPF in our ZigBee system is to reject the adjacent channel interference (ADCI), alternative channel interference (ALCI), and the double carrier frequency component generated by the coherent detection. The cutoff frequency of the LPF corresponds to the bandwidth of the baseband transmitted signal. Additionally, the impact of channel noise is bandlimited by the LPF resulting in the improvement of system performance. The low pass baseband in-phase and quadrature sub-carrier signals

are denoted by $z_I(t)$ and $z_Q(t)$, respectively. Processed by the sub-channel integrators and decision makers, the demodulated signal is P/S converted into the serial data sequence $\vec{x}(t)$. The Maximum Likelihood (ML) algorithm is adopted for the DSSS decoder. Finally after the DSSS decoding process and symbol-to-bit conversion, the bit message $\vec{s}(t)$ is obtained.

It can be seen that, after the O-QPSK coherent detection and the low pass filtering process, the remaining impulsive noise can cause the incorrect integral result $\vec{x}(t)$ to be transmitted to the following DSSS decoder. If the number of errors in $\vec{x}(t)$ exceeds the error correcting capability of the DSSS decoder, wrong symbols are decoded resulting in incorrect bit information being received by the user. In this case, additional impulsive noise suppression is warranted for ZigBee systems.

1.5 Dissertation Overview

The research presented in this dissertation focuses on the development of impulsive noise suppression approaches for OFDM and DSSS-based ZigBee systems. In the literature reviewed, three categories of impulsive noise suppression approaches have been addressed which are time domain suppression, frequency domain suppression, and the implementation of error-correcting coding techniques. The proposed approaches in this dissertation cover these three categories.

In Chapter 2, frequency domain impulsive noise estimation and time domain impulsive noise suppression for OFDM systems are proposed. The time domain suppression approach utilizes a proposed composite comparison value (CCV)-based filter. An RS coding process is also employed in this approach to achieve an enhanced

dual protection goal. Simulation-based results demonstrate the effectiveness of this proposed scheme.

In Chapter 3, the impulsive noise resistance of 915 MHz and 2.4 GHz band ZigBee systems is analyzed. An impulsive noise model is proposed and employed to compare the system performance of 915 MHz and 2.4 GHz band ZigBee systems in a heavy impulsive noise environment. The proposed model is based on the statistical characteristics of the impulsive noise measured in electricity substations. Results show that in the same signal-to-impulsive noise ratio scenario, the 2.4 GHz band ZigBee outperforms the 915 MHz band ZigBee in a BER comparison test.

In Chapter 4, the proposed CCV filter with RS coding is utilized with time domain noise estimation to mitigate the impulsive noise influence in ZigBee systems. The proposed scheme is compared with existing methods to access any advantages in system performance.

In Chapter 5, the distortion-noise relationship between the low pass filtering process in front of the sub-carrier integrators at the ZigBee receiver and the ZigBee system performance is analyzed. To facilitate an implementable filter response, a discrete wavelet transform (DWT)-based filtering algorithm is proposed and implemented to limit the impact of impulsive noise in the frequency domain. Simulation results demonstrate the BER improvement of the proposed DWT-based filter when compared to existing approaches which include the previously proposed CCV filter.

Chapter 2 Impulsive Noise Suppression for OFDM Communication Systems using a Dual Protection Scheme

2.1 Introduction

OFDM is widely used in various wireless communications and power-line communications. Compared with single carrier communication systems, OFDM has several advantages such as resistance to multipath distortion, improved spectral efficiency, and robustness to narrowband noise [32]. However, excessive impulse noise in terms of event probability, duration, and amplitude can cause difficulties in OFDM transmission [33, 34]. Impulsive noise is formalized as an additive channel noise component with typical characteristics such as spike-like with short time durations, random occurrence, wide bandwidth, and a high power spectral density. With respect to the latter, impulsive noise amplitude can be several dB over the received signal and other background noise [21]. As a result, impulsive noise can result in the performance degradation of OFDM systems, since its energy spreads to all the OFDM carriers through the receiver DFT demodulation process. This chapter is focused on improving the performance of the impulsive noise cancellation process as well as providing the ability to resist the influence of AWGN in OFDM systems. In this manner, we present a practical scheme which utilizes the frequency domain noise estimation, time domain nonlinear filtering, and RS coding for such a purpose.

To decrease the impact of impulsive noise, a basic suppression procedure was previously proposed, and is formulated using two basic steps: impulsive noise detection

and error correction [35, 36]. Based on these concepts, filtering and coding methods to manage impulsive noise have been previously proposed. For example, a blanking nonlinearity process is employed in OFDM systems to locate and filter an impulsive noise event if its amplitude exceeds an assigned threshold in the time domain [24, 37]. Although this technique has been found to improve the overall system BER, the performance gains are somewhat limited due to ill-defined impulse noise thresholds and the blanking of the data content. Recent research demonstrated several advantages of coding methods for error detection and correction in an impulsive noise environment, especially in regard to the Reed-Solomon coding scheme [38-40]. However, these proposed RS coding approaches are sensitive to increased levels of AWGN. Therefore we propose a dual faceted approach which utilizes the RS coding technique and a composite comparison value (CCV)-based filtering process to improve the impulsive noise resistance of OFDM systems. The CCV filter creates a more accurate estimate of the original OFDM signal after impulsive noise removal. The residual impulsive noise is then managed by an RS decoder in the second stage. Numerical results show the proposed approach outperforms the coding and filtering techniques alone.

The reminder of this chapter is organized as follows. In Section 2.2, the theoretical background and impact of impulsive noise on OFDM are introduced. Some existing impulsive noise suppression approaches which are based on filtering techniques are also described in this section. In Section 2.3, the details of our dual protection scheme are proposed. Finally, several simulations and numerical results are described in Section 2.4.

2.2 Impact of Impulsive Noise on OFDM

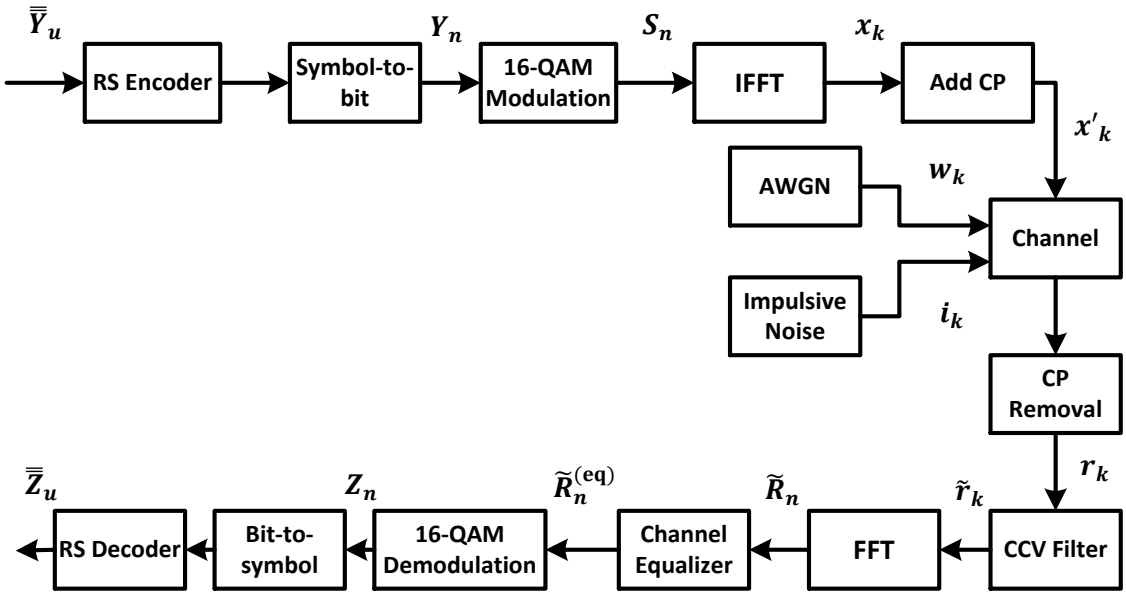

Figure 2.1 RS-OFDM with the CCV filter

The RS coded OFDM (RS-OFDM) with the proposed CCV filter is illustrated in Figure 2.1. The description of the basic OFDM is given in Chapter 1. The signal sequence to be transmitted, given as $\bar{\bar{Y}}_u$, is RS coded and converted into the bit sequence Y_n, where $0 \leq n \leq N-1$. With the OFDM modulation and insertion of CP, the signal to be transmitted is represented as x'_k. In the channel, the signal x'_k is interfered by AWGN w_k and impulsive noise i_k. Processed by CP removal, the received signal at the receiver is expressed as

$$r_k = x_k * h_k + i_k + w_k = x_k * h_k + n_k, 0 \leq k \leq N-1, \tag{2.1}$$

where h_k is the channel impulse response, and n_k is the aggregation of w_k and i_k. When a channel equalizer is not considered, the N-point FFT demodulation result can be represented as

$$R_n = S_n H_n + W_n + I_n \,, \tag{2.2}$$

where H_n is the channel frequency response, W_n and I_n are the AWGN and impulsive noise in frequency domain, respectively.

Referring to previous research work, impulsive noise i_k is normally accepted as the following expression [16]:

$$i_k = b_k g_k, \tag{2.3}$$

where b_k is a Bernoulli process indicating the arrival of the impulsive noise event and g_k is the random Gaussian process with zero mean and σ_i^2 variance. b_k contains independently distributed zeros and ones where the ones indicate the arrivals of impulsive noise events. The arrival rate of impulsive noise events is represented as $p = P(b_k = 1)$. The arrival and variance parameters can be altered to facilitate varying noise conditions. In this research, the probabilistic arrival rate of impulsive noise events p was set to 1% and 10%, and the variance was held constant.

In the time domain, the characteristics of impulsive noise can have significant differences when compared to transmitted signal and can be summarized as follows: (1) impulsive noise peak amplitudes can be much higher than that of the transmitted signal; (2) impulsive noise energy is concentrated into short periods. Given this, a method based on a blanking nonlinearity filter was proposed in [37]. The impulsive noise is suppressed by the process:

$$r_k^{(\text{comp})} = \begin{cases} r_k, \text{if } |r_k| < A_0, k = 0,1,\dots,N-1 \\ 0, \text{ otherwise} \end{cases}, \tag{2.4}$$

where r_k is the time domain signal at the receiver and A_0 is the experimental threshold value.

Also, Zhidkov proposed a promising peak detection method based on the variance of the estimated noise to mitigate the effect of impulsive noise at the receiver in the frequency domain [24]. The proposed method is denoted as variance-based filter (VBF).For the peak detection, a threshold value is estimated to recognize impulsive noise sequence $\hat{u} = [\hat{u}_0, \hat{u}_1, \dots, \hat{u}_{N-1}]$:

$$\hat{\sigma}^2 = \frac{1}{N} \sum_{k=0}^{N-1} \left|\hat{d}_k\right|^2, k = 0,1,\dots,N-1, \tag{2.5}$$

$$\hat{u}_k = \begin{cases} \hat{d}_k, \text{if } \left|\hat{d}_k\right|^2 > C\hat{\sigma}^2, k = 0,1,\dots,N-1 \\ 0, \text{ otherwise} \end{cases}, \tag{2.6}$$

where $\hat{d}_k$ is the integrated noise estimation in time domain, N is the number of $\hat{d}_k$, $\hat{u}_k$ is the estimated representation of the impulsive noise, and C is the threshold value that corresponds to the probability of false detection.

Although these approaches provide an effective way to reduce the effects of impulsive noise, the evaluation of the threshold value does not respond to changes in the characteristics of the impulsive noise and does not assess any correlation between the additive noise components.

2.3 The Proposed CCV Filtering Approach

As expected, the value of the impulsive noise threshold affects the performance of the impulsive noise suppression methodology. If the threshold value is too small, a

significant portion of the transmitted signal is replaced with zeros and the output signal-to-noise ratio (SNR) given by

$$SNR = 10\log_{10}\frac{\sum_{k=0}^{N-1} x'^{2}_{k}}{\sum_{k=0}^{N-1} n_k^2} = 10\log_{10}\frac{\mathrm{E}[x'^{2}_{k}]}{\mathrm{E}[n_k^2]} = 10\log_{10}\frac{\mathrm{E}[x'^{2}_{k}]}{\mathrm{E}^2[n_k]+\mathrm{Var}[n_k]}$$

$$= 10\log_{10}\frac{\mathrm{E}[x'^{2}_{k}]}{\mathrm{E}^2[w_k+i_k]+\mathrm{Var}[w_k+i_k]} = 10\log_{10}\frac{\mathrm{E}[x'^{2}_{k}]}{\mathrm{Var}[w_k]+\mathrm{E}[i_k^2]}$$

$$= 10\log_{10}\frac{\sum_{k=0}^{N-1} x'^{2}_{k}}{\sum_{k=0}^{N-1}(w_k^2+i_k^2)} \tag{2.7}$$

decreases, where E[·] denotes the expectation operation, Var[·] denotes the variance operation, and w_k and i_k are assumed to be independent. However, if the threshold value is set too high, impulsive noise events will go undetected and will corrupt the receiver demodulation process as shown by (2.2). Thus a good threshold value is needed to balance the false positive and negative detections of impulsive noise events.

Theoretically, the idea of a conventional mean filter is simply to replace each element in the transmitted data sequence with the mean or average value of its neighbors including itself [41, 42]. With a conventional mean filter only a rough approximation of the original OFDM transmitted signal is obtained. Although this is a poor representation of the original OFDM signal, some gain in receiver performance is achieved through the removal of the impulsive noise energy. In order to improve upon this, a new approach based on an improved mean windowing filter is proposed where the statistical property of every element and its neighbors is considered. The proposed filter attempts to remove impulsive noise rather than replace the OFDM signal with a mean value, thereby

retaining the original characteristics of the original OFDM signal less the impulsive noise.

2.3.1 Noise Estimation

As shown earlier, the transmitted signal at the OFDM receiver is expressed by (2.2). Assuming a reasonable channel estimate where $\widehat{H}_n \approx H_n$, the received signal $R_n^{(\mathrm{eq})}$ after frequency equalization can be represented as

$$R_n^{(\mathrm{eq})} = R_n \widehat{H}_n^{-1} = S_n + W_n \widehat{H}_n^{-1} + I_n \widehat{H}_n^{-1}, n = 0,1, \dots, N-1. \tag{2.8}$$

The total noise component N_n is the FFT of n_k, and is the sum of the impulsive noise and AWGN in frequency domain, that is,

$$N_n = W_n + I_n. \tag{2.9}$$

Our goal is to estimate the impulsive noise component I_n. To do this, the estimation of the integrated noise N_n from (2.9) represented as $\widehat{N}_n$ is given as

$$\widehat{N}_n = \widehat{H}_n\left(R_n^{(\mathrm{eq})} - \hat{S}_n\right), n = 0,1, \dots, N-1, \tag{2.10}$$

where $\hat{S}_n$ is the estimated transmitted signal that is obtained using a preliminary estimation processing [24]. This estimation procedure is organized as follows: (1) after removing the CP, all null subcarriers, which were previously created for the N-point IFFT, containing noise-induced non-zero data are reset to zero (2) the transmitted data is then de-mapped to the proper constellation points yielding $\hat{S}_n$.

2.3.2 Impulsive Noise Estimation using Composite Comparison Values

Once $\widehat{N}_n$ is estimated using (2.10), the following operation is considered,

$$\hat{n}_k = \mathrm{IFFT}(\widehat{N}_n) = \widehat{w}_k + \hat{\imath}_k, \tag{2.11}$$

where $\hat{n}_k$ is the time domain combination of AWGN and impulsive noise, $\hat{\imath}_k$ indicates the representation of the estimated impulsive noise, $\hat{w}_k$ indicates the representation of the estimated AWGN, and IFFT|·| is the IFFT operator. Once the impulsive noise component is estimated by our proposed filter, it can be subtracted from the received signal prior to decoding. The block diagram of the OFDM receiver with the CCV filter is shown in Figure 2.2.

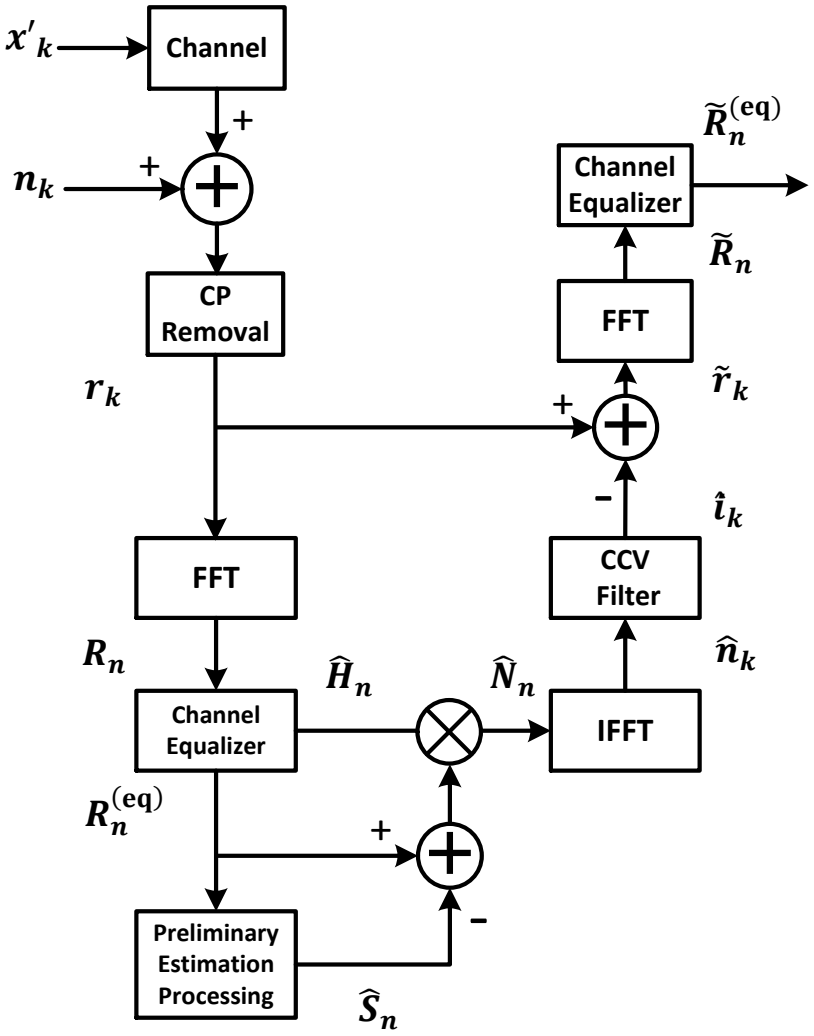

Figure 2.2 Diagram of the OFDM receiver with the CCV filter

In the time domain, the occurrence probability of the impulsive noise is fixed to 1% or 10 % as discussed in Section 2.2. The peak amplitude of the impulsive noise is decreased, in order to obtain a large SNR and the peak amplitude of the impulsive noise does not greatly differ from the transmitted signal. But compared with AWGN, the spike of the impulsive noise is assumed to be still detectable and in this case, we attempt to obtain the estimated total noise and then proceed with impulsive noise removal.

In order to mitigate the impact of the impulsive noise, a composite comparison value (CCV) algorithm is proposed to estimate $\hat{\imath}_k$ from $\hat{n}_k$. Initially, the estimated noise $\hat{n}_k$ is randomly sampled at the sampling rate $Q = (M/N) \times 100\%$, where M is the number of sampling positions and N is the number of the elements of the estimated noise $\hat{n}$ in the time domain, where $\hat{n} = [\hat{n}_0, \hat{n}_1, \ldots \hat{n}_k, \ldots, \hat{n}_{N-1}]$. A sampling sequence $s = [s_0, s_1, \ldots, s_m, \ldots, s_{M-1}]$ is then obtained, where $0 \leq m \leq M-1$ and $s \subset \hat{n}$. This process is shown in Figure 2.3.

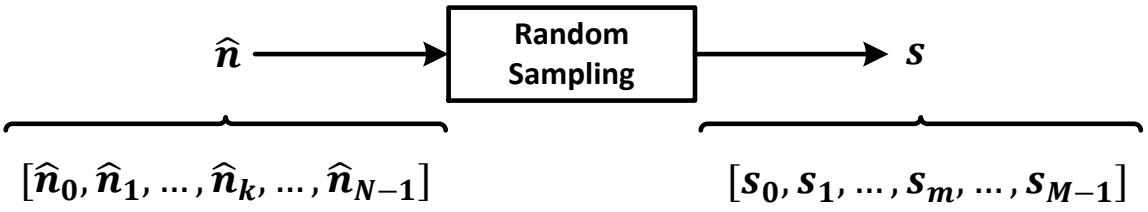

Figure 2.3 The random sampling process

Since $s \subset \hat{n}$, a sampling position locator (ρ, m) can be defined for the estimated noise $\hat{n}_k$ as

$$\hat{n}_{(\rho,m)} = s_m. \tag{2.12}$$

This is illustrated in Figure 2.4.

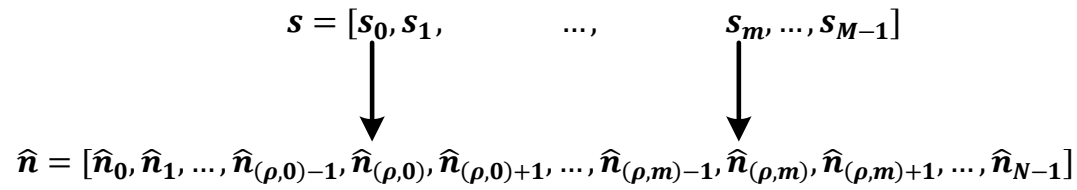

Figure 2.4 Illustration of the sampling position locator

A windowing process is then applied on every sampling position $\hat{n}_{(\rho,m)}$ of the estimated noise sequence $\hat{n}$. Figure 2.5 illustrates this process.

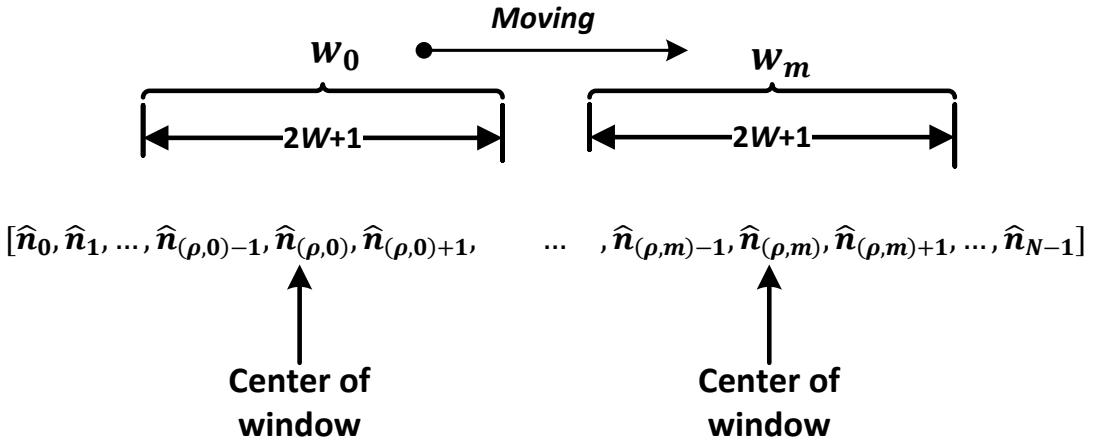

Figure 2.5 The windowing process

For each sampling position $\hat{n}_{(\rho,m)}$, the respective window w_m contains the following elements:

$$w_m = [\hat{n}_{(\rho,m)-W}, \hat{n}_{(\rho,m)-W+1}, \ldots, \hat{n}_{(\rho,m)}, \ldots, \hat{n}_{(\rho,m)+W-1}, \hat{n}_{(\rho,m)+W}], \qquad (2.13)$$

where w_m is the window on the estimated noise $\hat{n}_k$ and the width of w_m is $2W + 1$. Now the CCV λ_m is defined as

$$\lambda_m = \frac{\max|w_m| - \min|w_m|}{\text{mean}|w_m|}, \tag{2.14}$$

where max indicates the maximum value, min indicates minimum value, mean indicates the mean value, and $|\cdot|$ indicates the absolute value. Hence, after applying the window on all sampling positions, another mean value $\bar{\lambda}$ is obtained,

$$\bar{\lambda} = \frac{\sum_{m=0}^{M-1} \lambda_m}{M}. \tag{2.15}$$

Now the windowing process is applied on every element of the estimated noise $\hat{n}_k$ to obtain the window $\grave{w}_k$ for each element, that is,

$$\grave{w}_k = [\hat{n}_{k-W}, \hat{n}_{k-W+1}, \dots, \hat{n}_k, \dots, \hat{n}_{k-W-1}, \hat{n}_{k+W}]. \tag{2.16}$$

The CCV $\grave{\lambda}_k$ for every individual element of $\hat{n}_k$ is defined as

$$\grave{\lambda}_k = \frac{|\hat{n}_k| - \min|\grave{w}_k|}{\text{mean}|\grave{w}_k|}. \tag{2.17}$$

A proposed filtering process for impulsive noise removal is then defined as follows:

Step 1: If the absolute value of $\hat{n}_k$, which is also the center of the current window, is larger than the mean absolute value in the sampling sequence $s = [s_0, s_1, \dots, s_m, \dots, s_{M-1}]$:

$$|\hat{n}_k| \geq \text{mean}|s|, \tag{2.18}$$

the filtering process moves to **Step 2** for further analysis. Otherwise, the impulsive noise detection stops and the filtering process moves to the next data point $\hat{n}_{k+1}$.

Step 2: Once (2.18) is satisfied, the impulsive detection is triggered by considering the following condition:

$$\hat{\imath}_k = \begin{cases} \hat{n}_k, \text{if } \hat{\lambda}_k \geq \bar{\lambda} \\ 0, \text{ otherwise} \end{cases}, \tag{2.19}$$

where $\hat{\imath}_k$ is the representation of the impulsive noise obtained by the CCV filtering process. After this processing, the center signal of every window will be classified as either impulsive noise or not. Impulsive noise removal is then achieved as shown in Figure 2.2, that is,

$$\tilde{r}_k = r_k - \hat{\imath}_k, \tag{2.20}$$

where $\tilde{r}_k$ is the transmitted signal with the impulsive noise suppressed.

After the proposed impulsive noise filtering process, the received signal is processed by an FFT, that is

$$\tilde{R}_n = \text{FFT}(\tilde{r}_k), \tag{2.21}$$

where FFT$|\cdot|$ is the FFT operator. Finally with the processing of the equalizer, the received signal is represented as

$$\tilde{R}_n^{(\text{eq})} = \tilde{R}_n \hat{H}_n^{-1}. \tag{2.22}$$

In a low SNR environment with a fixed low occurrence probability of the impulsive noise, the peak amplitude of the impulsive noise in time domain is assumed to be much larger in comparison with the received signal r_k, and the impulsive noise generally results in a failure of the preliminary estimation processing discussed in Section 2.3.1. This is because the constellation arrangement of the QAM demodulation is incorrect due to the distortion introduced from the impulsive noise and results in additional errors in the estimation of the transmitted signal $\hat{S}_n$. As a result, the estimation of the total noise

component $\hat{n}_k$ is no longer accurate. To avoid this the CCV filter can be directly applied to the transmitted signal r_k rather than $\hat{n}_k$ and some BER improvement can be achieved. It should be noted, however, additional processing overhead is needed to assess the low SNR regime, possibly through power spectrum estimates from the OFDM receiver.

2.3.3 Application of the Reed-Solomon Decoding Process

In [28], it is found that RS code has the ability to correct burst errors. This is because RS decoder replaces the entire byte irrespective of the number of bits in error. In terms of $q - bit$ conventional RS(e, k) codes, where k is the number of data symbols and e is the number of code symbols of each coding block, that is,

$$(e, k) = (2^q - 1, 2^q - 2t - 1), \tag{2.23}$$

where t is the length of the correcting capability, thus $2t$ is the length of the parity symbols.

Now the impact of a random impulsive noise sequence on RS codeword is considered. As expected, the impulsive noise event will affect all OFDM subcarriers once processed by the FFT demodulation process, that is,

$$I_n = \text{FFT}(i_k) = \sum_{k=0}^{N-1} i_k \exp\left(-\text{j}\frac{2\pi nk}{N}\right), 0 \le n \le N - 1. \tag{2.24}$$

With the FFT representation of the impulsive noise in (2.24), the impact of a large impulsive noise error can exceed the error correcting capability of RS decoder. Therefore, one idea is to increase the accuracy of the decoding. More specifically, a traditional RS decoder employs syndromes to decrease the size of the dictionary which is used to determine the minimum Hamming distance [40]. Generally syndrome testing is defined as

$$\check{\mathrm{S}} = \check{\mathrm{R}}\check{\mathrm{H}}^T = \left(\check{\mathrm{C}} + \check{\mathrm{E}}\right)\check{\mathrm{H}}^T = \check{\mathrm{E}}\check{\mathrm{H}}^T = (\check{\mathrm{s}}_1, \check{\mathrm{s}}_2, \dots \check{\mathrm{s}}_{e-k}), \tag{2.25}$$

$$\check{\mathrm{H}}^T = \begin{bmatrix} \check{\mathrm{h}}_{1,1} & \cdots & \check{\mathrm{h}}_{1,e} \\ \vdots & \ddots & \vdots \\ \check{\mathrm{h}}_{e-k,1} & \cdots & \check{\mathrm{h}}_{e-k,e} \end{bmatrix}, \tag{2.26}$$

$$\check{\mathrm{E}} = (\check{\mathrm{e}}_1, \check{\mathrm{e}}_2, \dots \check{\mathrm{e}}_e), \tag{2.27}$$

where $\check{\mathrm{R}}$ is the received codeword, $\check{\mathrm{C}}$ is the original transmitted codeword, $\check{\mathrm{E}}$ is the error vector, and $\check{\mathrm{H}}^T$ is the transpose of the parity check. From (2.25), it is known that the syndrome only reflects the impact of error, irrespective of what the transmitted codeword is. To solve for the representation of $\check{\mathrm{E}}$, it is assumed that the codeword has t errors corresponding to the error correcting capability at locations $x^{f_1}, x^{f_2}, \dots, x^{f_t}$ with error value $y_{f_1}, y_{f_2}, \dots, y_{f_t}$. The error polynomial can be deduced as

$$\check{\mathrm{E}}(x) = y_{f_1}x^{f_1} + y_{f_2}x^{f_2} + \cdots + y_{f_t}x^{f_t}, \tag{2.28}$$

where the index f refers to the error location and $1,2, \dots, t$ refers to the first, second,…, tth error. In order to determine each location x^{f_l} and its error value y_{f_l}, where $l = 1,2, \dots, t$, an error location number is defined as $\varepsilon_l = a^{f_l}$, where α represents the basic elements of Galois Field. Next, a^c is substituted into the received polynomial, where $c = 1,2, \dots, 2t$. Then the $2t$ syndrome symbols are obtained:

$$\check{\mathrm{s}}_c = \check{\mathrm{R}}(a^c) = \sum_{l=1}^{t} y_{f_l}\varepsilon_l^c. \tag{2.29}$$

Hence the task is to find out the error value y_{f_l} and the location x^{f_l}. The error location polynomial $\Upsilon(x)$ is defined as

$$\begin{aligned} \Upsilon(x) &= (1 - \varepsilon_1 x)(1 - \varepsilon_2 x) \cdots (\varepsilon_t x) \\ &= \prod_{l=1}^{t} (1 - \varepsilon_l x) = \Upsilon_t x^t + \Upsilon_{t-1} x^{t-1} + \cdots \Upsilon_1 x + \Upsilon_0, \end{aligned} \tag{2.30}$$

where the solutions are $1/\varepsilon_1, 1/\varepsilon_2, \ldots 1/\varepsilon_t$, indicating the error locations $\varepsilon_1, \varepsilon_2, \ldots, \varepsilon_t$. In order to solve (2.30) with the given syndrome polynomial $\check{\mathrm{S}}$, the Berlekamp-Massey (BM) iterative algorithm is employed [43]. The BM algorithm is briefly summarized as follows. We define

$$\begin{cases} \check{\mathrm{S}}(x) = 1 + \check{\mathrm{s}}_1 x + \check{\mathrm{s}}_2 x^2 + \cdots + \check{\mathrm{s}}_{2t} x^{2t} \\ \mathcal{w}(x) = \check{\mathrm{S}}(x)\Upsilon(x) \\ \qquad = 1 + (\check{\mathrm{s}}_1 + \Upsilon_1)x + (\check{\mathrm{s}}_2 + \check{\mathrm{s}}_1\Upsilon_1 + 2\Upsilon_2)x^2 + \cdots + (\check{\mathrm{s}}_t + \Upsilon_1 + \check{\mathrm{s}}_{t-2}\Upsilon_2 + \cdots + \Upsilon_t)x^t \\ \qquad = 1 + \mathcal{w}_1 x + \mathcal{w}_2 x^2 + \cdots + \mathcal{w}_t x^t \end{cases}. \tag{2.31}$$

The key equation is obtained as

$$\check{\mathrm{S}}(x)\Upsilon(x) \equiv \mathcal{w}(x) \ (\mathrm{mod}\ x^{2t+1}), \tag{2.32}$$

where mod indicates a modulo division operation. For the BM iterative processing, a step-difference function d_j is employed, that is

$$\check{\mathrm{S}}(x)\Upsilon^{(j)}(x) \equiv (\mathcal{w}^{(j)}(x) + d_j x^{j+1}) \left(\mathrm{mod}\ x^{j+2}\right), \tag{2.33}$$

where j indicates the jth iteration.

Once the initial $d, \Upsilon(x), \mathcal{w}(x)$ are given, the iterations can be achieved as

$$\begin{cases} d_j = \check{\mathrm{s}}_{j+1} + \sum_{c=1}^{\partial \mathcal{w}^{(j)}(x)} \check{\mathrm{s}}_{j+1-c} \mathcal{w}_c{}^{(j)} \\ \Upsilon^{(j+1)}(x) = \begin{cases} \Upsilon^{(j)}(x) - d_j d_v^{-1} x^{j-v} \Upsilon^{(j)}(x), d_j \neq 0 \\ \Upsilon^{(j)}(x), d_j = 0 \end{cases} \\ \mathcal{w}^{(j+1)}(x) = \begin{cases} \mathcal{w}^{(j)}(x) - d_j d_v^{-1} x^{j-v} \mathcal{w}^{(j)}(x), d_j \neq 0 \\ \mathcal{w}^{(j)}(x), d_j = 0 \end{cases} \end{cases}, \tag{2.34}$$

where ∂ indicates a partial derivative operation, and v is corresponding to $\max(v - \partial\Upsilon^{(j)}(x))$.

The initial values are given as

$$\Upsilon^{(-1)}(x) = 1, \omega^{(-1)}(x) = 0, d_{-1} = 1, j = -1, \tag{2.35}$$

then we obtain

$$\Upsilon^{(0)}(x) = 1, \omega^{(0)}(x) = 1, d_0 = \check{s}_1, j = 0. \tag{2.36}$$

According to (2.34), the error location polynomial is obtained after $2t$ iterations:

$$\Upsilon(x) = \Upsilon^{(2t)}(x). \tag{2.37}$$

For (2.37), the Chien-search algorithm is employed to find the error locations with (2.30) [44]. With the RS encoder, we have

$$\varepsilon_{(z)}^{-1} = a^{-z}, \tag{2.38}$$

where $z = 0,1, \ldots, e$, and any $\varepsilon_{(z)}^{-1}$, satisfying the following condition

$$\Upsilon(x) = \Upsilon^{(2t)}(x) = \Upsilon\left(\varepsilon_{(z)}^{-1}\right) = 0, \tag{2.39}$$

is recorded as the error location number:

$$\varepsilon_l = \varepsilon_{(z)}. \tag{2.40}$$

The error value is then evaluated by the Forney Algorithm [45]:

$$y_{f_l} = -\frac{\omega\left(\varepsilon_l^{-1}\right)}{\Upsilon'\left(\varepsilon_l^{-1}\right)}, \tag{2.41}$$

where ′ indicates a derivative operation. Once the error polynomial $\check{E}(x)$ is obtained, decoding with error correction then follows.

2.4 Simulation Results

For our OFDM simulations using MATLAB, a $276k$ random bits baseband signal is transmitted via 200 subcarriers and a 512-point FFT/IFFT process. 16-QAM is used for baseband modulation and RS coding is added to provide additional impulsive noise resistance. A conventional bit-mapping arrangement for the 16-QAM symbol-to-voltage

conversion process was used and is shown in Table 2.1. Block interleaving then follows to provide additional channel robustness. At the receiver, the de-interleaver operates in reverse to arrange the encoded symbols in the original sequence. Since the effect of the impulsive noise on OFDM systems is the focus of this research, in order to lessen the impact of AWGN, the signal-to-AWGN ratio (SAR) is fixed to 20 dB, that is

$$SAR = 10\log_{10}\frac{\sum_{k=0}^{N-1} x'^{2}_{k}}{\sum_{k=0}^{N-1} w_k^2}, \tag{2.42}$$

and the impulsive noise amplitude was varied to achieve the desired SNR for all the following simulations. For the CCV filter, experimental results indicate that a reasonable sampling rate, Q, and window width, $2W+1$, are 10% and 41, respectively. The structure of our simulation tests is shown in Figure 2.1.

Table 2.1 The arrangement of 16-QAM Bit-mapping

Baseband bit block	I channel	Q channel
00	-3	-3
01	-1	-1
10	+1	+1
11	+3	+3

With the above configuration, several simulations with various probabilities of impulsive noise occurrence and RS code rates were performed to demonstrate the performance of the CCV filter with our practical RS decoding scheme.

2.4.1 Case 1: $p = 1\%$; $e = 15, k = 3$

The settings are arranged as follows for Case 1. The probability of the impulsive noise events occurrence is fixed to 1%. The length of the RS redundancy is fixed to 12 given the assumed impulsive noise characteristics. In order to limit the overhead of the RS coding process, the length of the codeword is fixed to a reasonable value of 15. Therefore the length of the data symbol is 3 and for RS$(15, k)$, every symbol contains 4 bits.

In the first simulation, the advantage of utilizing the CCV filter on the constellation of a 16-QAM demodulation process with 10 dB SNR is demonstrated. The differences between constellations of RS-OFDM with and without the CCV filter are shown in Figure 2.6. Clearly, the effectiveness of the CCV filter in improving the desired clustering of the QAM constellation points is seen.

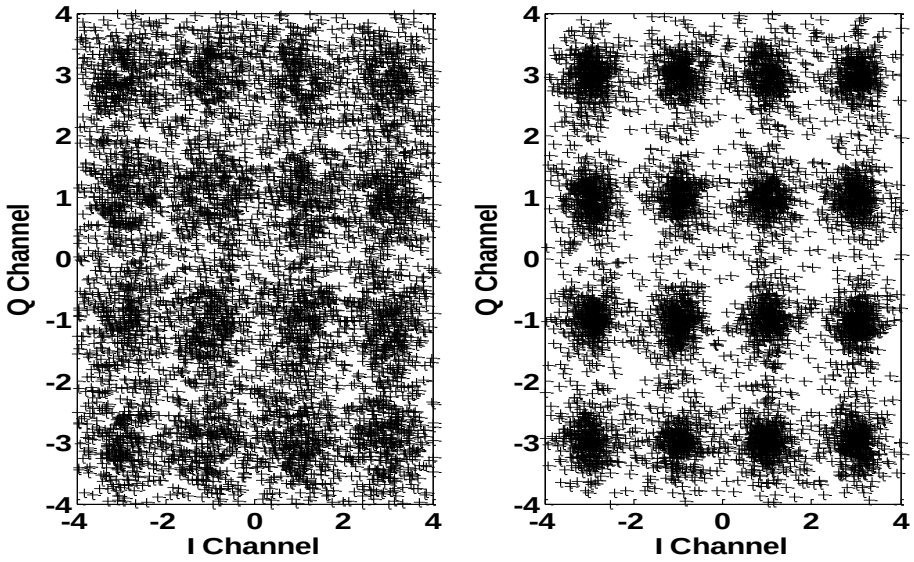

Figure 2.6 Left: constellation without the CCV filter; right: constellation with the CCV filter (SNR= 10 dB, $p = 1\%$)

In the second simulation, the BER performances of the conventional OFDM (OFDM), OFDM with VBF filter (VBF-OFDM) [24], OFDM with CCV filter (CCV-OFDM), RS-OFDM, and RS-OFDM with CCV filter (RSCCV-OFDM) are compared. The BER simulation results are shown in Figure 2.7. In these results the CCV-OFDM system shows an improved performance when compared to the VBF-OFDM system. As one can see, both the CCV filter and RS coding procedure improve the impulsive noise resistance of the OFDM system. Overall, the BER improvement of the proposed RSCCV-OFDM system is the largest when compared to all other methods.

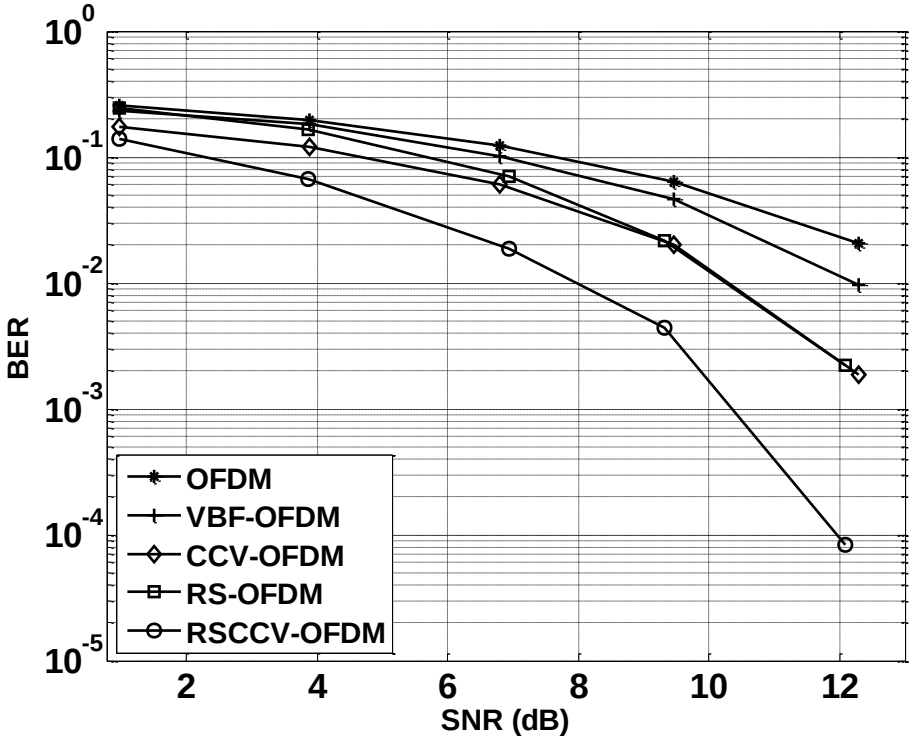

Figure 2.7 BER performances of the OFDM, VBF-OFDM, CCV-OFDM, RS-OFDM, and RSCCV-OFDM ($p = 1\%$)

2.4.2 Case 2: $p = 10\%$; $e = 15, k = 3$

In Case 2, the simulation settings are: the probability of the impulsive noise events occurrence is fixed to 10%, the length of the codeword is fixed to 15, the length of the data symbol is 3. The simulation results are shown in Figure 2.8. It is seen that RS-OFDM has fairly good impulsive noise resistance and is close in performance to RSCCV-OFDM but the latter having consistently the best BER performance. Based on the simulations of Case 1 and 2, it is found that the overall processing time of RS-OFDM utilizing CCV filter is approximately 6 times than the RS-OFDM without CCV filter. With specialized hardware, it is anticipated that this additional computational overhead can be significantly reduced.

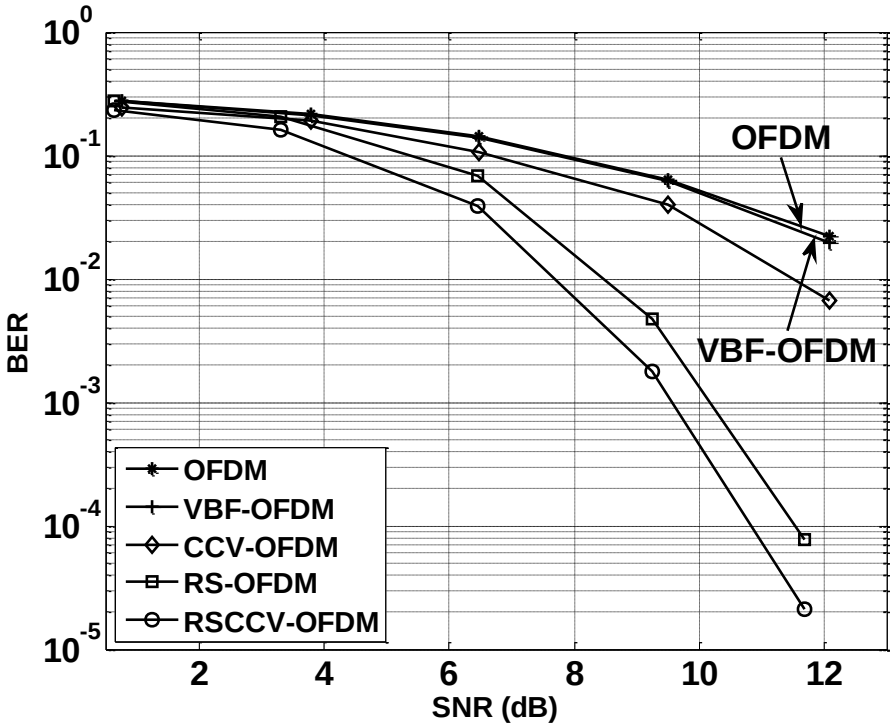

Figure 2.8 BER performances of the OFDM, VBF-OFDM, CCV-OFDM, RS-OFDM, and RSCCV-OFDM ($p = 10\%$)

2.4.3 Case 3: $p = 1\%$; $e = 15, k = 3, 5, 7, 9, 11$

In this case, the simulation settings are: the probability of the impulsive noise events occurrence is fixed to 1%, the length of the codeword is fixed to 15, the length of the data symbol is varying from 3 to 11.

Theoretically, if a coding scheme attempts to mitigate the effects of impulsive noise, the noise duration has to be only a small percentage of the codeword [28]. Therefore an increased size of the code block should enhance the error correcting capability but with the trade-off of more processing overhead. In this simulation, the BER performance of the RSCCV-OFDM with various RS redundancies is illustrated in Figure 2.9. As one can see, the results match theoretical expectations with the rate $3/15$ code yielding the best performance.

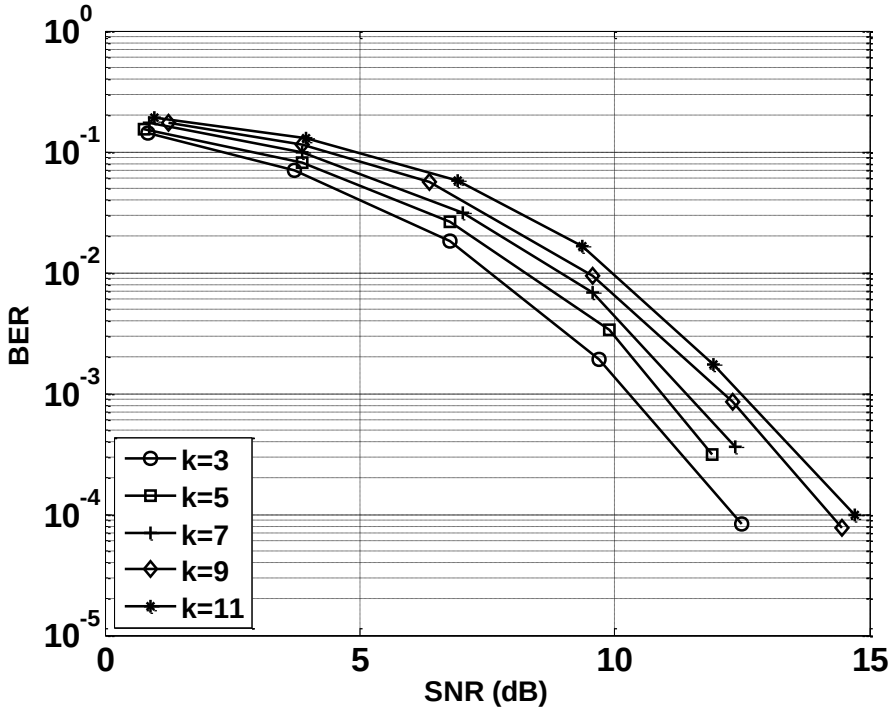

Figure 2.9 BER performance of the RSCCV-OFDM with various RS redundancies ($p = 1\%$)

2.4.4 Case 4: Multipath Channel: $p = 1\%$; $e = 15, k = 3$

In case 4, the simulation settings are arranged as follows. The probability of the impulsive noise events occurrence is fixed to 1%, the length of the codeword is fixed to 15, the length of the data symbol is 3. To facilitate a more realistic channel model, a time-invariant 7-path frequency-selective channel was utilized as an example to evaluate the performance of the proposed impulsive noise suppression algorithm. The resulting channel frequency response is shown in Figure 2.10. Although more difficult channel models could have been utilized, this example of a frequency-selective channel should suffice given our study focuses on point-to-point transceivers.

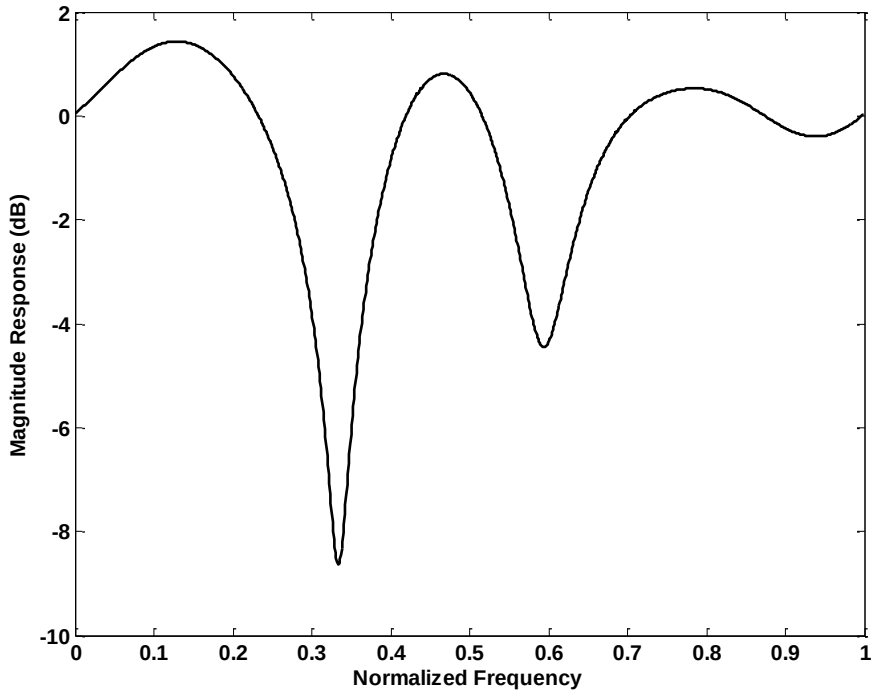

Figure 2.10 Multipath channel response

The BER and the symbol error rate (SER) are shown in Figure 2.11 and 2.12, respectively. From Figure 2.11, it can be seen that, to achieve the same bit error condition, CCV-OFDM obtains an average 9 dB and 6 dB SNR improvement when compared to OFDM and VBF-OFDM, respectively; RSCCV-OFDM also obtains a significant SNR improvement when compared to RS-OFDM. The system SER shows similar results.

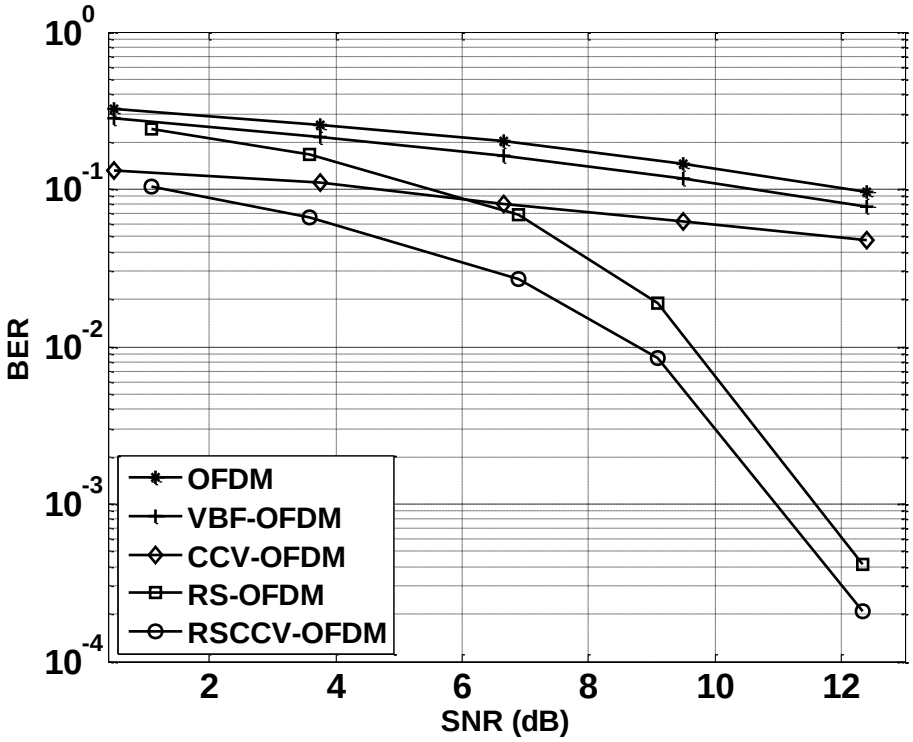

Figure 2.11 BER performances of the OFDM, VBF-OFDM, CCV-OFDM, RS-OFDM, and RSCCV-OFDM in a multipath channel

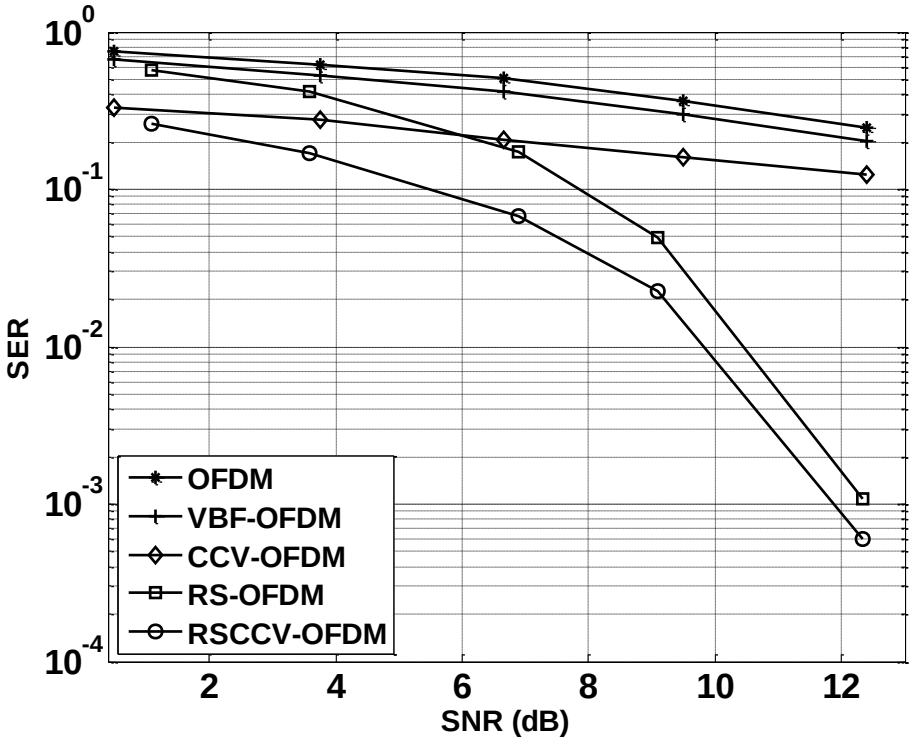

Figure 2.12 SER performances of the OFDM, VBF-OFDM, CCV-OFDM, RS-OFDM, and RSCCV-OFDM in a multipath channel

2.5 Conclusion

In this chapter, the dual protection scheme utilizing CCV filter and RS coding is proposed in order to mitigate the effect of impulsive noise in OFDM systems. The CCV pre-processing filter and practical RS decoding process with the frequency domain noise estimation are theoretically analyzed and confirmed through simulation. In comparison to other existing impulsive noise suppression algorithms, the proposed RSCCV-OFDM provides good resistance of impulsive noise and provides for additional performance gains over previously proposed methods. Numerous environmental regimes were tested including changes in impulsive noise rate and SNR.

Chapter 3 Impulsive Noise Resistance of 915 MHz and 2.4 GHz Band ZigBee Communication Systems

3.1 Introduction

The monitoring of electricity substation components is a critical task for substation operation as unnoticed equipment failure can create a safety hazard and/or be costly if pre-emptive measures are not taken. To facilitate the successful management of equipment faults, especially in high voltage systems, an efficient real time monitoring and communication system is required [46, 47]. In this regard, the wireless sensor network (WSN) allows for a flexible and cost-effective deployment in comparison to wireline sensor-based systems [48, 49]. Although a number of wireless technology candidates, such as WiFi, Bluetooth, DigiMesh, have been suggested for low-cost sensor nodes, the ZigBee standard draws significant attention from the electricity power industry, due to its open platform, low-power consumption, and security considerations [9, 50-52]. In this hazardous environment, a ZigBee-based WSN is also useful to achieve various industrial automations and helps to avoid potential bodily danger which improves industry efficiency [9].

However, when a ZigBee WSN is deployed under such difficult electromagnetic circumstances, as with many other wireless communication technologies, it can suffer from various noise difficulties such as the influence of AWGN and impulsive noise generated by high power electric devices. Particularly in a heavy power utility environment, impulsive noise is a common phenomenon [53]. Two main sources of

impulsive noise in substations are generally identified as partial discharge (PD) caused by deteriorated insulation and sferic radiation distortion from switching shock [46]. Furthermore, reviews of previous research indicate the relationship between an impulsive noise model and PD events [46, 54, 55]. It has been reported that PD impulsive noise may be the major source of external noise interference for wireless communication systems [48]. Recent research also reveals that impulsive noise occurring in electricity substations can degrade the performance of ZigBee systems [9, 46, 48]. In previous work, Gaouda compares the effect of high voltage noise, PD and impulsive events on the 2.4 GHz ZigBee band [9]. Numerical results of lost data packets are obtained from experiments which demonstrate the degraded system performance when the ZigBee nodes are close to impulsive faults. Also, Shan presented several laboratory results in the form of the byte error rate and BER for the 2.4 GHz band ZigBee band affected by impulsive noise [46]. In Bhatti's work, an impulsive noise model based on the symmetric α-stable distribution was proposed to evaluate the performance of ZigBee systems. Simulation results showed that when the power of impulsive noise is increased, the BER performance degradation of ZigBee systems is significant [48].

In this chapter, for the purpose of improving the deployment stability of ZigBee WSNs in high voltage electricity substations, an investigation of the performance of ZigBee systems in impulsive noise environments is described. Both the 915 MHz and 2.4 GHz band ZigBee systems utilize the DSSS baseband and O-QPSK modulation schemes with the corresponding carrier frequency and chip rate. Therefore, the noise performance of both of these ZigBee systems is evaluated in this chapter. Furthermore, to assess the impulsive noise performance of 915 MHz band and 2.4 GHz band ZigBee with computer

simulations, a novel PD impulsive noise model based on the statistical characteristics obtained from electricity substations is proposed [55]. Both theoretical and simulation results show the 2.4 GHz band ZigBee is less sensitive to PD impulsive noise in electricity substations, but it may be advantageous to deploy 915 MHz ZigBee if PD detection and concurrent telemetry data collection are desired.

The rest of this chapter is organized as follows. In Section 3.2, the theoretical noise performance of the DSSS coding modulation utilized in ZigBee systems is analyzed. Section 3.3 describes a novel model of PD impulsive noise based on the statistical results from previous research [55]. Finally, in Section 3.4, numerical simulation results are presented and the impact of PD impulsive noise on ZigBee systems operating at 915MHz and 2.4 GHz bands is discussed.

3.2 Noise Performance of the Coding Modulation in ZigBee Systems

The 915 MHz and 2.4 GHz bands on the PHY layer are part of the industrial, medical service, and science research bands. The 915 MHz band is used in North America and the 2.4 GHz band is accepted worldwide [56]. Therefore, our research will focus on these two bands of operation. General PHY specifications defined by IEEE 802.15.4 standard for the two bands are summarized in Table 1.1. As previously described in Chapter 1, the spreading mode for both frequency bands is DSSS while the modulation method for both frequency bands is O-QPSK.

According to coding theory, the length of the redundancy r, length of the data symbol k, and the correcting capacity t must meet the Plotkin bound [57]:

$$t \leq \frac{1}{2}\left(\frac{(r+k)\times 2^{k}}{2^{k}-1} - 1\right) . \tag{3.1}$$

With the same k, a greater r yields a greater correcting capacity t. For the DSSS coded ZigBee systems, the spreading gain $\text{Gain}_{\text{ZigBee}}$ is defined as

$$\text{Gain}_{\text{ZigBee}} = 10\log_{10}\frac{R_c}{R_b} = 10\log_{10}\frac{r+k}{k} \ , \tag{3.2}$$

where R_c is the chip rate and R_b is the bit rate respectively. Specifically, both the 2.4 GHz and 915 MHz ZigBee bands have the same k corresponding to the symbol length [58].

In O-QPSK systems, the channel bit error probability p_c is represented as

$$p_c = Q\left(\sqrt{\frac{2E_c}{N_0}}\right), \tag{3.3}$$

where E_c is the coded bit energy and N_0 is the noise power spectral density respectively [28]. Additionally, $Q(x)$ is the complementary error function (Q-function) defined as

$$Q(x) \approx \frac{1}{x\sqrt{2\pi}}\exp\left(-\frac{x^2}{2}\right), \tag{3.4}$$

and it is monotonically decreasing. We have

$$\frac{E_c}{N_0} = \frac{S}{N_0 B} = \frac{S}{N_0 R}, \tag{3.5}$$

where S is the signal power, B is the coded bit bandwidth, N is the noise power, and R is the code-bit rate. The code-bit rate corresponds to the spreading gain $\text{Gain}_{\text{ZigBee}}$ of the DSSS modulation. Hence, (3.3) can be modified as:

$$p_c = Q\left(\sqrt{\frac{2S}{N_0 R}}\right). \tag{3.6}$$

For a coded system, the coded block error probability p_M is represented as

$$p_M = \sum_{j=t+1}^{n}\binom{n}{j}p_c^j(1-p_c)^{n-j} \ . \tag{3.7}$$

Therefore, considering (3.6) and (3.7), with the condition of the same $\frac{S}{N_0}$ and a small p_c, the higher code-bit rate system has the less block error probability p_M compared to a lower bit rate system. Theoretically, a 2.4 GHz band ZigBee system should outperform its 915 MHz counterpart in terms of the error correcting capability.

3.3 Modelling the Sequence of PD Impulsive Noise

As early discussed in Section 3.1, it has been found that the radiation of PD impulsive events can lower the reliability of ZigBee systems working in high voltage environments. In order to identify the characteristics of the PD impulsive noise, Shan proposed a two-stage approach, utilizing a collection of the measured data at the 400/275/132 kV substation [55]. Since the measured impulsive noise events may be of low amplitude given the proximity and sensitivity of the measurement equipment, the resulting impulsive noise may be buried in other non-impulsive noise. Thus, the first step was to obtain the de-noised impulsive noise events from the original measurements using the wavelet packet transformation. The second stage includes the extraction of impulsive noise features and an assessment of a series of statistical distributions such as impulse rate, impulse amplitude, and impulse rise times. The statistical results are summarized in Table 3.1 where LBH and HBH are the low and high band quasi-transverse electromagnetic horn antennas, respectively [55].

Table 3.1 The parameters of fitted distributions from the measured data

Process	Antenna	Distribution	Parameters	
Impulse rate	LBH	Generalized extreme value	μ	$8.9 \times 10^4 s^{-1}$
			σ	$3.02 \times 10^4 s^{-1}$
			k	3.77×10^{-1}
	HBH	Generalized extreme value	μ	$1.08 \times 10^5 s^{-1}$
			σ	$1.16 \times 10^4 s^{-1}$
			k	2.34×10^{-1}
Impulse amplitude	LBH	Gaussian	μ	$-7.57 \times 10^{-2} mV$
			σ^2	$5.19 \times 10^{-1} mV$
	HBH	Gaussian	μ	$-1.48 \times 10^{-1} mV$
			σ^2	$1.94 \times 10^{-1} mV$
Impulse rise time	LBH	T location-scale	μ	$1.13 \times 10^2 ns$
			σ	$3.51 \times 10^1 ns$
			ν	1.95×10^0
	HBH	T location-scale	μ	$9.67 \times 10^1 ns$
			σ	$2.68 \times 10^1 ns$
			ν	9.05×10^{-1}

3.3.1 Time Domain Model

Based on the above summary, a simplified model of the PD impulsive noise sequence is proposed: the duration of the impulsive event is not included and the impulsive event is considered as an individual Dirac delta pulse, that is

$$I[n+1] = \sum_{n=0}^{N-1} \left(\left((A_0 + \hat{g}) \cos(2\pi \hat{e} t - \acute{n}) \right) \delta \left(t - n/\hat{e} - \frac{\acute{n}}{2\pi \hat{e}} \right) - A_0 \right). \quad (3.8)$$

Equation (3.8) is subject to

$$\begin{cases} \hat{g} \in G(\mu_G, \sigma_G^2) \\ \hat{e} \in GEV(k_{GEV}, \sigma_{GEV}, \mu_{GEV}) \\ \acute{n} \in U(0, 2\pi) \\ \text{ŧ} \in T(\mu_T, \sigma_T, \nu) \\ A_0 \gg \sigma_G^2 \end{cases}, \quad (3.9)$$

where G is a Gaussian process with a mean of μ_G and variance of σ_G^2, GEV is a Generalized Extreme Value process with a shape parameter of k_{GEV}, scale parameter of σ_{GEV} and location parameter of μ_{GEV}, U is a uniform process within the range of 0 to 2π, T is a T Location-scale process with a location parameter of μ_T, scale parameter of σ_T and shape parameter of v, and A_0 is the amplitude of the carrier. All relevant distributions in (3.9) correspond to the contents of Table 3.1 [55]. Therefore, our proposed model can be considered as an impulse-train sampling process with an amplitude modulation (AM) process to set amplitude values. This model has the following properties:

1. According to Shan's research, the time-interval between each nearby pulse is approximately constant suggesting a single dominant source of the impulsive noise. Correspondingly, the periodic sampling process extracting the positive peaks from the AM modulated signal ensures the time interval between each nearby impulse is constant, and the sampling frequency ê corresponds to the GEV distribution of the impulse rate in Table 3.1.

In [55], the occurrence intervals of impulsive events are uniformly distributed. In this regard, the initial phase ń of the AM signal is uniformly distributed from 0 to 2π in every AM carrier period which results in the impulses extracted by the periodic sampling process occurring arbitrarily and results in the occurrence times being uniformly distributed, as desired.

2. With AM modulation, the modulating signal is a Gaussian process $G(\mu_G, {\sigma_G}^2)$, hence the set of all positive peaks of the AM modulated signal deducted by A_0 can be considered as the periodic sampling process on $G(\mu_G, \sigma_G^2)$. We define the set of the

sampling results from the process $G(\mu_G, \sigma_G^2)$ as $G_s = [v_0, v_2, \dots, v_{q-1}]$. Assuming a random variable $\psi \in G_s$, we have

$$\sum_{i=0}^{q-1} P(\psi|v_i) = 1. \tag{3.10}$$

The expectation of the sample mean $\tilde{\mu}$ of G_s is μ_G and the variance of the mean is equal to $\frac{\sigma_G^2}{q}$. The expectation of sample variance $\tilde{\sigma}^2$ of G_s is σ_G^2 and the corresponding variance is equal to $\frac{4\sigma_G^2}{q-1}$. When q is large enough, we can assume

$$\begin{cases} \tilde{\mu} \approx \mu_G \\ \tilde{\sigma}^2 \approx \sigma_G^2 \end{cases} . \tag{3.11}$$

In order to simplify the identification process of the probability distribution density (PDF) for G_s, we assume the average power of G_s is zero and the variance is normalized to 1, and thus we have

$$\sum_{i=0}^{q-1} P(\psi|v_i) v_i^2 = 1 . \tag{3.12}$$

The entropy $H(\psi)$ of ψ is

$$H(\psi) = -\sum_{i=0}^{q-1} P(\psi|v_i) \ln P(\psi|v_i) . \tag{3.13}$$

To maximize $H(\psi)$, we employ the Lagrange multiplier λ, and the Lagrange function is

$$\Lambda = H(\psi) + \lambda\left(\sum_{i=0}^{q-1} P(\psi|v_i) v_i^2 - 1\right) , \tag{3.14}$$

which is subject to (3.12). According to (3.13) and (3.14), we have

$$\begin{aligned} \Lambda &= -\sum_{i=0}^{q-1} P(\psi|v_i) \ln P(\psi|v_i) + \lambda\left(\sum_{i=0}^{q-1} P(\psi|v_i) v_i^2 - 1\right) \\ &= \sum_{i=0}^{q-1} \left\{\lambda P(\psi|v_i) v_i^2 - P(\psi|v_i) \ln P(\psi|v_i)\right\} - \lambda . \end{aligned} \tag{3.15}$$

The partial derivative is

$$\frac{\partial \Lambda}{\partial P(\psi|v_i)} = \lambda v_i^2 - \ln P(\psi|v_i) = 0 \, . \tag{3.16}$$

Hence, we have

$$P(\psi|v_i) = e^{\lambda v_i^2} < 1 \, . \tag{3.17}$$

According to the property of the function $f(k) = e^k$, we have

$$\lambda v_i^2 < 0 \;\Rightarrow\; \lambda < 0 \, , \tag{3.18}$$

and, finally, we have the conclusion

$$P(\psi|v_i) = e^{\lambda v_i^2}, \lambda < 0 \, . \tag{3.19}$$

Compared to the standard normal distribution

$$f(\chi) = e^{-\pi \chi^2}, \tag{3.20}$$

it is concluded that the PDF of the periodic sampling process to a Gaussian process is also Gaussian distributed. This verifies that for the model suggested in (3.8), the amplitude is Gaussian distributed with the approximate mean μ_G and variance σ_G^2, respectively.

3.3.2 Frequency Domain Model

The common characteristics of impulsive noise from high voltage faults are of short time duration and high-energy content yielding broadband-like noise of significant power spectral density (PSD) levels. From previous research, impulsive noise can be modeled by a simple sinc function [59, 60], which leads to an extension of our PD impulsive noise model in time domain. To analyze the frequency properties, the individual impulsive noise event i is considered as a normalized sinc function with the parameter f_i, that is

$$\begin{cases} i = \mathrm{sinc}(2f_i t) = \frac{\sin(2\pi f_i t)}{2\pi f_i t} \\ F(f) = \begin{cases} 1, & |f| \le f_i \\ 0, & |f| > f_i \end{cases} \end{cases}, \tag{3.21}$$

where $F(f)$ is the Fourier transform of the sinc function and various f_i represent different frequency properties.

According to the IEEE 802.15.4 standard, when considering the alternative channel rejection and the 20dB PSD decay frequency limit, the operation frequency range for 915 MHz and 2.4 GHz band ZigBee are 902.8-927.2 MHz and 2396.5 MHz-2488.5 MHz, respectively. Thus, the sinc-like impulsive noise affecting the 915 MHz and 2.4 GHz band ZigBee are represented as i_1 and i_2, respectively, that is

$$\begin{cases} i_1 = \mathrm{sinc}(2f_{i,1}t), & f_{i,1} \ge 902.8 \text{ MHz} \\ i_2 = \mathrm{sinc}(2f_{i,2}t), & f_{i,2} \ge 2396.5 \text{ MHz} \end{cases}. \tag{3.22}$$

The rise time $\mathfrak{t}_i$ of i is defined as

$$\mathfrak{t}_i = |T_s - T_e| \ , \tag{3.23}$$

where T_s and T_e correspond the 10% and 90% of the sinc maximum amplitude, respectively [55]. One example is illustrated in Figure 3.1. With (3.23) and (3.24), the rise times of the impulsive noise affecting the 915 MHz and 2.4 GHz ZigBee bands are obtained and represented as $\mathfrak{t}_{i,1}$ and $\mathfrak{t}_{i,2}$, respectively. Based on Shan's results in Table 3.1, the results of the cumulative distribution function (CDF) C_T for $\mathfrak{t}_{i,1}$ and $\mathfrak{t}_{i,2}$ are summarized in Table 3.2, where C_T is obtained by the PDF P_T of the process $T(\mu_T, \sigma_T, v)$, that is

$$C_T(\mu_T, \sigma_T, v) = \int_{t=0}^{\mathfrak{t}_i} P_T(\mu_T, \sigma_T, v) d\, t \ . \tag{3.24}$$

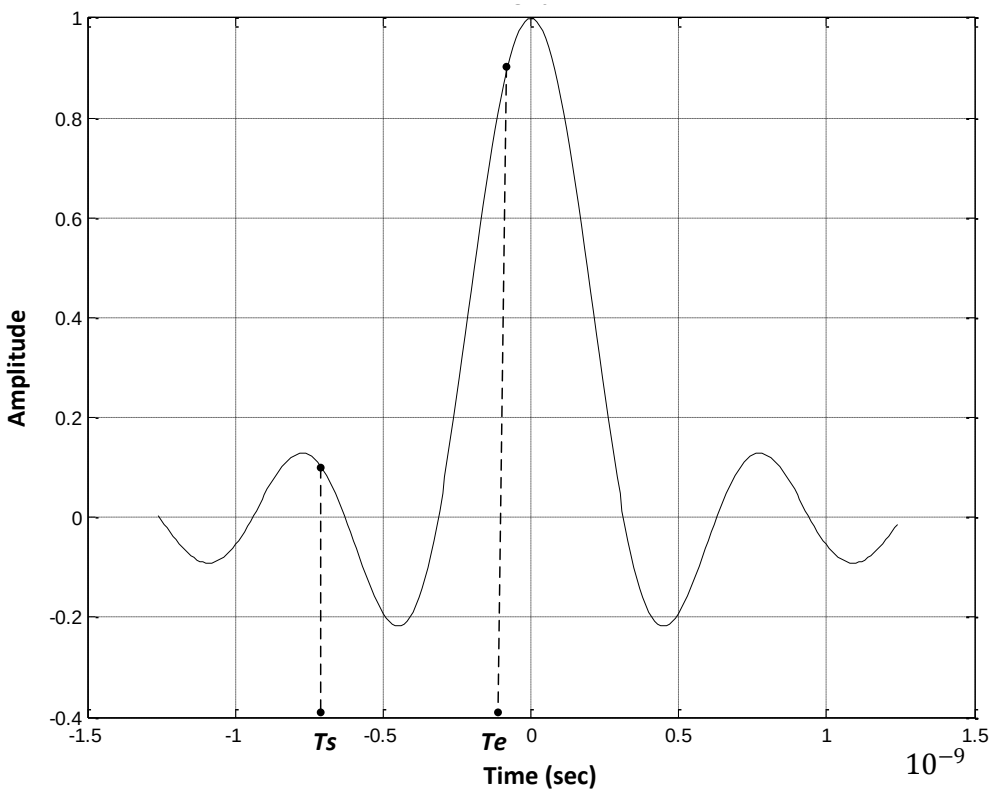

Figure 3.1 Illustration of the impulsive noise rise time

Table 3.2 The CDF of the rise time $t_{i,1}$ and $t_{i,2}$

Impulse rise time	$t_{i,1}$	$t_{i,2}$
CDF C_T	4.45%	0.426%

From this result, impulsive noise has a tenfold higher probability of impacting the 915 MHz band in comparison with the 2.4 GHz band.

3.4 Simulation

Based on our proposed model of the PD impulsive noise, numerical MATLAB simulations were performed. The simulation diagram of the PHY layer of both 915 MHz and 2.4 GHz ZigBee bands is shown in Figure 3.2. Detailed description of the ZigBee transmitter and receiver is given in Figure 1.3 and 1.4.

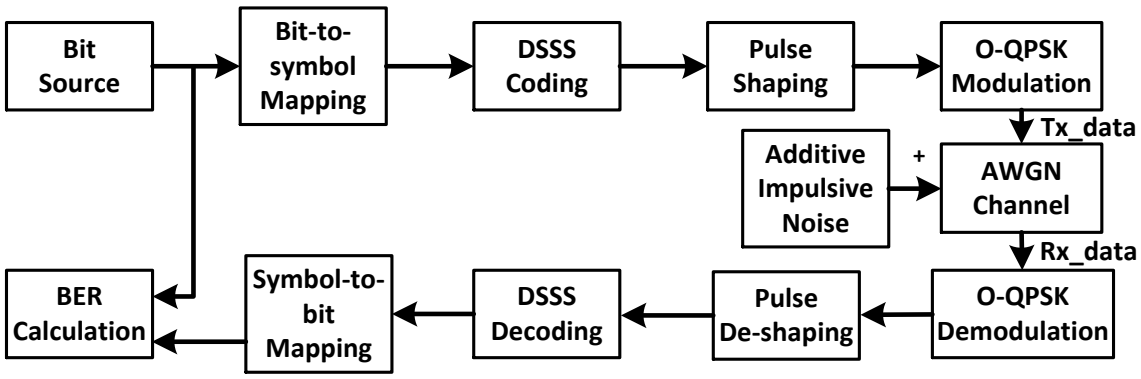

Figure 3.2 Diagram of the ZigBee system simulation

The simulation settings for both ZigBee bands are: the binary source generates 60000 bits; every 4 bits are converted into one symbol; the required DSSS and O-QPSK modulation with half-sine pulse shape follow the IEEE 802.15.4 standard; the SAR is fixed to 25dB for the AWGN channel; since the impulsive noise decays quickly with distance [55], the σ_G^2 in (3.9) is varied to achieve desired SNR. The BER result of 915 MHz and 2.4 GHz ZigBee bands is shown in Figure 3.3. This result shows the 2.4 GHz band outperforming the 915 MHz band, which is expected given the CDF results given in Table 3.2. It may be of interest, however, to utilize the poorer performance of the 915 MHz band for PD detection indicating a possible dielectric breakdown. One can envision

the deployment of 915 MHz sensor nodes for PD detection and concurrent telemetry data collection by those unaffected by impulsive noise. Additionally, with respect to the path loss of received signal power, the deployment of 915 MHz band ZigBee should obtain a better point-to-point communication distance when compared with the 2.4 GHz band given the same transmit power [28].

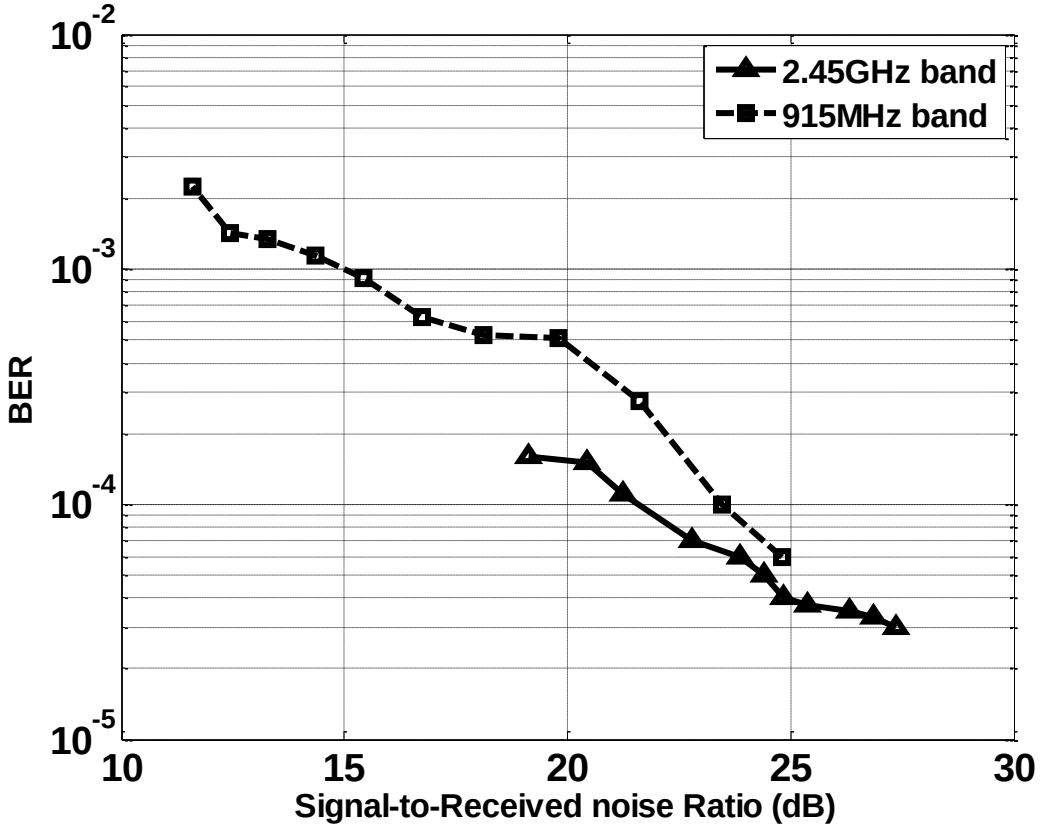

Figure 3.3 BER performances of 915 MHz and 2.4 GHz band ZigBee systems

3.5 Conclusion

In this chapter, an investigation of the performance of ZigBee systems at the 915 MHz and 2.4 GHz bands has been performed. A novel model of the PD impulsive noise sequence is proposed. The individual impulsive event is modeled by the sinc function for the frequency spectrum analysis and the influence of the sinc-like impulsive noise on ZigBee systems is assessed. In conclusion, simulation results verify the advantage of operating at 2.4 GHz over 915 MHz in harsh impulsive noise environments. However, this also points to the possible utilization of the 915 MHz band for the detection of close vicinity high voltage equipment failure (i.e. a high BER can indicate an equipment dielectric failure in close proximity to the sensor node) while allowing for concurrent telemetry data collection by unaffected sensor nodes.

Chapter 4 Time Domain Impulsive Noise Estimation and Mitigation for ZigBee Communication Systems

4.1 Introduction

In Chapter 3, the performance of 915 MHz and 2.4 GHz band ZigBee systems in an impulsive noise environment based on the measurements in electricity substations is assessed. Both theoretical and simulation results demonstrate the better impulsive noise resistance of the 2.4 GHz band ZigBee. Furthermore, as previously discussed, ZigBee-based WSNs have also been utilized in home automation, medical data collecting, and industrial monitoring due to its low power consumption and low cost characteristics [10, 12, 14]. However in these environments, impulsive noise events could also be generated by the power transmission lines, vehicle igniting, high voltage switching, and PD process [18-20]. Therefore, the deployment of 2.4 GHz band ZigBee WSNs in these scenarios is still challenged by the presence of impulsive noise. Therefore, in this chapter, we focus on improving the performance of the 2.4 GHz band ZigBee wireless communications in impulsive noise environments.

Impulsive noise mitigation has been previously addressed in the multicarrier communication systems and power-line communication systems [17, 61]. For DSSS-based communication systems, impulsive noise suppression schemes have also been previously proposed. In Lee's research, a robust data acquisition approach was proposed utilizing the median filter to mitigate impulsive noise in DSSS systems [62]. However, when the size of the filter window is decreased and the occurrence rate of impulsive noise

is increased, the performance of the impulsive noise detection deteriorates. Xu compared the performance of the passband clipping (PBC) and baseband clipping approaches for the impulsive noise rejection in DSSS systems [25]. Both simulation and experimental results demonstrated that the PBC outperformed the baseband clipping method. Silva developed a noise cancellation subsystem utilizing the Least Mean Square and Recursive Least Squares algorithm for Weiner Filtering [63]. The waveforms of filtered signal and unfiltered signal were compared to demonstrate the filter's performance in terms of noise rejection. However, the system resistance to AWGN was not considered in his research. According to Blackard's data collection, the measured amplitude of noise peaks could be several dB higher than various indoor wireless transmission signals located in the 918 MHz, 2.44 GHz, and 4 GHz license-free bands which cover the major operating bands of ZigBee WSNs [21]. With this in mind, an impulsive noise detection and filtering process utilizing the time domain characteristics of impulsive noise is proposed in this chapter.

The burst error correcting ability of the RS code was introduced and utilized for impulsive noise suppression in OFDM systems in previous chapters. In this chapter, the composite comparison value (CCV)-based filter is employed with time domain noise estimation and RS coding to detect and mitigate the impulsive noise in ZigBee systems. Numerical results show that the proposed impulsive noise suppression scheme improves the performance of 2.4 GHz band ZigBee systems. Furthermore, the performance of the proposed CCV filter with RS coding technique is compared with the conventional RS coding implemented alone in ZigBee systems. The comparison shows the advantage of our proposed CCV filter with RS coding for impulsive noise mitigation.

This chapter is organized as follows: in Section 4.2, the RS coded ZigBee (RS-ZigBee) system and the impulsive noise model are introduced, and in Section 4.3, the implementation of our composite comparison value-based filter with time domain noise estimation and RS coding is described in details. Simulation and numerical results are presented in Section 4.4.

4.2 ZigBee Systems with RS Coding and Impulsive Noise Model

In this chapter, improving the impulsive noise performance of 2.4 GHz band ZigBee systems is our focus since it was previously demonstrated that the 2.4 GHz band ZigBee has better impulsive noise resistance when compared with the 915 MHz band.

The burst error correction ability of the RS code is introduced in [28] indicating the RS decoder replaces the entire error-corrupted byte irrespective of the number of error bits. For an m-bit RS(c, l) code, where l is the number of data symbols to be coded and c is the number of code symbols of each coding block, the code form can be defined by

$$(c, l) = (2^m - 1, 2^m - 2t - 1), \tag{4.1}$$

where t is the length of the correcting capability; thus the length of the parity symbols is $2t$. In our system, the bit source of the signal to be transmitted is first RS coded before entering the ZigBee modulator and then is decoded at the receiver. The RS-ZigBee system with the proposed CCV filter is illustrated in Figure 4.1 where our proposed approach is inside the dotted line block.

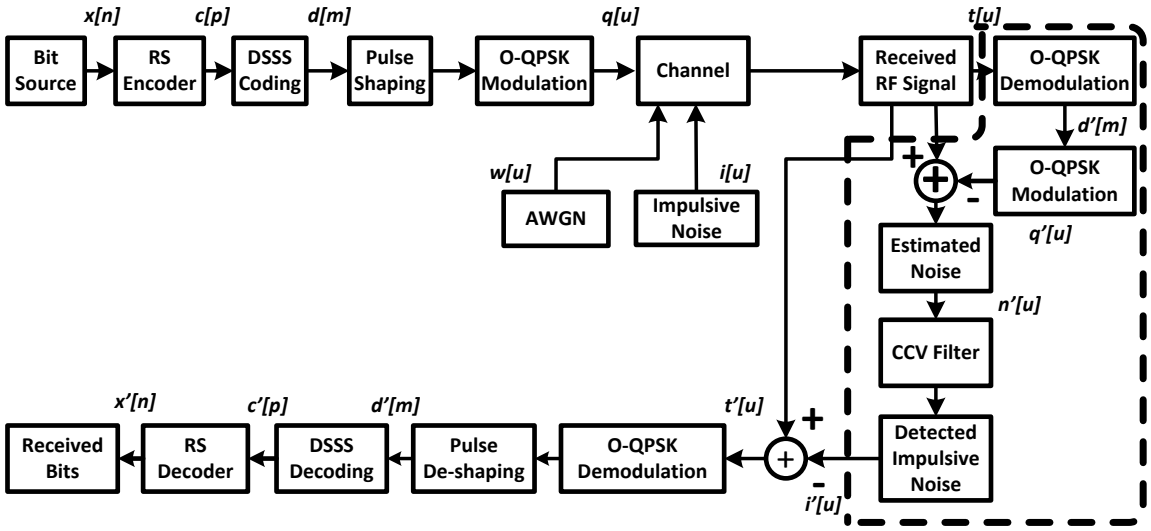

Figure 4.1 RS coded ZigBee system with the CCV filter

The impulsive noise in our research is represented by the following model referring to previous research [16]:

$$i[u] = b[u]g[u], \quad u = 0,1, \dots, N-1, \tag{4.2}$$

where N is the number of the noise sequence, u is the sequence index, and $g[u]$ indicates the Gaussian process that has zero mean and σ_g^2variance. $b[u]$ is a Bernoulli process that contains independently distributed zeros and ones. The ones in $b[u]$ indicate the occurrence of the impulsive noise event. The rate between the number of ones and the length of the noise sequence defines the occurrence rate p of the impulsive noise. The occurrence rate p and the variance parameters can be altered to facilitate noise strength. In this research, the occurrence rate is experimentally set to 1% and 5%, and the variance σ_g^2 is varied in order to achieve the desired SNR. The SNR is given by:

$$SNR = 10\log_{10}\frac{\sum_{u=0}^{N-1} q^2[u]}{\sum_{u=0}^{N-1} n^2[u]}, \tag{4.3}$$

where $q[u]$ is the transmitted signal. $n[u]$ is the entire channel noise component expressed by

$$n[u] = i[u] + w[u]\,, \tag{4.4}$$

where $w[u]$ is the AWGN in the channel. Assuming $i[u]$ and $w[u]$ are independent, substitution of (4.4) into (4.3) yields the identical result shown in (2.7).

4.3 The Proposed Filtering Scheme

In this section, our CCV time domain filter is proposed to provide an additional improvement to impulsive noise resistance of ZigBee systems. The noise filtering process is split into two stages: the first stage is the time domain noise estimation process followed by the second stage, the impulsive noise cancellation process. It should be noted that the channel response is considered to be ideal given that our focus is on noise effects only.

4.3.1 Noise Estimation

In Figure 4.1, the RF signal $T[u]$ is represented as:

$$t[u] = q[u] + w[u] + i[u], \;\; 0 \le u \le N-1, \tag{4.5}$$

where $q[u]$ is the output of the O-QPSK modulator. Our main goal is to detect and remove the impulsive noise component $i[u]$ from the received signal $t[u]$. To do this, we demodulate $q[u]$ and then re-modulate this result using the O-QPSK modulation to form

the estimation of $q[u]$, which is represented as $q'[u]$. Although errors in $q'[u]$ still exist, the re-modulation process enhances the ability to accurately estimate the impulsive noise amplitude and location with further processing. The total noise component estimation $n'[u]$ is then obtained as:

$$n'[u] = t[u] - q'[u]. \tag{4.6}$$

This term will then be processed to formulate an estimation of the impulsive noise component to be excised from the received signal.

4.3.2 Impulsive Noise Mitigation

As discussed in Section 4.2, the impulsive noise occurrence rate p is fixed to constant values, and the variance σ_g^2 is varied in order to obtain the desired SNR. In the case of a large SNR, the amplitude of impulsive noise does not greatly differ from the RF signal $q[u]$. Assuming a reasonable level of AWGN, the impulsive noise event is assumed to be still detectable. In this case, once the noise component $n'[u]$ is estimated as shown in (4.6), the CCV filtering process is performed on $n'[u]$ which attempts to detect and remove the impulsive noise component $i[u]$.

The CCV filtering process is previously introduced in Chapter 2 for impulsive noise suppression in OFDM systems. In this chapter, the application of the CCV filter in ZigBee systems is briefly described. With the random sampling process, the locator sequence which is used to obtain the mean CCV is generated from the estimated noise $n'[u]$ and denoted by $n'_\delta[f]$. For each locator in $n'_\delta[f]$, the corresponding CCV $V[f]$ can be obtained with the windowing process. After calculating the mean CCV $\bar{V}$ from the set of

$V[f]$, the CCV acquiring process for each $n'[u]$ is then performed. The resulting CCV corresponding to $n'[u]$ is represented as $V_{n'}[u]$. After $V_{n'}[u]$ and $\bar{V}$ are obtained, the impulsive noise detection scheme is given as follows:

Step 1: if $|n'[u]| < \text{mean}|n'_{\delta}[f]|$, $n'[u]$ is not considered as impulsive noise, and is recorded by marking $i'[u] = 0$, where $i'[u]$ is the estimated impulsive noise sequence. Otherwise, the detection process moves to **Step 2**.

Step 2: since in this step, $|n'[u]| \geq \text{mean}|n'_{\delta}[f]|$, $n'[u]$ is classified as either impulsive noise or not by the following condition:

$$i'[u] = \begin{cases} n'[u], & \text{if } V_{n'}[u] \geq \bar{V} \\ 0, & \text{otherwise} \end{cases}. \tag{4.7}$$

Hence, the estimation of the impulsive noise is completed and then removed from the received RF signal, that is,

$$t'[u] = t[u] - i'[u]. \tag{4.8}$$

Following the O-QPSK demodulation, pulse de-shaping, DSSS decoding and RS decoding, the received signal $x'[n]$ is obtained as shown in Figure 4.1.

Figure 4.2 shows an example of a received RF signal $T[u]$ with the noise condition of SNR=4 dB and impulsive noise occurrence rate $p = 5\%$. The estimation of the entire noise sequence with the corresponding CCV, the detected impulsive noise, and the impulsive noise added in the channel are illustrated in Figure 4.3, Figure 4.4, and Figure 4.5, respectively. As shown in Figure 4.4 the detected impulsive noise provides a reasonable facsimile to that shown in Figure 4.5 and thus BER improvements should be expected.

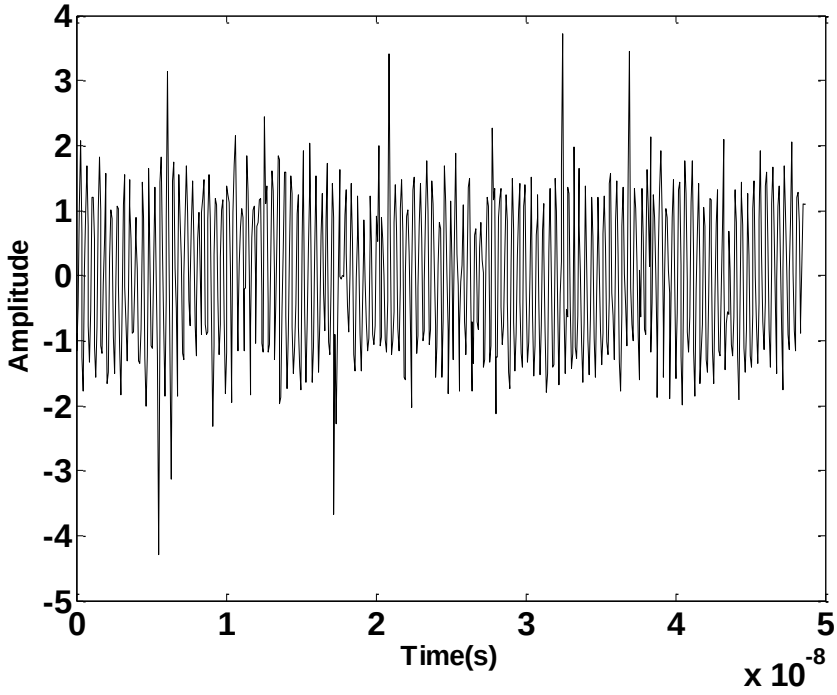

Figure 4.2 Received RF signal $T[u]$

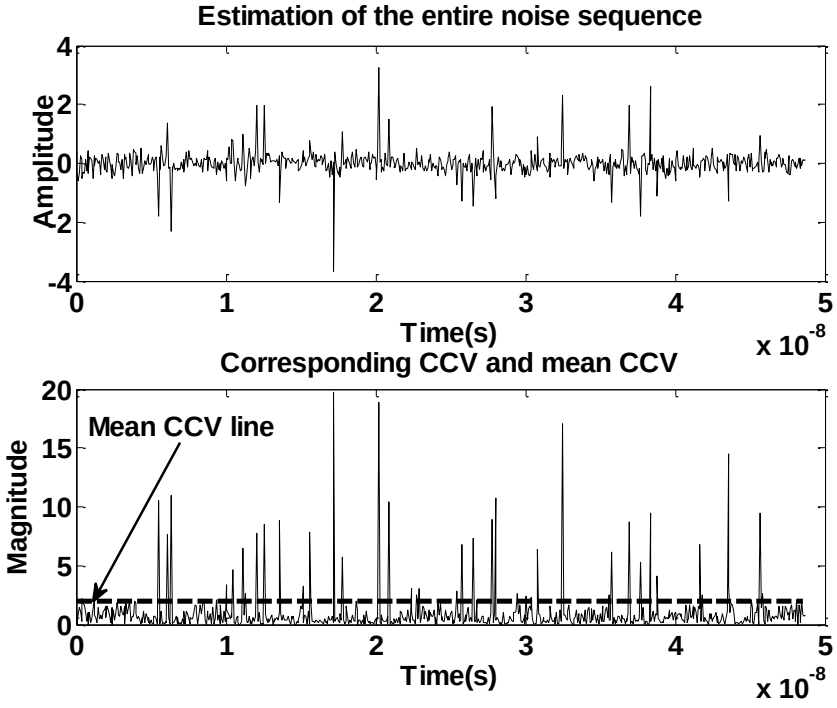

Figure 4.3 Estimation of the entire noise sequence $n'[u]$ and the corresponding CCV

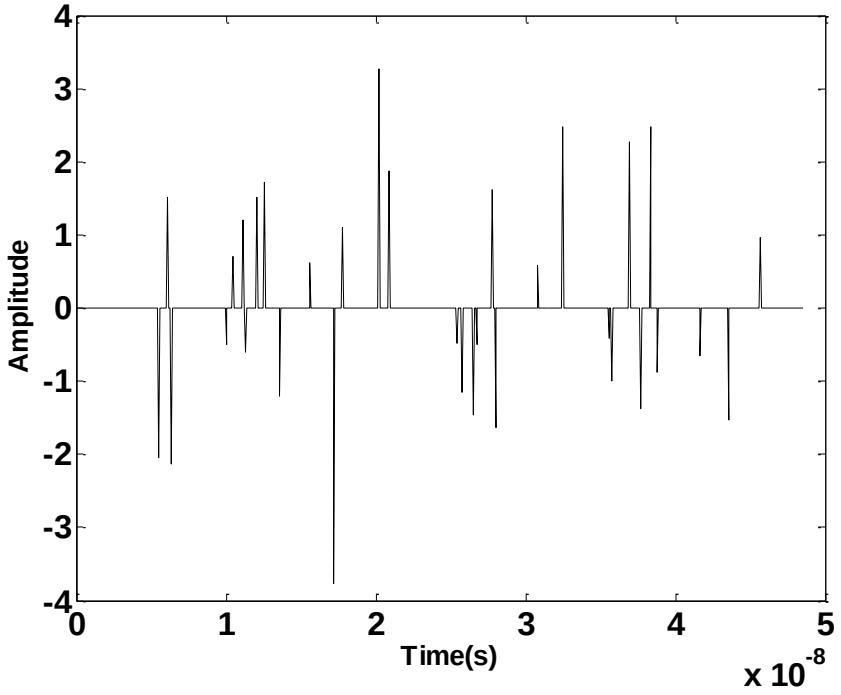

Figure 4.4 Detected impulsive noise $i'[u]$ by the CCV filter

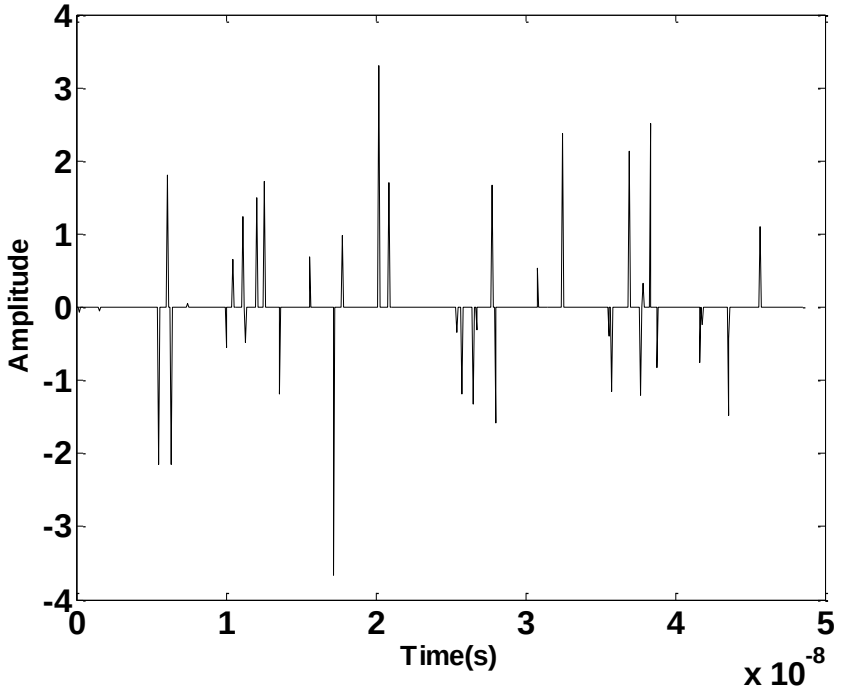

Figure 4.5 Impulsive noise $i[u]$ added in the channel

4.4 Numerical Results

In order to evaluate the performance of our proposed filtering system, several simulation tests were performed using MATLAB. The simulation diagram using the RS encoder and CCV filter is shown in Figure 4.1. The simulated ZigBee PHY follows IEEE 802.15.4 standard which comes with the symbol-to-chip mapping and 2.4 GHz carrier of the O-QPSK RF modulation. In these simulation results, a sequence of 15200 random bits is generated as the source of message which is represented as $x[n]$ in Figure 4.1. Also, since impulsive noise suppression is the primary focus of our work, the SAR is reasonably fixed to 10dB, and the impulsive noise variance σ_g^2 is varied to achieve the desired SNR. Two case studies are presented where the occurrence rate of the impulsive noise is varied from 1% to 5%. A (31, 19) RS encoder is employed which is experimentally corresponding to the assumed characteristics of additive channel noise component. Every four bits of $x[n]$ are converted into one integer symbol and every 19 symbols are grouped for the previously indicated RS coding process that follows. For our proposed CCV filter, based on the experimental results, the random sampling rate r and window width $2w + 1$ are reasonably set to 10% and 41, respectively.

Based on the above settings, the BER performances of the conventional ZigBee, RS-ZigBee, CCV filtered ZigBee (CCV-ZigBee), and RS-ZigBee with CCV filter (RSCCV-ZigBee) are compared. Two cases with an occurrence rate $p = 1\%$ and $p = 5\%$ are investigated, and the BER results are shown in Figure 4.6 and Figure 4.7, respectively. As one can see, with $p = 1\%$ and 5%, the performance of the RS coding is limited. With both occurrence rates, the CCV-ZigBee has better impulsive noise resistance compared to the conventional ZigBee system. Overall, the proposed RSCCV-ZigBee consistently has

the best noise performance when the system is interfered by the impulsive noise, even in a severe impulsive noise environment which is when $p = 5\%$.

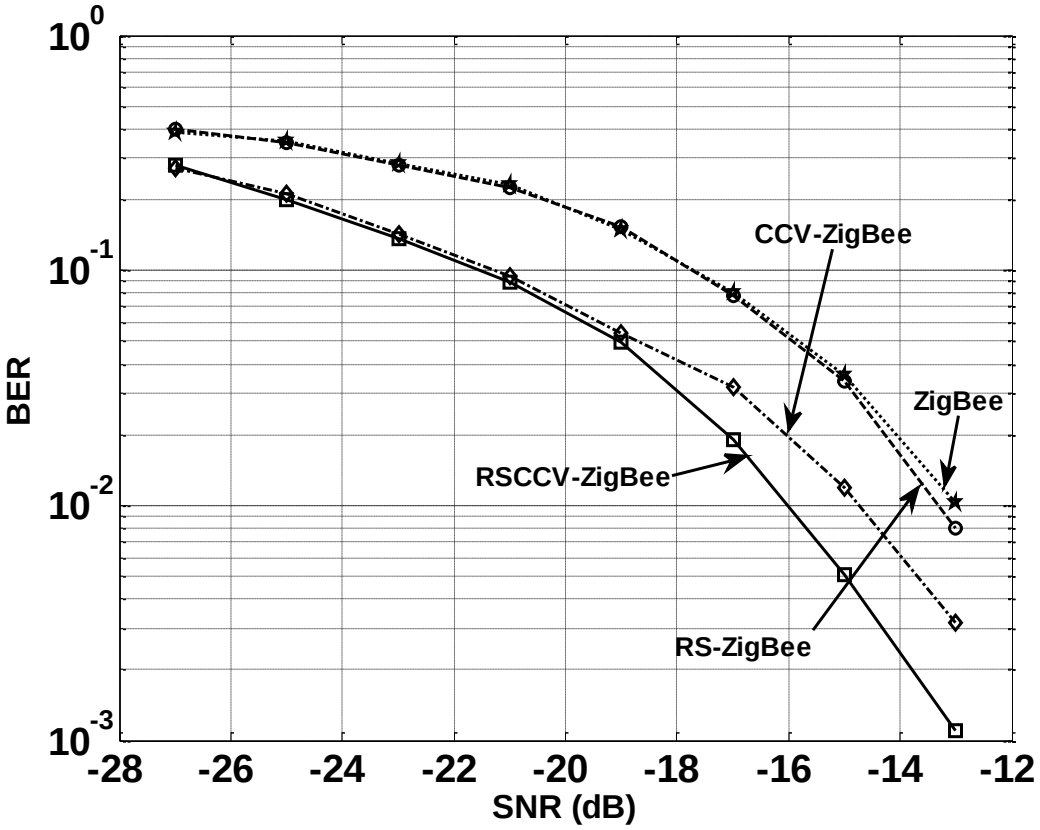

Figure 4.6 BER performances of the ZigBee, RS-ZigBee, CCV-ZigBee, and RSCCV-ZigBee ($p = 1\%$)

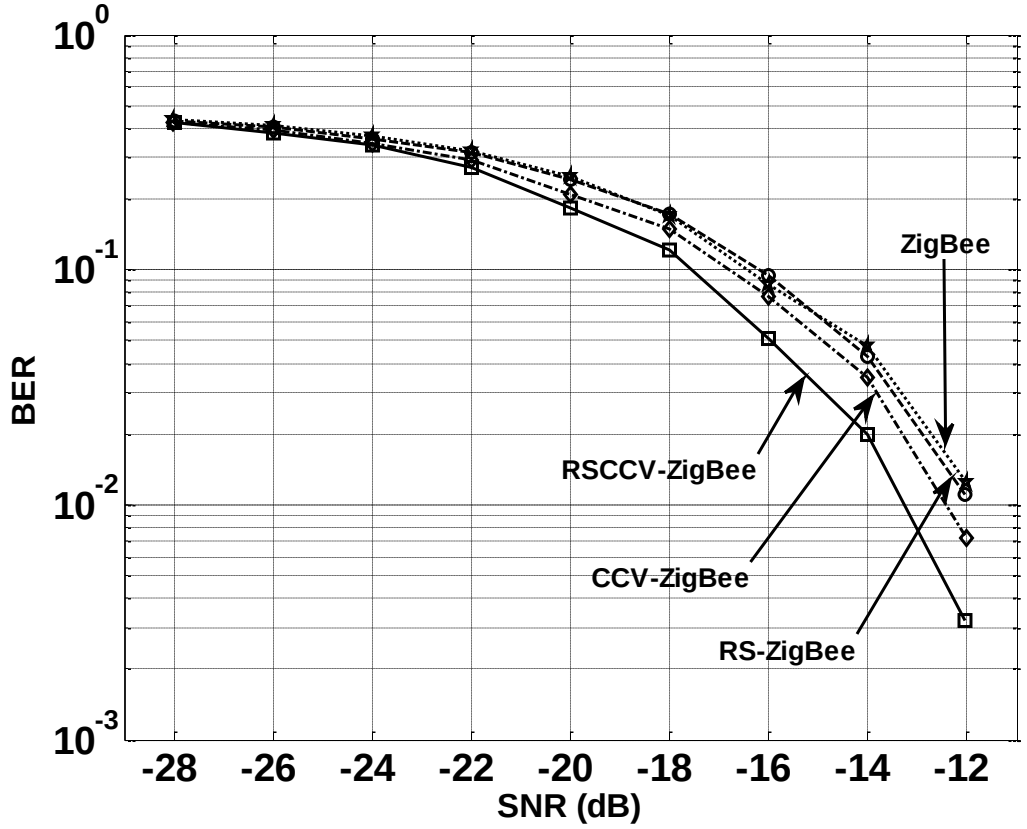

Figure 4.7 BER performances of the ZigBee, RS-ZigBee, CCV-ZigBee, and RSCCV-ZigBee ($p = 5\%$)

4.5 Conclusion

A RS coded ZigBee with the aid of the proposed CCV filter is described in this chapter for the impulsive noise suppression. The CCV filtering system focuses on the time domain characteristics of impulsive noise and includes two stages: time domain noise estimation and impulsive nose cancellation. Numerical simulations based on IEEE 802.15.4 standard were performed in order to evaluate the noise resistance of our proposed approach. Compared with the conventional ZigBee system and RS coded ZigBee system, RSCCV-ZigBee provides additional system performance gain with respect to BER vs. SNR.

Chapter 5 Impulsive Noise Rejection for ZigBee Communication Systems based on Frequency Multiresolution Analysis

5.1 Introduction

In Chapter 4, we propose a CCV filter-based impulsive noise suppression approach based on the time domain characteristics of impulsive noise. Another notable characteristic of impulsive noise is its wide band spectrum that can reach up to several GHz. Therefore, in this chapter, we focus on the frequency domain features of impulsive noise. From previous research work, impulsive noise was found to degrade the communication quality of ZigBee sensors due to its wide band spectrum and high-energy content within a short time duration [9, 48, 64]. It was shown that the impulsive noise contains significant energy at frequencies up to 3 GHz [22]. However, the latest report even indicated that the impulsive noise event can be found in frequencies up to 7 GHz [64]. This circumstance may cause notable spectrum distortion on ZigBee wireless transmission which is typically operated with carrier frequency of less than 2.5 GHz [31]. Therefore, in this chapter, we propose an impulsive noise rejection approach in frequency domain which improves the mean squared error (MSE) of the received ZigBee signal corrupted by impulsive noise.

In the frequency domain, Hussien managed channel interference, including AWGN, flicker noise, impulsive noise, 5MHz offset ADCI, and 10 MHz offset ALCI, using an LPF for a 2.4 GHz band ZigBee transceiver [27]. In this work, it was found that an increased LPF bandwidth allows more interference noise to be down converted into the

baseband, whereas a smaller bandwidth generates more distortion on the demodulated signal. That said a detailed analysis using a more formal approach for determining the LPF bandwidth was not presented.

Within our research scope, our primary focus is the impulsive noise rejection in 2.4 GHz band ZigBee systems, which have better impulsive noise resistance compared with the 915 MHz band. Due to the wide bandwidth nature of impulsive noise, a filter bandwidth improvement can be employed to remove the significant out-of-band spectrum content while balancing the residual effects of filter distortion. In this chapter, we first discuss the O-QPSK demodulation performance and the bandwidth/distortion trade-off of a pre-detection LPF used within the ZigBee receiver. A novel wavelet filtering-based scheme to limit the bandwidth of the O-QPSK demodulator output is also proposed for the purpose of improving the quality of the baseband decoding procedure and overall system BER performance.

The remainder of this chapter is described as follows. In Section 5.2, discussions on the characteristics of impulsive noise and its impact on ZigBee systems are described. In Section 5.3, the effect of the LPF introduced within the symbol detector is analyzed. Based on the bandwidth improvement analysis, our low pass Error-Balanced Wavelet (EB-Wavelet) filtering is proposed in Section 5.3. Finally, in Section 5.4, several simulations using MATLAB are presented.

5.2 Characteristics of Additive Impulsive Noise in ZigBee Systems

To ensure the quality of communication, IEEE 802.15.4 defines the required packet error rate (PER) as a maximum value of 1%. It is reported that severe impulsive noise

added in the channel can easily exceed this maximum PER and may even cause network termination [9].

5.2.1 Analysis of Impulsive Noise in ZigBee Systems

The system architectures of the 2.4 GHz band ZigBee transmitter and receiver are respectively illustrated in Figure 1.4 and 1.5 where both AWGN $w(t)$ and impulsive noise $i(t)$ are considered as the channel noise. However, as the impact of impulsive noise is our main focus, the power of $w(t)$ is fixed to a small level, and the power of $i(t)$ is varied in order to achieve various channel SNR scenarios.

To model the features of channel additive impulsive noise which include the extremely short event duration and high-energy component compared with conventional AWGN, the Bernoulli-Gaussian process is utilized in this research and is represented as:

$$i(t) = b(t) \cdot g(t) \,, \tag{5.1}$$

where $b(t)$ is a binary Bernoulli process and $g(t)$ is a zero-mean Gaussian process representing the random occurrence and amplitude of the impulsive noise event, respectively [16]. The PDF $f_B(b)$ of $b(t)$ is given as:

$$f_B(b) = \begin{cases} p, & \text{if } b = 1 \\ 1 - p, & \text{if } b = 0 \end{cases} . \tag{5.2}$$

When $b = 1$ an impulsive noise event has occurred, and therefore in this case, p is the occurrence rate of the impulsive noise.

For the rest of this chapter, $\mathrm{E}[\cdot]$ denotes the expectation operator and $\mathrm{Var}[\cdot]$ denotes the variance operator. The expectation and variance of $b(t)$ is obtained as:

$$\begin{cases} \mathrm{E}[b(t)] = 0 \cdot (1-p) + 1 \cdot p = p \\ \mathrm{E}[b^2(t)] = 0^2 \cdot (1-p) + 1^2 \cdot p = p \\ \sigma_b^2 = \mathrm{E}[b^2(t)] - \mathrm{E}^2[b(t)] = p(1-p) \end{cases}, \tag{5.3}$$

where σ_b^2 is the variance of $b(t)$. For $g(t)$, the expectation is given by $\mathrm{E}[g(t)] = 0$ and the variance is expressed by σ_g^2. Therefore for $i(t)$, we have

$$\mathrm{E}[i(t)] = \mathrm{E}[b(t)g(t)] = \mathrm{E}[b(t)]\mathrm{E}[g(t)] = p \cdot 0 = 0, \tag{5.4}$$

assuming $b(t)$ and $g(t)$ are independent. The variance σ_i^2 of $i(t)$ is then obtained as

$$\begin{aligned} \sigma_i^2 &= \mathrm{Var}[b(t)g(t)] = \mathrm{E}^2[g(t)]\sigma_b^2 + \mathrm{E}^2[b(t)]\sigma_g^2 + \sigma_b^2\sigma_g^2 \\ &= 0^2 \cdot p(1-p) + p^2\sigma_g^2 + p(1-p)\sigma_g^2 = p\sigma_g^2. \end{aligned} \tag{5.5}$$

$g(t)$ is assumed to be an AWGN process where the PSD is $S_g(f) = N_0/2$. The corresponding autocorrelation function is $R_g(\tau) = N_0\delta(\tau)/2$ where $\delta(\tau)$ is the Dirac Delta function. For a digital system with a sampling rate, f_s, the received power PW_g of $g(t)$ is assumed to be band-limited, that is,

$$\mathrm{PW}_g = \int_{-f_s/2}^{f_s/2} S_g(f)df = N_0 f_s/2 = \sigma_g^2. \tag{5.6}$$

Referring to (5.3), the autocorrelation function $R_b(\tau)$ and the power PW_b of $b(t)$ are represented as

$$\begin{cases} R_b(\tau) = \mathrm{E}[b(t)b(t-\tau)] = \begin{cases} p^2, \tau \neq 0 \\ p, \tau = 0 \end{cases}. \\ \mathrm{PW}_b = R_b(0) = p \end{cases} \tag{5.7}$$

Given $p < 1$, we can assume $p^2 \ll p$. According to the representation of $R_b(\tau)$ in (5.7), we can reasonably consider the PSD $S_b(f)$ of $b(t)$ to be approximately flat within the corresponding BW based on f_s. Therefore, $S_b(f)$ is calculated as

$$\begin{cases} \mathrm{PW}_b = p = \int_{-f_s/2}^{f_s/2} S_b(f)df = S_b(f)\, f_s \\ S_b(f) = p/f_s \end{cases}. \tag{5.8}$$

For $i(t)$, we have the autocorrelation $R_i(\tau)$ by

$$R_i(\tau) = \mathrm{E}[i(t)i(t-\tau)] = \mathrm{E}[b(t)g(t)b(t-\tau)g(t-\tau)]$$

$$= \mathrm{E}[b(t)b(t-\tau)]\mathrm{E}[g(t)g(t-\tau)] = R_b(\tau)R_g(\tau) = pN_0\delta(\tau)/2. \tag{5.9}$$

Thus the PSD $S_i(f)$ of $i(t)$ is

$$S_i(f) = pN_0/2. \tag{5.10}$$

Likewise the power PW_i of $i(t)$ is then expressed as

$$\mathrm{PW}_i = \int_{-f_s/2}^{f_s/2} S_i(f)df = pN_0f_s/2 = \sigma_i^2. \tag{5.11}$$

It can be seen from (5.11), PW_i is a function of p and N_0 given a fixed f_s. Varying N_0 and holding the occurrence rate p of the impulsive noise constant is one option to represent various levels of the impulsive noise power. Our research follows this arrangement to achieve various channel SNR conditions. As a reference for the following sections of this chapter, the characteristics of $b(t)$, $g(t)$ and $i(t)$ are summarized in Table 5.1.

Table 5.1 Characteristics of impulsive noise

	$\boldsymbol{b(t)}$	$\boldsymbol{g(t)}$	$\boldsymbol{i(t)}$
Expectation	p	$N_0f_s/2$	$pN_0f_s/2$
Variance	$p(1-p)$	$N_0f_s/2$	$pN_0f_s/2$
Autocorrelation	$\begin{cases} p^2, \tau \neq 0 \\ p, \tau = 0 \end{cases}$	$N_0\delta(\tau)/2$	$pN_0\delta(\tau)/2$
PSD	p/f_s	$N_0/2$	$pN_0/2$
Power	p	$N_0f_s/2$	$pN_0f_s/2$

5.2.2 Performance of ZigBee Systems with Impulsive Noise

As shown in Figure 1.4, $x_I(t)$ and $x_Q(t)$ are the polar nonreturn-to-zero (NRZ) signal transmitted in the in-phase and quadrature sub-channels, respectively. $x_I(t)$ and $x_Q(t)$ are then processed by the required pulse shaping and represented as $x_{I,s}(t)$ and $x_{Q,s}(t)$, respectively. Therefore, we have the RF modulated signal $y(t)$ as

$$y(t) = A_c\left(x_{I,s}(t)\cos 2\pi f_c + x_{Q,s}(t)\sin 2\pi f_c\right), \tag{5.12}$$

where A_c and f_c are the amplitude and frequency of the carrier, respectively. With the additive impulsive noise, $i(t)$, we have

$$r_i(t) = y(t) + i(t), \tag{5.13}$$

where $r_i(t)$ is the received signal interfered by $i(t)$. We assume the relevant coherent detection is without phase error distortion, and the demodulated sub-channel signal $z_a(t)$ and $z_b(t)$ processed by the pulse de-shaping fully pass the LPF with the 0 dB in-band gain. The received in-phase signal $z_I(t)$ shown in Figure 1.5 is then obtained as

$$z_I(t) = x_{I,A}(t) + i_{L,m}(t), \tag{5.14}$$

with

$$\begin{cases} x_{I,A}(t) = A_c x_I(t) \\ i_m(t) = 2i(t)\cos 2\pi f_c t \end{cases}, \tag{5.15}$$

and

$$i_{L,m}(t) = \text{LPF}|i_m(t)|, \tag{5.16}$$

where LPF$|\cdot|$ denotes the linear filtering process of the LPF with the cutoff frequency B_{LPF}.

The effect of the pulse de-shaping operated on $i_m(t)$ is ignored since the out-of-band component with the significant de-shaping gain is later removed by the LPF. Using (5.14), (5.15), and (5.16), the output D of the in-phase sub-channel integrator is

$$D = \int_0^{T_{\text{symbol}}} \left[x_{I,A}(t) + i_{L,m}(t)\right] dt = \pm A_c T_{\text{symbol}} + M, \tag{5.17}$$

where T_{symbol} is the O-QPSK symbol duration and

$$M = \int_0^{T_{\text{symbol}}} i_{L,m}(t)\, dt. \tag{5.18}$$

The PDF $f_I(i)$ of $i(t)$ is given as [16]

$$f_I(i) = \underbrace{(1-p)\delta(i)}_{\textbf{Term 1}} + \underbrace{p f_g(i)}_{\textbf{Term 2}}, \tag{5.19}$$

where $f_g(i)$ is

$$f_g(i) = \frac{1}{\sigma_g \sqrt{2\pi}} \exp[-\frac{i^2}{2\sigma_g^2}]. \tag{5.20}$$

It can be seen from (5.19), Term 1 describes the absence of the impulsive noise in $b(t)$ due to the property of $\delta(i)$, and Term 2 is Gaussian distributed with the factor p. Hence to evaluate the performance of O-QPSK, $i(t)$ can be approximated as a Gaussian process and the probability of error (PE) $P_{e,i,\text{OQPSK}}$ in the presence of LPF and $i(t)$ is derived in Appendix B and is represented as

$$P_{e,i,\text{OQPSK}} = Q\left(\frac{A_c T_{\text{symbol}}}{\sqrt{pN_0\left(T_{\text{symbol}} - \frac{\left(1-\cos 2\pi B_{\text{LPF}} T_{\text{symbol}}\right)}{2\pi B_{\text{LPF}}}\right)}}\right), \tag{5.21}$$

where $Q(\cdot)$ is the Q-function operator. Based on this analysis, the PE $P_{e,w,\text{OQPSK}}$ resulting from AWGN $w(t)$ can be simply expressed as

$$P_{e,w,\mathrm{OQPSK}} = Q\left(\frac{A_c T_{\mathrm{symbol}}}{\sqrt{N_{0,w}\left(T_{\mathrm{symbol}} - \frac{\left(1-\cos 2\pi B_{\mathrm{LPF}} T_{\mathrm{symbol}}\right)}{2\pi B_{\mathrm{LPF}}}\right)}}\right), \tag{5.22}$$

where $N_{0,w}/2$ is defined as the PSD of $w(t)$.

Given the received signal $r(t)$ expressed as

$$r(t) = y(t) + i(t) + w(t), \tag{5.23}$$

and since $i(t)$ and $w(t)$ are assumed to be independent, the system PE $P_{\mathrm{e,OQPSK}}$ is therefore given as

$$P_{e,\mathrm{OQPSK}} = P_{e,i,\mathrm{OQPSK}} + P_{e,w,\mathrm{OQPSK}}\,. \tag{5.24}$$

Assuming $i(t)$ is the dominant source of noise,

$$P_{e,\mathrm{OQPSK}} \approx P_{e,i,\mathrm{OQPSK}}\,. \tag{5.25}$$

With the DSSS decoding performed on $\vec{x}(t)$ in Figure 1.5, the system performance is improved by the error correcting ability of the chip-to-symbol conversion [65]. Given by IEEE 802.15.4, the maximum and minimum codeword distance for the 2.4 GHz band ZigBee PHY is 20 and 12, respectively, and by using a Maximum Likelihood decoding algorithm, the error correcting capability is 5 [28]. The PE of the DSSS decoding process is then obtained as

$$P_{e,\mathrm{DSSS}} = \sum_{i=6}^{32} \binom{32}{6} \left(1 - P_{e,\mathrm{OQPSK}}\right)^{32-i} P_{e,\mathrm{OQPSK}}^{i}\,, \tag{5.26}$$

where

$$\binom{j}{i} = \frac{j!}{i!(j-i)!}\,. \tag{5.27}$$

Given a small $P_{e,\mathrm{OQPSK}}$, $P_{e,\mathrm{DSSS}}$ can be approximately expressed using only the first term of the summation that is

$$P_{e,\mathrm{DSSS}} \approx \frac{32!}{6!26!}\left(1 - P_{e,\mathrm{OQPSK}}\right)^{26} P_{e,\mathrm{OQPSK}}^{6}\,. \tag{5.28}$$

Based on the maximum codeword distance, the BER result BER_{ZigBee} of the 2.4 GHz band ZigBee is represented as

$$\begin{aligned} BER_{\mathrm{ZigBee}} &\approx \frac{5 \times 32!}{8 \times 6!\,26!}\left(1 - P_{e,\mathrm{OQPSK}}\right)^{26} P_{e,\mathrm{OQPSK}}^{6} \\ &= 566370\left(1 - P_{e,\mathrm{OQPSK}}\right)^{26} P_{e,\mathrm{OQPSK}}^{6}\,. \end{aligned} \tag{5.29}$$

5.3 Improving the Performance of O-QPSK Demodulation

From (B.3), it can be seen that the variance $\sigma_{i_{L,m}}^2$ of $i_{L,m}(t)$ can be obtained as

$$\sigma_{i_{L,m}}^2 = \int_{-B_{\mathrm{LPF}}}^{B_{\mathrm{LPF}}} S_{i_{L,m}}(f)df = 2B_{\mathrm{LPF}}pN_0. \tag{5.30}$$

Considering (5.21), (5.25), (5.29), and (5.30), it is found that the noise-limiting B_{LPF} suppresses the power of $i_{L,m}(t)$ and can theoretically improve the BER performance. However, this result is based on the condition that the LPF balances filtering distortion on the demodulated baseband signal and its noise rejection properties. Excessively limiting B_{LPF} in order to limit noise will significantly distort the baseband signal in both of the parallel O-QPSK sub-channels. In this regard, the effects of this band limiting operation on the input signal prior to the demodulation integrator is described. This is followed by our proposed impulsive noise filtering scheme based on the multiresolution property of discrete wavelet transform to perform the needed low pass filtering operation.

5.3.1 Mean Squared Error Improvement

As shown in Figure 1.5, $z_I(t)$ is the input of the in-phase sub-channel integrator. The PSD $S_{x_{I,A}}(f)$ of $x_{I,A}(t)$ is represented as [28]

$$S_{x_{I,A}}(f) = A_c^2 T_{\text{symbol}} \text{sinc}^2(T_{\text{symbol}} f). \tag{5.31}$$

According to (5.14), (5.31), and (B.3), $S_{x_{I,A}}(f)$ shown with the PSD of $i_{L,m}(t)$ is illustrated in Figure 5.1. All magnitudes are normalized with respect to the peak value of $S_{x_{I,A}}(f)$.

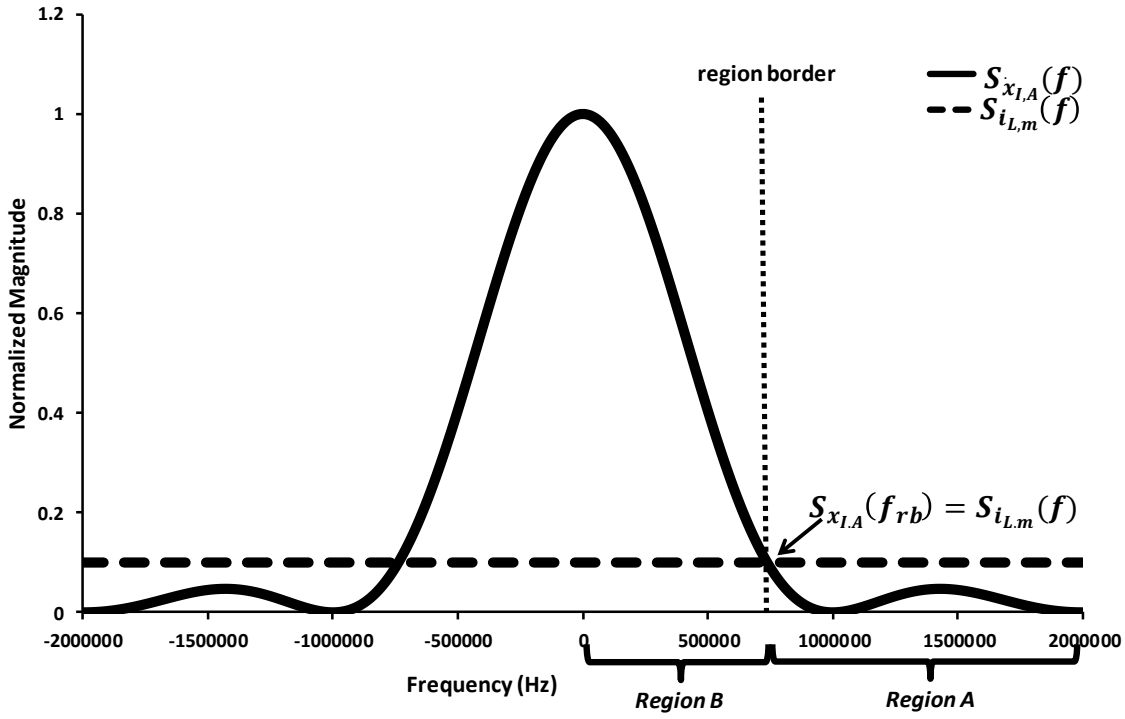

Figure 5.1 PSD of $x_{I,A}(t)$ and $i_{L,m}(t)$

Due to the 5 MHz offset of the ADCI and 1.5 MHz bandwidth of $x_{I,A}(t)$ required by

IEEE 802.15.4, B_{LPF} is initially set to $2/T_{\mathrm{symbol}}$ equal to 2 MHz. This initial arrangement ensures $x_{I,A}(t)$ filtered by the LPF is fairly undistorted and both ADCI and ALCI are rejected. To introduce significant levels of impulsive noise, $S_{i_{L,m}}(f)$ is set to be greater than the first side lobe of $S_{x_{I,A}}(f)$. Two regions of the frequency spectrum within the range of B_{LPF} are assigned as the Region A and B and illustrated in Figure 5.1 where the border frequency f_{rb} is defined as $S_{x_{I,A}}(f_{rb}) = S_{i_{L,m}}(f)$.

An LPF with the cutoff frequency located in the Region A is denoted as LPF_A. The MSE, MSE_A, between $x_{I,A}(t)$ and the LPF_A filtered $z_I(t)$ thus can be represented as

$$\mathrm{MSE}_A = \mathrm{E}\left[\left(\mu_{I,A}(t) + i_{A,m}(t)\right)^2\right] = \mathrm{E}\left[\mu_{I,A}^2(t) + 2\mu_{I,A}(t)i_{A,m}(t) + i_{A,m}^2(t)\right]$$

$$= \mathrm{E}\left[\mu_{I,A}^2(t)\right] + \mathrm{E}\left[i_{A,m}^2(t)\right] + 2\mathrm{E}[\mu_{I,A}(t)i_{A,m}(t)], \tag{5.32}$$

where $\mu_{I,A}(t)$ is the distortion term due to the application of a non-ideal LPF and $i_{A,m}(t)$ is the result of the linear filtering operation on $i_m(t)$. $\mu_{I,A}(t)$ and $i_{A,m}(t)$ are assumed to be independent, thus (5.32) can be rewritten as

$$\mathrm{MSE}_A = \mathrm{E}\left[\mu_{I,A}^2(t)\right] + \mathrm{Var}[i_{A,m}(t)]. \tag{5.33}$$

Substituting (5.31) and (B.3) into (5.33), (5.33) can be expanded to

$$\mathrm{MSE}_A = 2\int_{B_{\mathrm{LPF},A}}^{\frac{2}{T_{\mathrm{symbol}}}} S_{x_{I,A}}(f)\,df + 2\int_0^{B_{\mathrm{LPF},A}} S_{i_{L,m}}(f)\,df\,, \tag{5.34}$$

where $B_{\mathrm{LPF},A}$ is the cutoff frequency of LPF_A and $f_{rb} < B_{\mathrm{LPF},A} < 2/T_{\mathrm{symbol}}$.

An LPF with the cutoff frequency located in the Region B is denoted as LPF_B and $B_{\mathrm{LPF},B}$ is its respective cutoff frequency. The MSE, when the cutoff frequency of the LPF is equal to f_{rb} and located in the Region B, is represented as MSE_{rb} and MSE_B, respectively. According to (5.34), we have

$$\begin{cases} \mathrm{MSE}_{rb} = 2\int_{f_{rb}}^{\frac{2}{T_{\mathrm{symbol}}}} S_{x_{I,A}}(f)\,df + 2\int_{0}^{f_{rb}} S_{i_{L,m}}(f)\,df \\ \mathrm{MSE}_{B} = 2\int_{B_{\mathrm{LPF},B}}^{\frac{2}{T_{\mathrm{symbol}}}} S_{x_{I,A}}(f)\,df + 2\int_{0}^{B_{\mathrm{LPF},B}} S_{i_{L,m}}(f)\,df \end{cases}, \tag{5.35}$$

where $0 < B_{\mathrm{LPF},B} < f_{rb}$.

The MSE gain, MG, is used to compare the MSE performance of MSE_A, MSE_{rb}, and MSE_B, that is

$$\begin{cases} MG_{A,rb} = \mathrm{MSE}_A - \mathrm{MSE}_{rb} \\ MG_{rb,B} = \mathrm{MSE}_{rb} - \mathrm{MSE}_B \end{cases}, \tag{5.36}$$

and, therefore,

$$\begin{cases} MG_{A,rb} = 2\int_{f_{rb}}^{B_{\mathrm{LPF},A}} \left(S_{i_{L,m}}(f) - S_{x_{I,A}}(f)\right) df \\ MG_{rb,B} = 2\int_{B_{\mathrm{LPF},B}}^{f_{rb}} \left(S_{i_{L,m}}(f) - S_{x_{I,A}}(f)\right) df \end{cases}. \tag{5.37}$$

Since

$$\begin{cases} S_{i_{L,m}}(f) > S_{x_{I,A}}(f), \text{ when } f_{rb} < f < B_{\mathrm{LPF},A} \\ S_{i_{L,m}}(f) < S_{x_{I,A}}(f), \text{ when } B_{\mathrm{LPF},B} < f < f_{rb} \end{cases}, \tag{5.38}$$

MG becomes

$$\begin{cases} MG_{A,rb} = 2\int_{f_{rb}}^{B_{\mathrm{LPF},A}} \left(S_{i_{L,m}}(f) - S_{x_{I,A}}(f)\right) df > 0 \\ MG_{rb,B} = 2\int_{B_{\mathrm{LPF},B}}^{f_{rb}} \left(S_{i_{L,m}}(f) - S_{x_{I,A}}(f)\right) df < 0 \end{cases}. \tag{5.39}$$

It can be seen from (5.39), when the cutoff frequency of the LPF is moved from the Region A to the border frequency f_{rb}, the MSE is improved and when it is moved from f_{rb} to the Region B, the MSE condition deteriorates. Therefore, the cutoff frequency f_{MinMSE} of the LPF corresponding to the minimal MSE is $f_{\mathrm{MinMSE}} = f_{rb}$. Using (5.31) and (B.3), this intersection yields

$$A_c^2 T_{\mathrm{symbol}} \mathrm{sinc}^2\left(T_{\mathrm{symbol}} f_{rb}\right) = pN_0, \tag{5.40}$$

and solving for frequency gives

$$f_{\text{MinMSE}} = f_{rb} = \frac{\text{sinc}^{-1}\left(\frac{1}{A_c}\sqrt{\frac{pN_0}{T_{\text{symbol}}}}\right)}{T_{\text{symbol}}}, \tag{5.41}$$

where sinc^{-1} denotes the inverse sinc function. Based on this analysis, by continuously limiting the bandwidth of the LPF from $2/T_{\text{symbol}}$, one can further improve system performance bounded by the conditions given by (5.39) and (5.41).

5.3.2 The Proposed Error-Balanced Wavelet Filtering Scheme

Given a constant A_c and T_{symbol} in (5.41), f_{MinMSE} is a function of pN_0 only. However in a realistic O-QPSK demodulation system, $S_{i_m}(f)$ is usually unknown and the cutoff frequency f_{MinMSE} cannot be directly determined. Thus an Error-Balanced Wavelet (EB-Wavelet) filtering scheme is proposed for the determination of the cutoff frequency in order to improve the system performance. The proposed scheme utilizes the multiresolution analysis (MRA) of the discrete wavelet transform (DWT).

The DWT includes two portions: the decomposition and reconstruction [66]. Considering a discrete noisy signal $m[t]$ where $t = 0, 1, \cdots, N-1$, and N is the power of two, the MRA of $m[t]$ using the DWT decomposition is given as

$$\begin{cases} a_{j+1}[k] = \sum_{n=-\infty}^{+\infty} a_j[n]h_0[n-2k] = a_j[k] * \bar{h}_0[2k] \\ d_{j+1}[k] = \sum_{n=-\infty}^{+\infty} a_j[n]h_1[n-2k] = a_j[k] * \bar{h}_1[2k] \end{cases}, \tag{5.42}$$

where $a_{j+1}[k]$ and $d_{j+1}[k]$ are respectively the approximation coefficients and detail coefficients, $\bar{h}[k] = h[-k]$, $*$ denotes the convolution, and the resolution level $j = 0, 1, \cdots, log_2 N$. For the purpose of reducing computational complexity, at the initial level

$j = 0$, the condition $a_0[k] = m[t]$ is employed. The filter impulse responses, $h_0[k]$ and $h_1[k]$, are the LPF and highpass filter (HPF) of DWT, respectively. However $h_0[k]$ and $h_1[k]$ are not independent and are related by

$$\begin{cases} h_1[k] = (-1)^k h_0[1-k] \\ H_1(z) = -z^{-1} H_0(-z^{-1}) \end{cases}, \tag{5.43}$$

where $H(z)$ is the z-Transform of $h[k]$. MRA using the wavelet filter bank of $h_0[k]$ and $h_1[k]$ divides signal into two frequency sub-bands at each resolution level while all information of signal is preserved. The coefficients $a_j[k]$ and $d_j[k]$ describe the approximation and detail information of $m[t]$ for a certain wavelet space corresponding to the resolution level j. Considering the downsampling process represented by the term $[n-2k]$ in (5.42), at a certain resolution level J, the corresponding sampling rate is reduced by half compared with the lower level $J-1$. Hence the frequency range FR of MRA at the resolution level J for $h_0[k]$ and $h_1[k]$ can be represented as

$$\begin{cases} FR_{h_0,J} = \left[0, \frac{f_s}{2^{J+1}}\right] \\ FR_{h_1,J} = \left[\frac{f_s}{2^{J+1}}, \frac{f_s}{2^J}\right] \end{cases}. \tag{5.44}$$

Figure 5.2 illustrates $FR_{h_0,j}$ and $FR_{h_1,j}$ at several adjacent resolution levels where the corresponding frequencies are normalized by the factor f_s.

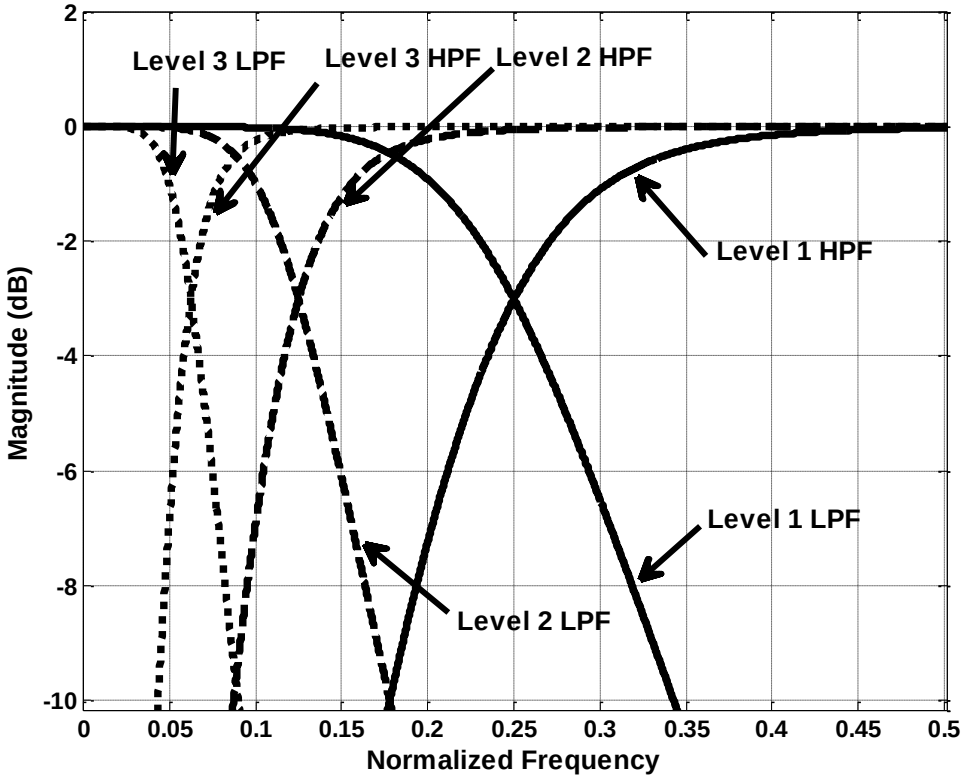

Figure 5.2 MRA frequency ranges

The DWT reconstruction iteration is expressed as

$$a_j[k] = \sum_{n=-\infty}^{+\infty} a_{j+1}[n]h_0[k-2n] + \sum_{n=-\infty}^{+\infty} d_{j+1}[n]h_1[k-2n]. \qquad (5.45)$$

Equations (5.44) and (5.45) suggest that managing $a_{j+1}[k]$ and $d_{j+1}[k]$ during the reconstruction iterations, it is possible to remove unwanted components within the corresponding frequency range and partially recover $m[t]$ for certain processing purpose. Given a resolution level J and discarding $d_{j+1}$where $0 \le j \le J-1$ for the reconstruction of $m[t]$, the information within the frequency range of $\left[0, \frac{f_s}{2^{J+1}}\right]$ is to be recovered. Such

an operation can be considered as a low pass filtering process where the cutoff frequency $f_{\text{cutoff,w,J}}$ is approximately equal to $\frac{f_s}{2^{J+1}}$. Given f_{MinMSE} in (5.41), the suggested resolution level $J_{\text{suggested}}$ corresponding to f_{MinMSE} for impulsive noise suppression can be obtained as follows:

1. Define the frequency difference function $\Delta_{fd}(j)$ for resolution level j as

$$\Delta_{fd}(j) = \left| f_{\text{cutoff,w,j}} - \frac{1}{T_{\text{symbol}}} \right|, j = 1, \cdots, log_2 N. \tag{5.46}$$

2. The minimal value $\Delta_{fd,\min}$ of $\Delta_{fd}(j)$ is then determined as

$$\Delta_{fd,\min} = \min\left[\Delta_{fd}(j)\right], \tag{5.47}$$

where $\min[\cdot]$ indicates the minimal value acquiring operator.

3. The suggested resolution level $J_{\text{suggested}}$ is obtained as

$$J_{\text{suggested}} = \Delta_{fd}^{-1}\left(\Delta_{fd,\min}\right), \tag{5.48}$$

where Δ_{fd}^{-1} is the inverse function of $\Delta_{fd}(j)$. The corresponding cutoff frequency $f_{\text{cutoff,w},J_{\text{suggested}}}$ of $h_0[k]$ at the suggested resolution level $J_{\text{suggested}}$ is thus represented as

$$f_{\text{cutoff,w},J_{\text{suggested}}} = \frac{f_s}{2^{J_{\text{suggested}}+1}} . \tag{5.49}$$

After $J_{\text{suggested}}$ is determined, the wavelet low pass filtering process is performed on $z_I(t)$ and $z_Q(t)$ by discarding all the detail coefficients from resolution level $J_{\text{suggested}}$ to level 1, that is

$$\begin{cases} z_{I,wl,J_{\text{suggested}}}(t) = \text{wrecon}_{z_I,A}\left(J_{\text{suggested}}\right) \\ z_{Q,wl,J_{\text{suggested}}}(t) = \text{wrecon}_{z_Q,A}\left(J_{\text{suggested}}\right) \end{cases}, \tag{5.50}$$

where $\text{wrecon}_{z_{I,A}}(j)$ and $\text{wrecon}_{z_{Q,A}}(j)$ represent the DWT reconstruction process shown in (5.45) for $z_I(t)$ and $z_Q(t)$, respectively.

As the ratio of the frequency range between two adjacent resolution levels j and $j+1$ is $\frac{2^{j+1}}{2^j} = 2$, the frequency difference between $f_{\text{cutoff,w},J_{\text{suggested}}}$ and f_{MinMSE} should be considered. Based on the analysis given in Section 5.3.1, $f_{\text{cutoff,w},J_{\text{suggested}}}$ may possibly reside in the Region A or Region B rather than exactly at f_{MinMSE}. Therefore, the filter distortion and $i_{L,m}(t)$ need to be further processed. To manage this, an error balancing operation is performed on both of the wavelet reconstruction results $z_{I,wl,J_{\text{suggested}}}(t)$ and $z_{Q,wl,J_{\text{suggested}}}(t)$. The EB-Wavelet filtering output is defined as follows

$$z_{I,wl,\text{Balanced}}(t) = \begin{bmatrix}\lambda_1\\ \lambda_2\\ \lambda_3\\ \lambda_4\end{bmatrix}^T \times \begin{bmatrix}z_{I,wl,J_{\text{suggested}}-1}(t)\\ z_{I,wl,J_{\text{suggested}}}(t)\\ z_{I,wl,J_{\text{suggested}}+1}(t)\\ z_{I,wl,J_{\text{suggested}}+2}(t)\end{bmatrix}, \tag{5.51}$$

where $z_{I,wl,\text{Balanced}}(t)$ is the error-balanced result of $z_{I,wl,J_{\text{suggested}}}(t)$, T denotes the matrix transpose, and the weighting matrix Λ is expressed as

$$\Lambda = [\lambda_1 \quad \lambda_2 \quad \lambda_3 \quad \lambda_4]. \tag{5.52}$$

Based on evaluations using MATLAB simulations, Λ is experimentally set to obtain the minimal MSE between $z_{I,wl,\text{Balanced}}(t)$ and $x_{I,A}(t)$, that is

$$\Lambda = \left[\frac{1}{4.8} \quad \frac{1.7}{4.8} \quad \frac{1.1}{4.8} \quad \frac{1}{4.8}\right], \tag{5.53}$$

where the sum of the weighting terms is normalized to 1.

5.4 Assessment by Simulations

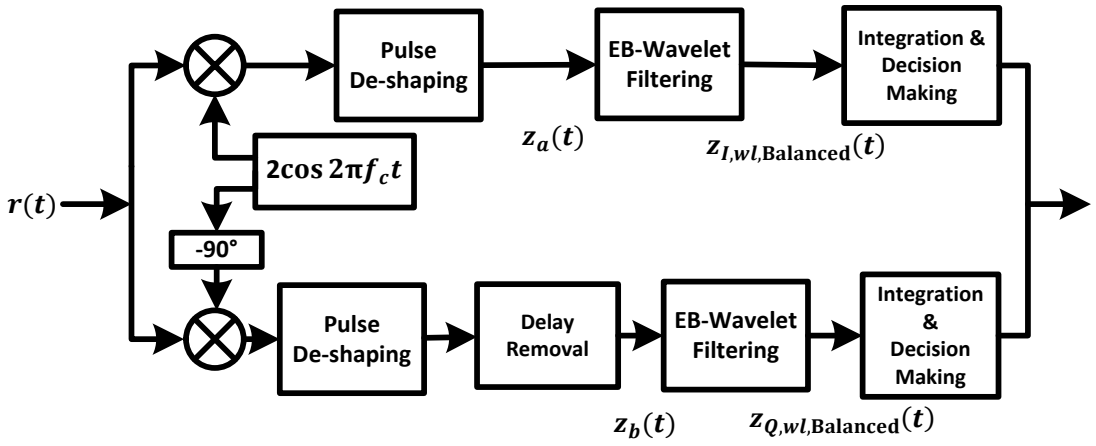

Figure 5.3 O-QPSK demodulator with the EB-Wavelet filter

In this section, several MATLAB simulations were performed in order to evaluate the performance of the proposed EB-Wavelet filtering approach for ZigBee systems. The specifications of the bit-to-symbol mapping, symbol-to-chip mapping, pulse shaping, and O-QPSK modulation follow IEEE 802.15.4 standard [58]. The O-QPSK carrier frequency f_c is set to 2.4 GHz and the sampling rate f_s is set to 4 times the carrier frequency. The proposed EB-wavelet filter is placed prior to the in-phase and quadrature sub-channel integrators as shown in Figure 5.3. Based on the setting of f_s and T_{symbol}, the suggested resolution level for the proposed EB-Wavelet filtering is obtained as $J_{\text{suggested}} = 12$. The variance of the $g(t)$ component in the impulsive noise model is used to set the power of the impulsive noise while the occurrence rate p is held constant.

The SAR is fixed to 20 dB and the impulsive noise power is varied to provide the desired channel SNR. The channel response is assumed flat within the corresponding O-QPSK transmission bandwidth and AWGN and impulsive noise are the only sources of the channel interference.

5.4.1 Selection of Wavelet Filter Type

In the simulation, the performances of EB-Wavelet filters using different wavelets are compared. p is set to 10% in order to test the impulsive noise rejection ability of various wavelets in a severe noise environment. The weighting matrix given in (5.53) is adopted for all the employed wavelets as it gives the best BER results based on simulation results. The BER results of ZigBee are shown in Figure 5.4. It can be found that EB-Wavelet filter using the haar wavelet has the best impulsive noise rejection capability when compared with other wavelet basis functions such as db4, bior2.2, and sym2. This is mostly due to the similar characteristics between the $h_0[k]$ of the haar filter bank and the polar NRZ signal transmitted in the parallel sub-channels of O-QPSK.

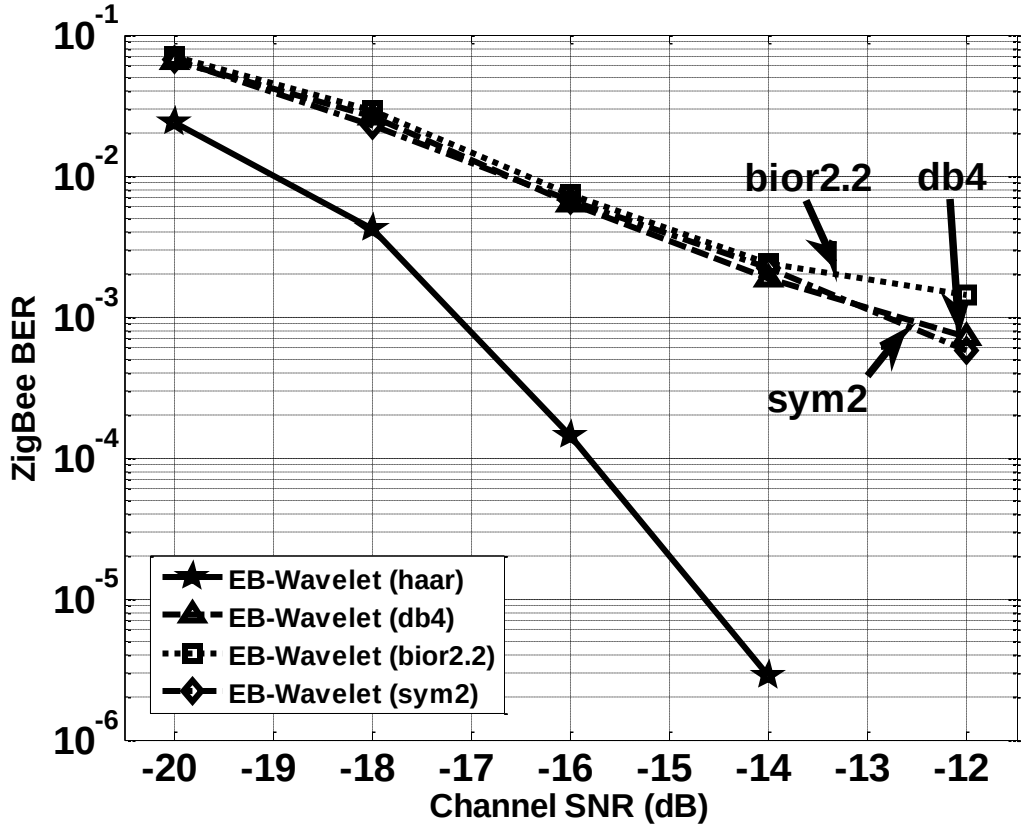

Figure 5.4 BER performances of EB-Wavelet filters using the haar, db4, bior2.2, and sym2 (p = 10%)

In the next simulation, the demodulated in-phase sub-channel signal $z_a(t)$ is filtered by the proposed EB-Wavelet filter with $J_{\text{suggested}} = 12$ and an LPF with 1 MHz cutoff frequency denoted by LPF_1. The 1 MHz LPF was utilized by Hussien in his ZigBee transceiver design to obtain the best BER performance [27]. For our simulations, LPF_1 was implemented as a basic 3rd order Butterworth FIR design and higher orders were found to provide limited gains in the system performance. The channel SNR and the occurrence rate p of the impulsive noise is set to -20 dB and 10%, repectively. The

results are compared with the baseband signal $x_{I,A}(t)$ of the in-phase sub-channel without any interference. The comparison is shown in Figure 5.5 and the effectiveness of our proposed filter in suppressing impulsive noise is clearly seen. The detector input signal fidelity is notably enhanced by the EB-Wavelet filter which should result in improved system performance.

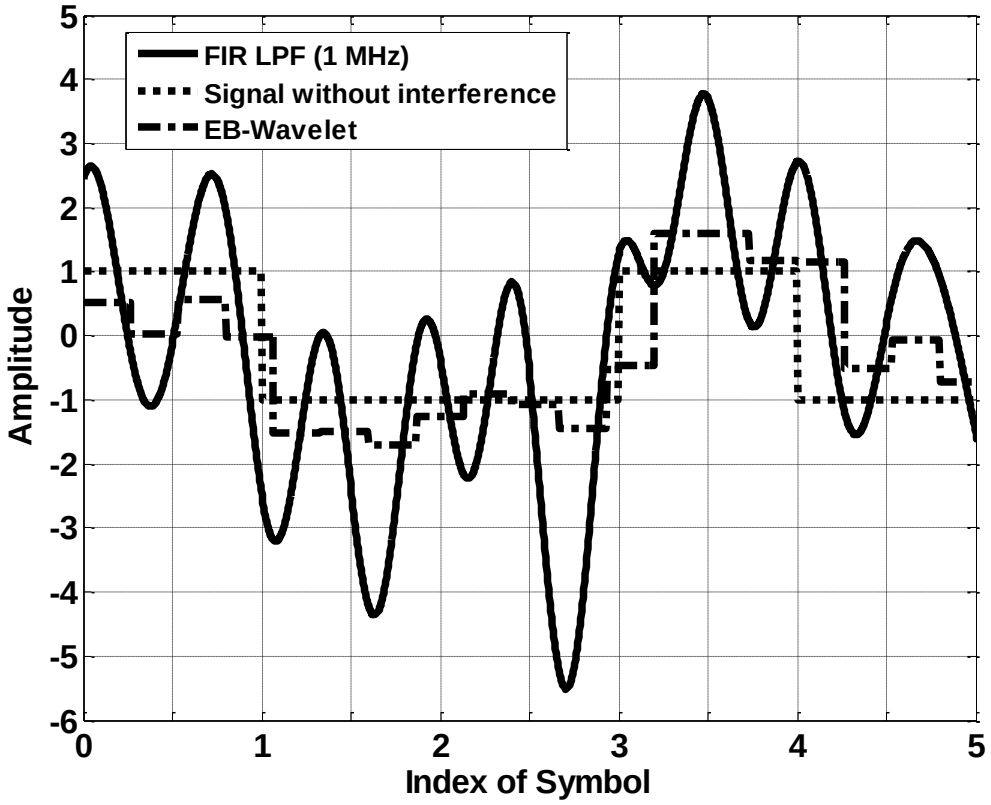

Figure 5.5 Comparison of the EB-Wavelet filtered signal and FIR LPF filtered signal (Channel SNR= -20 dB, $p = 10\%$)

5.4.2 MSE Performance

In this simulation, comparative MSEs were obtained by filtering $z_a(t)$ using the 1 MHz LPF (LPF_1), EB-Wavelet filter, and an FIR LPF with the cutoff frequency corresponding to the minimal MSE given in (5.41) (LPF_{MinMSE}). p is initially set to 1% and later increased to 10% in order to facilitate a more severe impulsive noise environment. The MSE results are compared in Figure 5.6 and Figure 5.7. These results show the application of LPF_{MinMSE} results in greatest improvement in MSE at all evaluated SNR conditions. However, the cutoff frequency of LPF_{MinMSE} requires an estimate of the impulsive noise PSD which increases the complexity of the receiver design. The EB-Wavelet filter also provides a notable MSE improvement but is more convenient to implement as no noise estimation process is needed.

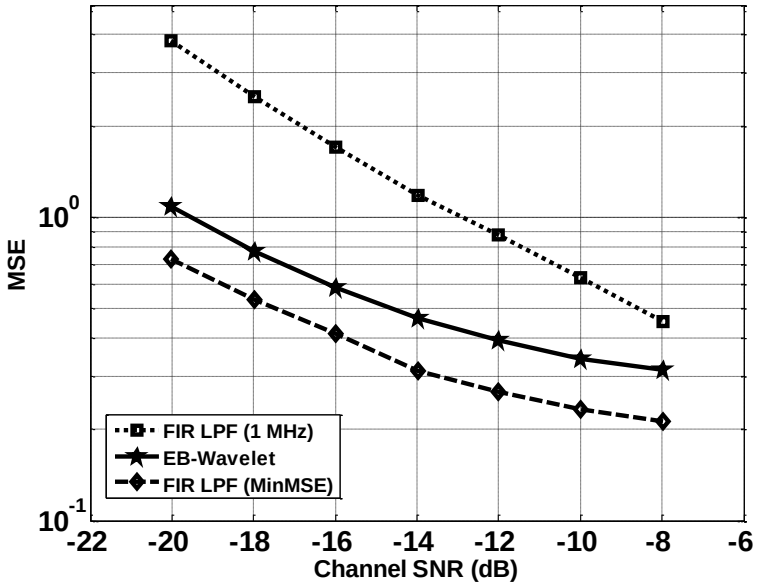

Figure 5.6 MSE performances of the FIRs filtered and EB-Wavelet filtered in-phase sub-channel signal ($p = 1\%$)

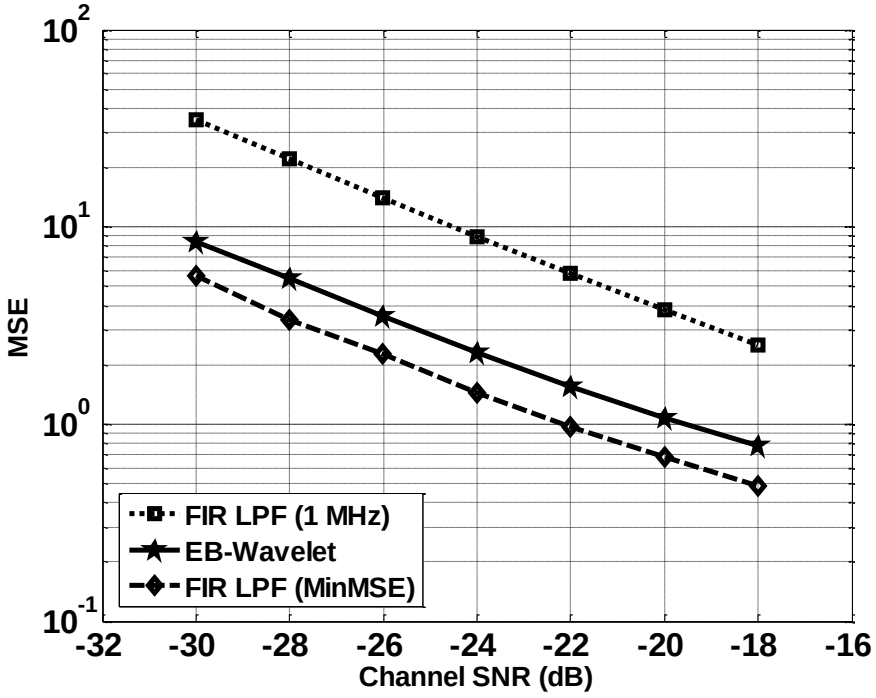

Figure 5.7 MSE performances of the FIRs filtered and EB-Wavelet filtered in-phase sub-channel signal ($p = 10\%$)

5.4.3 BER Performance

In this simulation, the resulting BER performance of the O-QPSK demodulator with and without the EB-Wavelet filter is shown. p is set to 1% and 10%, respectively. These results focus solely on the detection process without the added benefit of the DSSS error correction. As seen in Figure 5.8 and Figure 5.9, the O-QPSK demodulation with EB-Wavelet offers the expected BER performance improvement given the MSE shown in the previous results. In the next simulation, the overall ZigBee BER performance is shown in Figure 5.10 and Figure 5.11. As expected, the EB-Wavelet filter consistently yields a

better BER performance when compared with LPF_1. For example, to achieve the same BER 10^{-4} in the case of $p = 1\%$, the EB-Wavelet filter yields a 2 dB SNR gain when compared with ZigBee filtered by LPF_1. Similarly, for the case of $p = 10\%$, to achieve the same BER 10^{-1}, the SNR gain is 3 dB when comparing the same filter. Overall, LPF_{MinMSE} provides the best BER performance but with the EB Wavelet filter providing almost the same level of performance at all SNR levels.

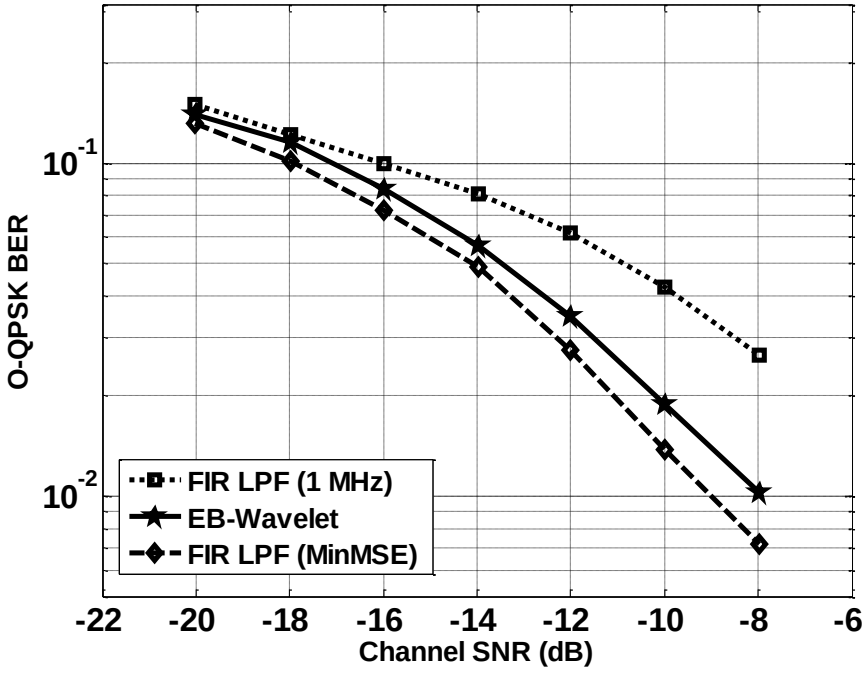

Figure 5.8 BER performance of the O-QPSK demodulator with FIR LPFs and EB-Wavelet ($p = 1\%$)

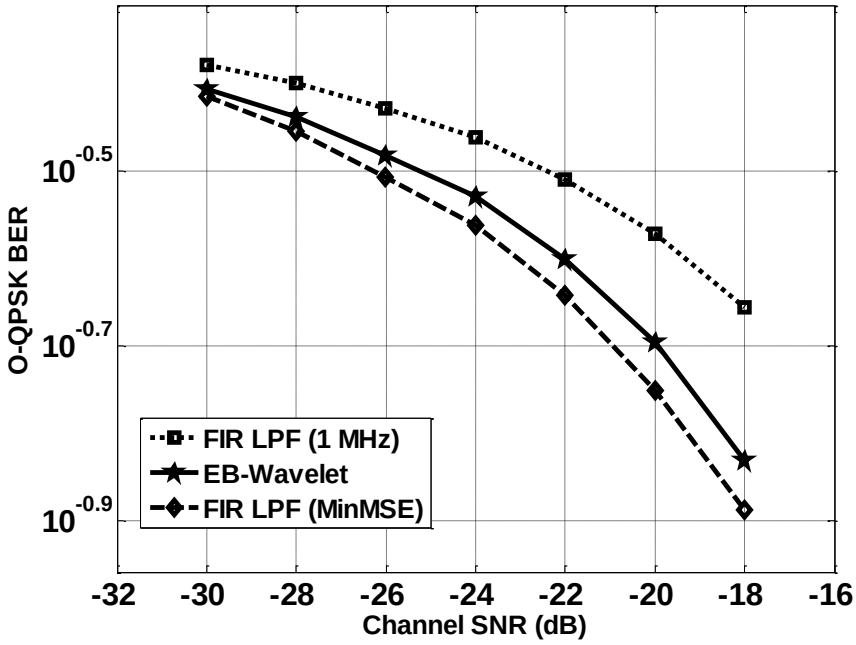

Figure 5.9 BER performance of the O-QPSK demodulator with FIR LPFs and EB-Wavelet (p = 10%)

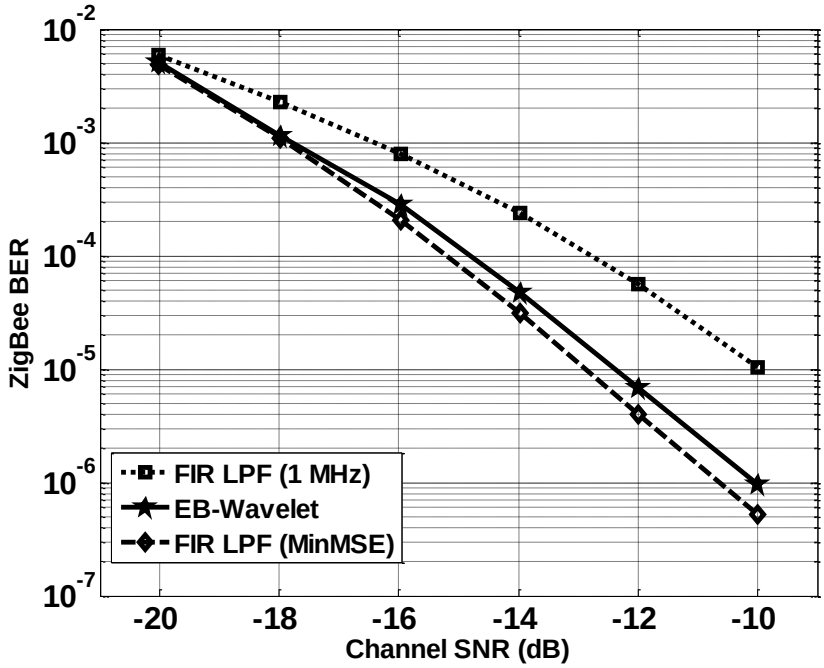

Figure 5.10 BER performance of the ZigBee with FIR LPFs and EB-Wavelet (p = 1%)

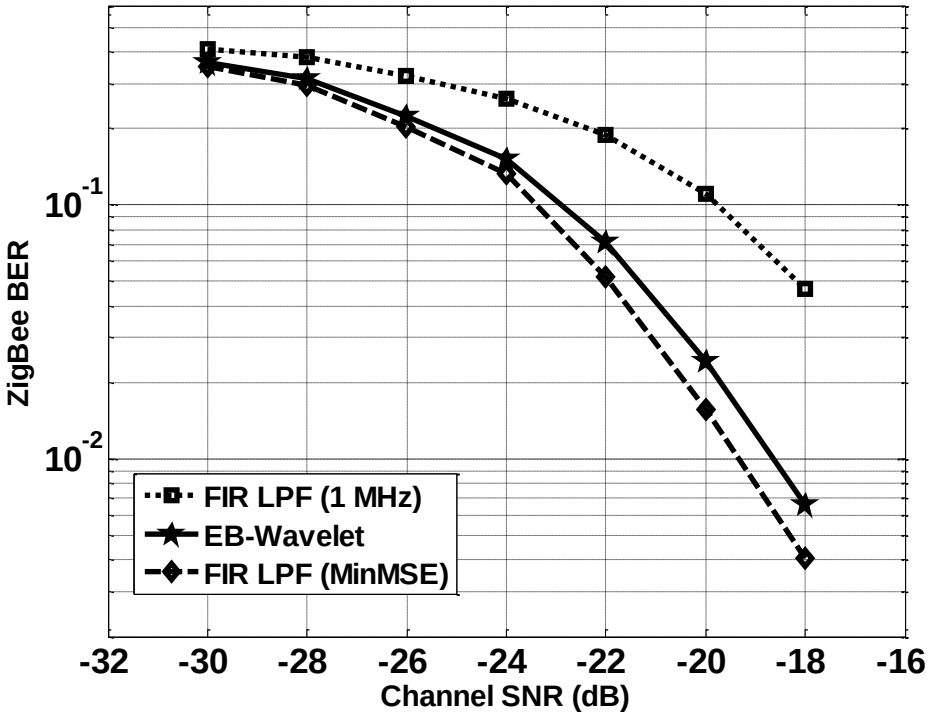

Figure 5.11 BER performance of the ZigBee with FIR LPFs and EB-Wavelet ($p = 10\%$)

5.4.4 EB-Wavelet Compared with Other Proposed Methods

In the last simulation, the BER performance of the EB-Wavelet filter is compared with LPF_1, CCV filter which is proposed in Chapter 4, and PBC which was introduced in [25]. Simulation results are shown in Figure 5.12. The simulation setting is arranged as follows: p is set to 10%; for the CCV filter, the random sampling rate used to obtain the mean CCV and the window width used for the CCV filtering process are respectively set to 10% and 41 as introduced in Chapter 4; for the PBC approach, the clipping ratio is set to 5 dB as it gives the best BER performance [25]. Preliminary BER comparisons show the proposed EB-Wavelet filter to outperform both the CCV and PBC filtering

approaches. For example, to achieve the same BER 10^{-2}, the proposed EB-Wavelet obtains a 2 dB and 4 dB SNR gain when compared to the CCV and PBC methods, respectively.

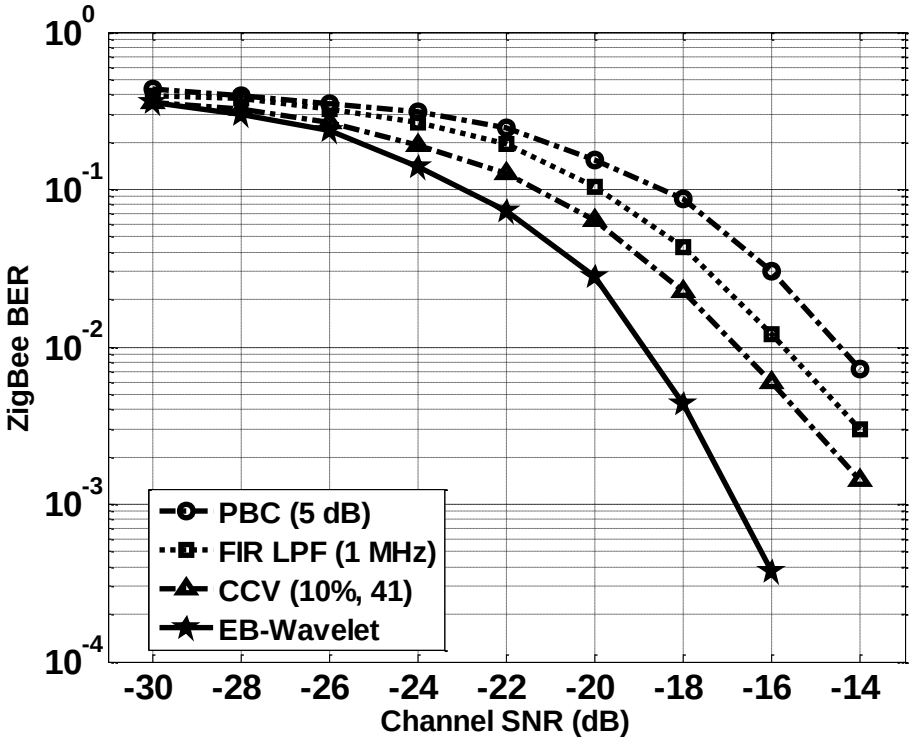

Figure 5.12 BER performance of the EB-Wavelet compared to the CCV filter and the PBC method ($\boldsymbol{p = 10\%}$)

5.5 Conclusion

In this chapter, the relationship between the minimum MSE bandwidth of the receiver LPF and the presence of impulsive noise for ZigBee systems is analyzed. Also, a novel Error-Balanced Wavelet filtering scheme based on the desired LPF bandwidth is

proposed for the purpose of impulsive noise rejection. This solution provides approximately the same BER results as the minimum MSE result without the added receiver complexity. This wavelet-based technique includes two key innovations: determination of the suggested resolution level for MRA and the improved BER performance using an error-balancing weighting matrix to combine adjacent decomposition levels. Several MATLAB-based simulations were performed to evaluate the performance of the proposed EB-Wavelet filter at various SNR levels. Results show the EB-Wavelet filter using the haar wavelet to outperform a 1 MHz FIR LPF as well as two previously proposed impulsive noise rejection techniques.

Chapter 6 Conclusion

In this dissertation, we address the impact of impulsive noise on OFDM-based communication systems [1-3] and ZigBee wireless communication systems [31, 58]. Impulsive noise is considered as one type of channel additive noise which can be generated by power transmission lines, vehicle ignition, defective electric transients, partial discharge and sferic radiation [17-20]. Impulsive noise has the following unique characteristics: random occurrence, high-energy content within short time duration, and wide band spectrum [16, 21, 22, 64]. Due to its random spike-like time domain characteristics and wide band PSD in frequency domain, excessive impulsive noise may degrade the performance of OFDM-based communications and ZigBee WSNs [9, 33, 34, 46, 48]. For example, the impulsive noise may spread to all OFDM sub-carriers during the FFT demodulation; it may cause difficulties to ZigBee O-QPSK demodulation and DSSS decoding process. This can result in transmitting incorrect messages to users. Therefore, mitigating the influence of impulsive noise becomes a critical task for improving the communication transmission quality. In this research, several impulsive noise rejection schemes have been presented for both OFDM and ZigBee communication systems.

6.1 Summary of Contributions

In Chapter 2, we focus on the impulsive noise suppression in OFDM communication systems. To achieve this goal, a dual faceted approach is proposed. We employ the Reed-Solomon (RS) channel coding technique in a conventional OFDM system termed RS-OFDM to provide the first stage protection. A frequency domain noise estimation process

is then performed as a pre-detection process. With a direct blanking or clipping operation on the received signal, the originally transmitted signal may be also blanked or clipped by false impulsive noise detection. Correspondingly the systems performance improvement is limited due to the ill-defined threshold [24, 25, 37]. However, this type of pre-detection followed by impulsive noise suppression performed on the estimated noise could offer some advantages. After the estimated noise is obtained, a composite comparison value (CCV)-based time domain filtering process is formulated to detect and remove the impulsive noise as the second stage protection. Our proposed filtering process utilizes a novel and efficient CCV-based threshold for a more accurate detection. Simulation results demonstrate the BER performance improvement of the proposed CCV filter with the aid of the RS coding when compared with the previously proposed methods in various impulsive noise environments and a multipath channel [24, 28].

In Chapter 3, we compare the performances of 915 MHz and 2.4 GHz band ZigBee systems in the presence of impulsive noise. Both of these ZigBee systems utilize the DSSS and O-QPSK as the PHY layer infrastructure. First, the theoretical analysis of the noise performance of the 915 MHz and 2.4 GHz band ZigBee systems is developed, and it is revealed that the 2.4 GHz band ZigBee has a better impulsive noise resistance. In order to perform a simulation assessment, an impulsive noise model based on the statistical characteristics of the impulsive noise measured in electricity substations is presented [55]. The proposed impulsive noise model is formed by sampling an amplitude modulation process where each sampled point is modulated with a sinc function. This process forms a sinc-like pulse train impulsive noise model which corresponds to the statistical characteristics of the measured impulsive noise such as impulse amplitude,

impulse rate, and impulse rise time. By employing the proposed impulsive noise model, several simulations are performed to compare the impulsive noise resistance of these two ZigBee systems. Results also verify that the 2.4 GHz band ZigBee outperforms the 915 MHz band given the same signal-to-impulsive noise ratio scenario. However, as a trade-off, more DSSS coding redundancy results in an increase of the baseband bandwidth for the 2.4 GHz band ZigBee given the fixed data rate [58], and the 915 MHz band ZigBee may be possibly deployed for PD detection due to its greater sensitivity to impulsive noise.

In Chapter 4, the CCV filter with a time domain impulsive noise estimation and RS coding is employed with the ZigBee receiver. Noise estimation in the time domain attempts to avoid extra errors generated by the false detection and is performed directly on the received original signal interfered by impulsive noise. The effect of the RS coding against impulsive noise was previously shown to be effective in OFDM systems due to its burst error correcting ability. Simulation results show that the CCV filter alone outperforms RS coding implemented across a wide range of SNRs. However, the combination of the CCV and RS coding gives the best BER result for the 2.4 GHz band ZigBee system.

In Chapter 5, a frequency domain filtering approach is proposed to suppress the impulsive noise for the 2.4 GHz band ZigBee system. First, the BER performance of the 2.4 GHz band ZigBee receiver employing an LPF for the O-QPSK coherent detection is analyzed in an impulsive noise environment. It is shown that for the purpose of reducing BER, the bandwidth of LPF is related to the impulsive noise power which is theoretically not constant. A simple LPF with a fixed bandwidth, therefore, cannot effectively suppress

the impulsive noise. However, a flexible bandwidth LPF increases the complexity of the receiver design as the impulsive noise power needs to be continuously estimated. Based on this consideration, we propose a less complex but more elegant solution: an Error-Balanced Wavelet (EB-Wavelet) filtering process. The EB-Wavelet filter includes two portions: a wavelet-based low pass filtering process utilizing the multiresolution analysis property of a DWT and an error balancing process using a proposed weighting matrix. The performance of the EB-Wavelet filter is compared with an FIR LPF with 1 MHz cutoff frequency and an LPF with the cutoff frequency corresponding to the minimal MSE on the O-QPSK demodulator [27]. Simulation results show the LPF with the cutoff frequency corresponding to the minimal MSE to have the best performance. However, the EB-Wavelet filter provides almost the same level of improvement but is more convenient to implement. The proposed EB-Wavelet filter is also compared with the time domain CCV filter and the previously proposed PBC method [25]. Results demonstrate the EB-Wavelet filter outperforms these two filters.

6.2 Future Work

For the CCV filtering with RS coding approach introduced in Chapter 2 and Chapter 4, the RS codeword and redundancy extension should be further analyzed in the case of a greater occurrence probability of impulsive noise. RS coding with increased redundancy is able to correct more errors, but minimal redundancy is still needed to obtain the highest possible code rate. Moreover, according to both simulation results and theoretical analysis, the decoding failure of the proposed RS decoding algorithms still exists. Hence

analysis of the probability of decoding failure of the proposed RS decoding algorithms with various occurrence probabilities of impulsive noise is warranted.

In Chapter 3, the proposed impulsive noise model is based on the measured data in substations. It can be seen that the time-interval between each nearby impulsive noise is approximately constant according to the statistical distribution. This suggests a dominant periodic impulsive noise source during measurements in the electricity substation. However, the random occurrence is more acceptable as the common characteristic of impulsive noise [16, 33, 67]. Therefore, field measurements in various impulsive noise environments, such as the indoor environments, distributed power substations, and industrial workshops, could be used in order to improve the accuracy of the modelling process for different practical impulsive noise sources.

In Chapter 5, for the DWT-based impulsive noise rejection approach in ZigBee communication systems, the adopted value of the weighting matrix is determined by simulation results. However, a theoretical optimization of the weighting matrix can be considered to further improve system performance. When compared with other tested wavelets, the haar wavelet demonstrates the best performance which is mostly due to the similar characteristics between the haar wavelet and the polar NRZ signal. However, the theoretical relation between the selection of wavelet basis function and resulting filter performance could be further analyzed. In addition, the creation of a new wavelet basis function may be considered to further improve the system performance.

Bibliography

[1] R. W. Chang, "Synthesis of band-limited orthogonal signals for multichannel data transmission," *The Bell System Technical Journal*, vol. 45, pp. 1775-1796, Dec, 1966.

[2] S. Weinstein and P. Ebert, "Data Transmission by Frequency-Division Multiplexing Using the Discrete Fourier Transform," *IEEE Trans. on Communi. Techno.*, vol. 19, pp. 628-634, Oct., 1971.

[3] L. J. Cimini, "Analysis and Simulation of a Digital Mobile Channel Using Orthogonal Frequency Division Multiplexing," *IEEE Trans. on Communi.*, vol. 33, pp. 665-675, Jan., 1985.

[4] Y. H. Lee, T. H. Yu, K. K. Huang and A. Y. Wu, "Rapid IP design of variable-length cached-FFT processor for OFDM-based communication systems," in *Proc. 2006 IEEE Worksh. on Signal Proces. Syste. Design and Implem.*, Banff, Canada, 2006, pp. 62-65.

[5] C. Pan, L. Dai and Z. Yang, "TDS-OFDM based HDTV transmission over fast fading channels," *IEEE Trans. on Consu. Electro.*, vol. 59, pp. 16-23, Feb., 2013.

[6] A. Ghosh, R. Ratasuk, B. Mondal, N. Mangalvedhe and T. Thomas, "LTE-advanced: next-generation wireless broadband technology," *IEEE Trans. on Wireless Communi.*, vol. 17, pp. 10-22, Jun., 2010.

[7] P. Torio and M. G. Sánchez, "Intrasymbol interference in OFDM," *IEEE Trans. on Consu. Electro.*, vol. 56, pp. 447-449, May, 2010.

[8] J. Zhang, "Narrowband interference suppression in OFDM-based communication systems," *Dept. Electri. Comp. Eng. , University of New Brunswick, Canada,* 2009.

[9] A. Gaouda, F. Sallabi, A. El-Hag and M. Salama, "ZigBee performance during severe interruptions in electric power systems," in *Proc. the International Conf. on Electrical Power Quality and Utilisation,* Lisbon, Portugal, 2011, pp. 1-6.

[10] Y. Du, Y. Lee, Y. Lu, C. Lin, M. Wu, C. Chen and T. Chen, "Development of a telecare system based on ZigBee mesh network for monitoring blood pressure of patients with hemodialysis in health care centers," *Springer Journal of Medi. Syst.,* vol. 35, pp. 877-883, Oct., 2011.

[11] J. Zhang, G. Song, G. Qiao, T. Meng and H. Sun, "An indoor security system with a jumping robot as the surveillance terminal," *IEEE Trans. on Consu. Electro.,* vol. 57, pp. 1774-1781, Nov., 2011.

[12] K. Hwang, B. Choi and S. Kang, "Enhanced self-configuration scheme for a robust ZigBee-based home automation," *IEEE Trans. on Consu. Electro.,* vol. 56, pp. 583-590, May, 2010.

[13] J. Yao, Z. Zhang, P. Dong and K. Holtman, "A ZigBee controlled lighting system with improved resistance to wireless interference," in *Proc. IEEE Asia Pacific Confer. on Wireless and Mobile,* Bali, Indonesia, 2014, pp. 219-225.

[14] W. Sung and C. Hsu, "Intelligent environment monitoring system based on innovative integration technology via programmable system on chip platform and ZigBee network," *IET Communi.*, vol. 7, pp. 1789-1801, Nov., 2013.

[15] P. Yi, A. Iwayemi and C. Zhou, "Developing ZigBee deployment guideline under WiFi interference for smart grid applications," *IEEE Trans. on Smart Grid*, vol. 2, pp. 110-120, Mar., 2011.

[16] S. Vaseghi, *Advanced Digital Signal Processing and Noise Reduction.* NJ, USA: Wiley, 2009.

[17] G. Ndo, P. Siohan and M. H. Hamon, "Adaptive noise mitigation in impulsive environment: application to power-line communications," *IEEE Trans. on Power Deliv.*, vol. 25, pp. 647-656, Mar., 2010.

[18] J. A. Cortes, L. D. Diez and F. J. Canete, "Analysis of the indoor broadband power-line noise scenario," *IEEE Trans. on Electromagn. Compat.*, vol. 52, pp. 849-858, Nov., 2010.

[19] G. Bedicks, C. E. S. Dantas, F. Sukys, F. Yamada, L. T. M. Raunheitte and C. Akamine, "Digital Signal Disturbed by Impulsive Noise," *IEEE Trans. on Broadca.*, vol. 51, pp. 322-328, Aug., 2005.

[20] Q. Shan, I. Glover, R. Atkinson, S. Bhatti, I. Portugues, P. Moore, R. Rutherford, M. Viera, A. Lima and B. Souza, "Estimation of impulsive noise in an electricity substation," *IEEE Trans. on Electromag. Compatib.*, vol. 53, pp. 653-663, Aug., 2011.

[21] K. L. Blackard, T. S. Rappaport and C. W. Bostian, "Measurements and models of radiofrequency impulsive noise for indoor wireless communications," *IEEE Journ. on Selected Areas in Communi.,* vol. 11, pp. 991-1001, Sep., 1993.

[22] M. D. Judd, O. Farish, J. S. Pearson and B. F. Hampton, "Dielectric windows for UHF partial discharge detection," *IEEE Trans. on Dielectri. and Electr. Insula.,* vol. 8, pp. 953-958, Dec., 2011.

[23] U. Epple and M. Schnell, "Adaptive threshold optimization for a blanking nonlinearity in OFDM receivers," in *Proc. IEEE Global Communications Conf.,* Anaheim, USA, 2012, pp. 3661-3666.

[24] S. V. Zhidkov, "Impulsive noise suppression in OFDM-based communication systems," *IEEE Trans. on Consu. Electro.,* vol. 49, pp. 944-948, Nov., 2003.

[25] X. Xu, S. Zhou, H. Sun, A. K. Morozov and Y. Zhang, "Impulsive noise suppression in per-survivor processing based DSSS systems," in *Proc. 2014 Oceans - St. John'S,* St. John's, Canada, 2014, pp. 1-5.

[26] S. Nayyef, C. Tsimenidis, A. Al-Dweik, B. Sharif and A. Hazmi, "Time- and frequency-domain impulsive noise spreader for OFDM systems," in *Proc. IEEE 11th Interna. Confer. on Trust, Security and Privacy in Computing and Commu.,* Liverpool, UK, 2012, pp. 1856-1861.

[27] F. A. E. Hussien, "Ultra low power IEEE 802.15.4/ZigBee compliant transceiver," *Dept. Elec. Eng. , Texas A&M University, USA,* 2009.

[28] B. Sklar, *Digital Communications: Fundamentals and Applications.* Upper Saddle River, NJ, USA: Prentice Hall, 2001.

[29] G. V. Meerbergen, M. Moonen and H. D. De, "Combining reed-solomon codes and OFDM for impulse noise mitigation: RS-OFDM," in *Proc. IEEE Conf. on Acoustics, Speech and Signal Processing,* Toulouse, France, 2006, pp. 657-660.

[30] ITU Standard G.9903-2014, "Part 7: Physical layer specification," 2014.

[31] IEEE Standard 802.15.4-2011, "Part 8: General PHY requirements," 2011.

[32] Y. Wu and W. Y. Zou, "Orthogonal frequency division multiplexing: a multi-carrier modulation scheme," *IEEE Trans. on Consumer Electronics,* vol. 41, pp. 392-399, Aug, 1995.

[33] Y. H. Ma and P. L. So, "Performance analysis of OFDM systems for broadband power line communications under impulsive noise and multipath effects," *IEEE Trans. on Power Delivery,* vol. 20, pp. 674-682, Apr., 2005.

[34] M. Mirahmadi, A. Al-Dweik and A. Shami, "BER Reduction of OFDM Based Broadband Communication Systems over Multipath Channels with Impulsive Noise," *IEEE Trans. on Communi.*, vol. 61, pp. 4602-4615, Nov., 2013.

[35] S. V. Vaseghi and P. J. W. Rayner, "Detection and suppression of impulsive noise in speech communication systems," in *IEE Proc. Communi., Speech and Vision,* vol. 137, pp. 38-46, Feb, 1990.

[36] S. J. Godsill and P. J. Rayner, "Statistical reconstruction and analysis of autoregressive signals in impulsive noise using the Gibbs sampler," . *IEEE Trans. on Speech and Audio Processing*, vol. 6, pp. 352-372, Jul., 1998.

[37] T. C. Giles, "On the design of HF radio modems," *Depart. of Electri. and Electro. Eng. , University of Adelaide, Australia*, 1995.

[38] F. Marvasti, M. Hasan, M. Echhart and S. Talebi, "Efficient algorithms for burst error recovery using FFT and other transform kernels," *IEEE Trans. on Signal Processing*, vol. 47, pp. 1065-1075, Apr, 1999.

[39] R. Kumaresan, "Rank reduction techniques and burst error-correction decoding in real/complex fields," in *Proc. of 9th Asilomar Conf. on Circuits, Systems and Computers*, Pacific Grove, USA, 1985, pp. 457-461.

[40] S. Dlhan and P. Farkas, "Impulsive noise cancellation in systems with OFDM modulation," *Journ. of Electr. Eng.*, vol. 59, pp. 310-316, 2008.

[41] X. Wang, "NFIR nonlinear filter," *IEEE Trans. on Signal Processing*, vol. 39, pp. 1705-1708, Jul., 1991.

[42] D. Stranneby and W. Walker, *Digital Signal Processing and Applications* . Boston, USA: Newnes, 2004.

[43] J. L. Berlekamp, *Algebraic Coding Theory*. NY, USA: McGraw-Hill, 1968.

[44] R. T. Chien, "Cyclic decoding procedures for the bose-chaudhuri-hocquenghem codes," *IEEE Trans. on Information Theory*, vol. 10, pp. 357-363, Oct., 1964.

[45] G. D. Forney, "On decoding BCH codes," *IEEE Trans. on Information Theory,* vol. 11, pp. 549-557, Oct., 1965.

[46] Q. Shan, I. A. Glover, P. J. Moore, I. E. Portugues, R. J. Watson and R. Rutherford, "Performance of ZigBee in electricity supply substations," in *Proc. 2007 Int. Wireless Communications, Networking and Mobile Computing Conf.,* Shanghai, China, 2007, pp. 3871-3874.

[47] M. M. Nordman and M. Lehtonen, "A wireless sensor concept for managing electrical distribution networks," in *Proc. 2004 IEEE PES Power Systems Conf. and Exposition,* NY, USA, 2004, pp. 1198-1206.

[48] S. A. Bhatti, Q. Shan, R. Atkinson, M. Vieira and I. A. Glover, "Vulnerability of ZigBee to impulsive noise in electricity substations," in *Proc. 2011 XXXth URSI General Assembly and Scientific Symposium,* Istanbul, Turkey, 2011, pp. 1-4.

[49] Y. C. Wu, L. F. Cheung, K. S. Lui and P. W. T. Pong, "Efficient communication of sensors monitoring overhead transmission lines," *IEEE Trans. on Smart Grid,* vol. 3, pp. 1130-1136, Sept., 2012.

[50] L. Wei, H. Zhu, Q. Jiao and Z. Huang, "The research and design of wireless communication system for substation," in *Proc. 2010 China Int. Electricity Distribution Conf.,* Nanjing, China, 2010, pp. 1-9.

[51] S. A. Bhatti, I. A. Glover, R. Atkinson, Q. Shan, Y. Yang, J. M. R. S. Neto and Neto, J. S. D. R., "Vulnerability of bluetooth to impulsive noise in electricity transmission substations," in *Proc. 2010 IET Int. Wireless Sensor Network Conf.*, Beijing, China, 2010, pp. 53-58.

[52] P. P. Parikh, T. S. Sidhu and A. Shami, "A comprehensive investigation of wireless LAN for IEC 61850 based smart distribution substation applications," *IEEE Trans. on Industrial Informatics,* vol. 9, pp. 1466-1476, Oct., 2012.

[53] A. Hakam, N. A. Aly and S. Jimaa, "Impulsive noise mitigation in a MIMO-OFDM communication system," in *Proc. 6th Int. New Techno;Ogies, Mobility and Security Conf.*, Dubai, UAE, 2014, pp. 1-5.

[54] S. Xiao, P. J. Moore, M. D. Judd and I. E. Portugues, "An investigation into electromagnetic radiation due to partial discharges in high voltage equipment," in *Proc. 2007 IEEE Power Engineering Society General Meeting,* Vancouver, Canada, 2007, pp. 1-7.

[55] Q. Shan, S. Bhatti, I. A. Glover, R. Atkinson, I. E. Portugues, P. J. Moore and R. Rutherford, "Characteristics of impulsive noise in electricity substations," in *Proc. 17th European Signal Processing Conf.*, Glasgow, UK, 2009, pp. 2136-2140.

[56] R. Kanna, "Design of ZigBee transceiver for IEEE 802.15.4 using Matlab/Simulink," *Dept. Elec. Comm. Eng. , National Institute of Technology, India,* 2011.

[57] G. C. Clark and J. B. Cain, *Error-Correction Coding for Digital Communications.* NY, USA: Springer Science & Business Media, 1981.

[58] IEEE Standard 802.15.4-2011, "Part 10: O-QPSK PHY," 2011.

[59] T. Shirai, T. Nishiyama, M. Itami, H. Ohta and K. Itoh, "A study on adaptive cancellation of impulsive noise from OFDM signal under multi-path environment," in *Proc. 7th Int. Symp. Power-Line Communications and its Applications,* Kyoto, Japan, 2003, pp. 215-220.

[60] T. Hirakawa, M. Fujii, M. Itami and K. Itoh, "A study on iterative impulsive noise reduction in OFDM signal by recovering time domain samples," in *Proc. 2006 IEEE Int. Symp. on Power Line Communications and its Applications* , Orlando, USA, 2006, pp. 325-330.

[61] G. Ren, S. Qiao, H. Zhao, C. Li and Y. Hei, "Mitigation of periodic impulsive noise in OFDM-based power-line communications," *IEEE Trans. on Power Delivery,* vol. 28, pp. 825-834, Jan., 2013.

[62] Y. Lee and S. Kim, "Median-prefiltering-based robust acquisition of direct-sequence spread-spectrum signals in wide-band pulse jamming," *IEEE Trans. on Veh. Technol.,* vol. 51, pp. 171-179, Jan., 2002.

[63] K. V. R. Silva, N. D. Suraweera, D. S. Talagala, D. K. Thilakarathna and D. Dias, "ZigBee based local communication system for high noise environments," in *Proc. 9th Int. Information Technology Conf.,* Las Vegas, USA, 2008, pp. 72-78.

[64] P. Torio and M. Sanchez, "Improving capability of detecting impulsive noise," *IEEE Trans. on Electromagn. Compat.*, vol. 55, pp. 66-73, Jul., 2012.

[65] X. Li, C. Yu, M. Hizlan, W. Kim and S. Park, "Physical layer watermarking of direct sequence spread spectrum signals," in *Proc. IEEE Military Communications Conf.*, San Diego, USA, Nov. 2013, pp. 476-481.

[66] S. Mallat, *A Wavelet Tour of Signal Processing: The Sparse Way*. MA, USA: Elsevier, 2009.

[67] F. Sacuto, F. Labeau and B. L. Agba, "Wide Band Time-Correlated Model for Wireless Communications under Impulsive Noise within Power Substation," *IEEE Trans. on Wireless Communications*, vol. 13, pp. 1449-1461, Jan, 2014.

Appendix A

Improvement of Bandwidth Efficiency using 16-QAM Modulation in OFDM Systems

An OFDM modulation system transmits bit information at the bit rate R. Assuming each OFDM symbol contains N bits, an N-point IFFT is therefore performed. The OFDM symbol duration is expressed as

$$T_{os} = \frac{N}{R}. \tag{A.1}$$

The frequency interval of OFDM sub-carriers is hence

$$f_{si} = \frac{1}{T_{os}} = \frac{R}{N}, \tag{A.2}$$

and the required bandwidth of the OFDM baseband transmission is

$$B_b = \frac{N}{2} \cdot f_{si} = \frac{R}{2}. \tag{A.3}$$

With a 2^M-ary QAM modulation, every QAM symbol contains M bits, hence the QAM symbol duration is

$$T_{qs} = \frac{M}{R}. \tag{A.4}$$

To transmit the same N bits, the number of QAM symbols is N/M which is also the IFFT points for the corresponding OFDM modulation. With the N/M-point IFFT operation, the duration of the OFDM symbol carrying the QAM symbols is the same as the duration of the OFDM symbol carrying the bits, that is

$$T_{osq} = T_{os}. \tag{A.5}$$

The frequency interval of sub-carriers is therefore the same as f_{si}. The required bandwidth of the baseband transmission is hence obtained as

$$B_{b1} = \frac{1}{2} \cdot \frac{N}{M} \cdot f_{si} = \frac{R}{2M}. \quad \text{(A.6)}$$

A bandwidth gain of the baseband transmission is defined to evaluate the bandwidth efficiency of the QAM modulation, that is

$$\text{Gain}_q = 10\log_{10} \frac{B_{b1}}{B_b} = 10\log_{10} M \text{ (dB)}. \quad \text{(A.7)}$$

For the 16-QAM modulation, the bandwidth gain is about 6 dB. Therefore, to transmit the same number of bits, a 16-QAM modulated OFDM system requires a -6 dB bandwidth when compared to the OFDM system modulating the bit information directly which shows the improvement of bandwidth efficiency.

Appendix B

BER Performance of O-QPSK in the Presence of Channel Impulsive Noise and Coherent Detection with an LPF

The autocorrelation $R_{i_m}(\tau)$ of $i_m(t)$ is obtained as

$$R_{i_m}(\tau) = \mathrm{E}[i_m(t)i_m(t-\tau)] = \mathrm{E}[2i(t)\cos 2\pi f_c t \cdot 2i(t-\tau)\cos 2\pi f_c(t-\tau)]$$

$$= \mathrm{E}[4i(t)i(t-\tau)]\mathrm{E}[\cos 2\pi f_c t \cos 2\pi f_c(t-\tau)] = 4R_i(\tau)\cdot\frac{1}{2}\cos 2\pi f_c\tau = pN_0\delta(\tau). \quad \text{(B.1)}$$

The PSD $S_{i_m}(f)$ of $i_m(t)$ is thus

$$S_{i_m}(f) = pN_0. \quad \text{(B.2)}$$

The PSD $S_{i_{L,m}}(f)$ and autocorrelation $R_{i_{L,m}}(\tau)$ of $i_{L,m}(t)$ is hence can be represented as

$$\begin{cases} S_{i_{L,m}}(f) = \begin{cases} pN_0, |f| \le B_{\mathrm{LPF}} \\ 0, |f| > B_{\mathrm{LPF}} \end{cases} \\ R_{i_{L,m}}(\tau) = 2pB_{\mathrm{LPF}}N_0\mathrm{sinc}(2B_{\mathrm{LPF}}\tau) \end{cases}. \quad \text{(B.3)}$$

Finally considering the condition $T_{\mathrm{symbol}} > \frac{1}{B_{\mathrm{LPF}}}$ the variance σ_M^2 of M is obtained as

$$\sigma_M^2 = \mathrm{E}[M^2] = \mathrm{E}\left[\left(\int_0^{T_{\mathrm{symbol}}} i_{L,m}(t)\,dt\right)^2\right] = \int_0^{T_{\mathrm{symbol}}}\int_0^{T_{\mathrm{symbol}}} \mathrm{E}\left[i_{L,m}(t)i_{L,m}(a)\right]dtda$$

$$= \int_0^{T_{\mathrm{symbol}}}\int_0^{T_{\mathrm{symbol}}} R_{i_{L,m}}(t-a)dtda = \int_0^{T_{\mathrm{symbol}}}\left(T_{\mathrm{symbol}}-\tau\right)R_{i_{L,m}}(\tau)d\tau$$

$$= \int_0^{T_{\mathrm{symbol}}} T_{\mathrm{symbol}}R_{i_{L,m}}(\tau)d\tau - \int_0^{T_{\mathrm{symbol}}} \tau R_{i_{L,m}}(\tau)d\tau$$

$$\approx pN_0T_{\mathrm{symbol}} - \int_0^{T_{\mathrm{symbol}}} 2\tau pB_{\mathrm{LPF}}N_0\frac{\sin 2\pi B_{\mathrm{LPF}}\tau}{2\pi B_{\mathrm{LPF}}\tau}d\tau$$

$$= pN_0\left(T_{\mathrm{symbol}} - \frac{\left(1-\cos 2\pi B_{\mathrm{LPF}}T_{\mathrm{symbol}}\right)}{2\pi B_{\mathrm{LPF}}}\right), \quad \text{(B.4)}$$

where $\tau = t - a$. According to (5.19) and (5.20), M can be approximately considered as a Gaussian process with zero mean as a result of linear operations on $i(t)$. The PDF $f_M(m)$ of M is thus given as

$$f_M(m) = \frac{\exp(-m^2/2\sigma_M^2)}{\sigma_M\sqrt{2\pi}}. \tag{B.5}$$

The PE $P_{e1,i,\mathrm{OQPSK}}$ of the integrator output in the in-phase sub-channel is therefore derived as

$$P_{e1,i,\mathrm{OQPSK}} = \int_{-\infty}^{-A_cT_{\mathrm{symbol}}} f_M(m)dm = \int_{-\infty}^{-A_cT_{\mathrm{symbol}}} \frac{\exp(-m^2/2\sigma_M^2)}{\sigma_M\sqrt{2\pi}}\,dm. \tag{B.6}$$

Let $l = \frac{m}{\sigma_M}$, (B.6) can be rewritten as

$$P_{e1,i,\mathrm{OQPSK}} = \int_{\left(\frac{A_cT_{\mathrm{symbol}}}{\sigma_M}\right)}^{+\infty} \frac{\exp(-l^2/2)}{\sigma_M\sqrt{2\pi}}\sigma_M dl = Q\left(\frac{A_cT_{\mathrm{symbol}}}{\sigma_M}\right)$$

$$= Q\left(\frac{A_cT_{\mathrm{symbol}}}{\sqrt{pN_0\left(T_{\mathrm{symbol}} - \frac{\left(1-\cos 2\pi B_{\mathrm{LPF}}T_{\mathrm{symbol}}\right)}{2\pi B_{\mathrm{LPF}}}\right)}}\right). \tag{B.7}$$

The PE of the integrator output in the quadrature sub-channel and O-QPSK system are denoted as $P_{e2,i,\mathrm{OQPSK}}$ and $P_{e,i,\mathrm{OQPSK}}$, respectively. It can be found that

$$P_{e1,i,\mathrm{OQPSK}} = P_{e2,i,\mathrm{OQPSK}} = P_{e,i,\mathrm{OQPSK}}. \tag{B.8}$$

Curriculum Vitae

Candidate's full name: Jia Jia

Universities attended:

University of New Brunswick, Fredericton, NB, Canada
Doctor of Philosophy (Ph. D.) 2009-2015

University of Bradford, Bradford, W. Yorkshire, England
Master of Philosophy (M. Phil.) 2006-2009

University of Electronic Science and Technology of China, Chengdu, Sichuan, China
Bachelor of Science (B. Sc.) 2001-2005

Publications:

Jia Jia, Julian Meng, "Impulsive Noise Rejection for ZigBee Communication Systems using Error-Balanced Wavelet Filtering," submitted to *Elsevier AEU International Journal of Electronics and Communications.*

Jia Jia, Julian Meng, "A Novel Approach for Impulsive Noise Mitigation in ZigBee Communication Systems," in *Proceedings of Global Information Infrastructure and Networking Symposium*, Montreal, Quebec, Sept. 2014.

Jia Jia, Julian Meng, "A Dual Protection Scheme for Impulsive Noise Suppression in OFDM Systems," *Elsevier AEU International Journal of Electronics and Communications*, vol. 68, no. 1, Jan. 2014.

Jia Jia, Julian Meng, "Partial Discharge Impulsive Noise in Electricity Substations and the Impact on 2.4 GHz and 915 MHz ZigBee Communications," in *Proceedings of IEEE Power and Energy Society General Meeting*, Vancouver, British Columbia, Jul. 2013.

Jia Jia, Jianmin Jiang, Dong Wang, "Recognition of Hand Gesture based on Gaussian Mixture Model," in *Proceedings of International Workshop on Content-Based Multimedia Indexing*, London, England, Jun. 2008.